Van Wagenen First Author 1971-1983

View   Arrange By   Action   Share   Edit Tags   Search

Name

Van Wagenen 1971? Activated Carbon Artificial Kidney Parts 1 and 2.pdf

Van Wagenen 1975 Activated Carbons lentz steggall.pdf

Van Wagenen 1975 Particulates coleman.pdf

Van Wagenen 1976 Streaming potential J Electrochem hibbs.pdf

Van Wagenen 1980 Flat Streaming Potential.pdf

Van Wagenen 1980 Organic Coatings preprints TIRF albumin Zdasiuk.pdf

Van Wagenen 1981 Polymer Streaming Potent...leman king triolo brostrom smith gregonis.pdf

Van Wagenen 1982 Cooper Peppas ACS Bk TIRF rockhold.pdf

Van Wagenen 1983?? draft unpublished TIRF IgG Dunn.pdf

Walker 1976 Activated Carbon Kidney International denti van wagenen.pdf

ACTIVATED CARBON AND THE ARTIFICIAL KIDNEY I

R. Van Wagenen
J. D. Andrade

Institute for Biomedical Engineering
University of Utah
Salt Lake City, Utah 84112

Activated Carbon

Activated carbon (charcoal) has been utilized in industry for many years to decolorize and purify gases and organic liquids. There are a variety of grades of activated carbon used for many specialty applications, including municipal water purification, sugar refining, winemaking, radioactive gas adsorption, air purification, and various catalyst support systems. The purification process is one of adsorption (physical attachment by secondary bonding) of solute or gas molecules directly to the surface of the carbon. The extremely high adsorption capacity of activated carbon is a result of its large surface area. In some cases, this area can be as much as 1000-1400 m^2/gram. The high surface area is created by the presence of an extensive porosity in the carbon substructure. Macropores (greater than 1000 Å in diameter) originate at the surface of the activated carbon particle and penetrate into the bulk carbon. Micropores (10 Å to 1000 Å in diameter) branch off from the macropores in the interior of the carbon; it is in these micropores where most of the solute adsorption occurs.

The adsorptive properties of a specific grade of activated carbon are due to its total surface area (which is dependent on the micropore size distribution), the pore structure, and the chemical nature of the carbon surface. The pore structure and total surface area depend upon the material used to produce the activated carbon and the methods of activation. Many organic materials (coal, peat, bone, petroleum, shells, wood, etc.) have been used at one time or another as a basis of activated carbon production. These materials are usually carbonized by high temperature treatment. The amorphous part of the carbon is then removed either chemically or with high temperature steam resulting in an extensive porous network of high surface area. The generation of this porous network is termed "activation" of the carbon.

If the major contribution to surface area and thus adsorption capacity is located in the micropores of molecular dimensions, then adsorption specificity depends on the molecular size of the solute molecules. For instance, a large solute molecule cannot penetrate into a micropore of too small diameter or of irregular shape. Thus these big molecules are "screened out" and prevented from adsorbing in the micropores. Even though the large molecules could adsorb in the large pores to which they could gain access, adsorption capacity would be small due to the small contribution to the total surface area provided by the macropores. Figure 1 illustrates the concept that for any molecule the effective surface area for adsorption exists only in the pores to which the molecule can gain access. Figure 2 is a photomicrograph of the surface of an activated carbon particle.

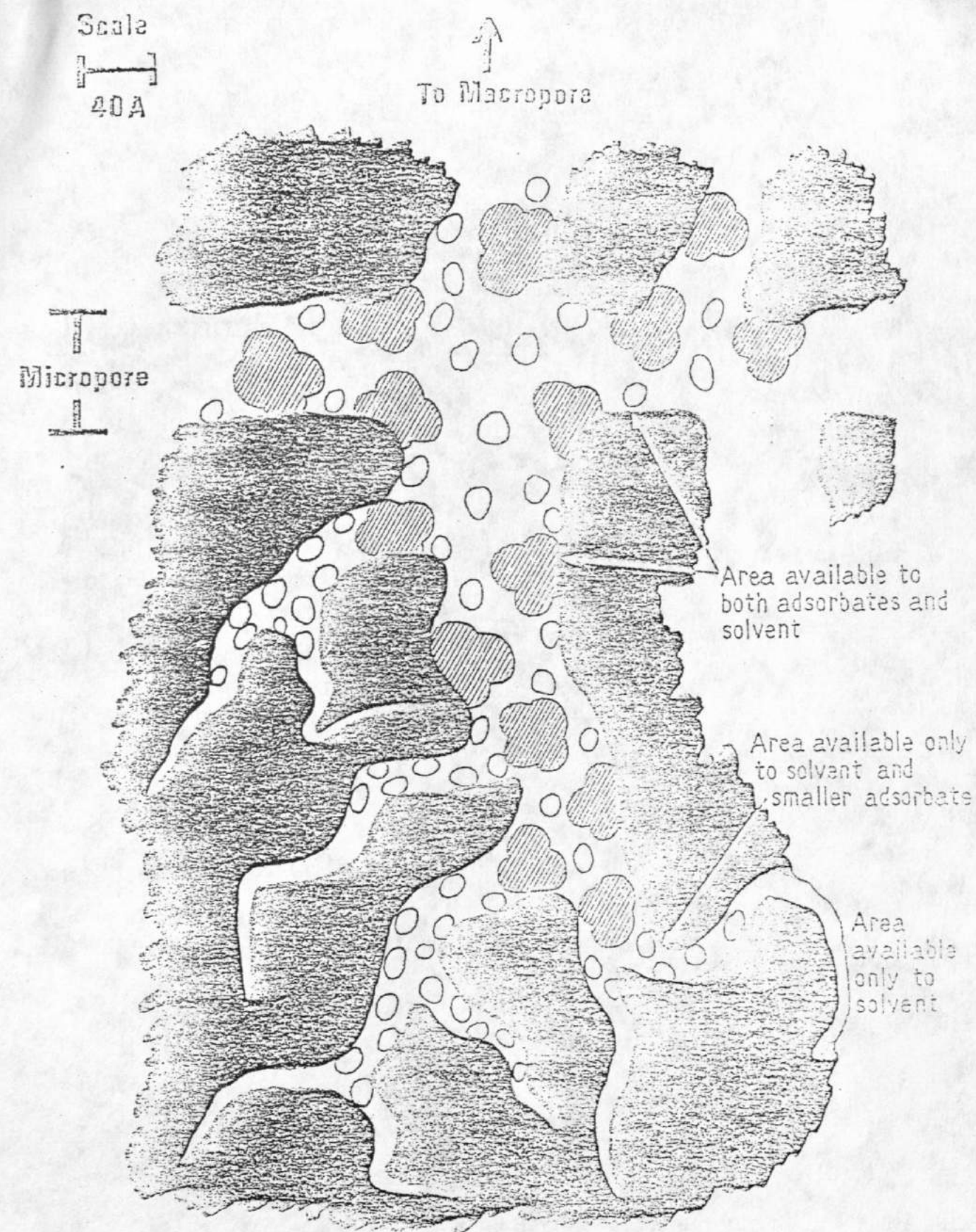Figure 1. A schematic cross-sectional view of the pore structure in an activated carbon particle. Two kinds of solute molecules in a solvent (not shown) compete for adsorbent surface. The small micropores are inaccessible to the large solute molecules. The greater diffusional mobility and the smaller size of the second solute molecule allows it to reach the micropores and adsorb in large quantities. (Redrawn from Ref. 1, p. 7.)
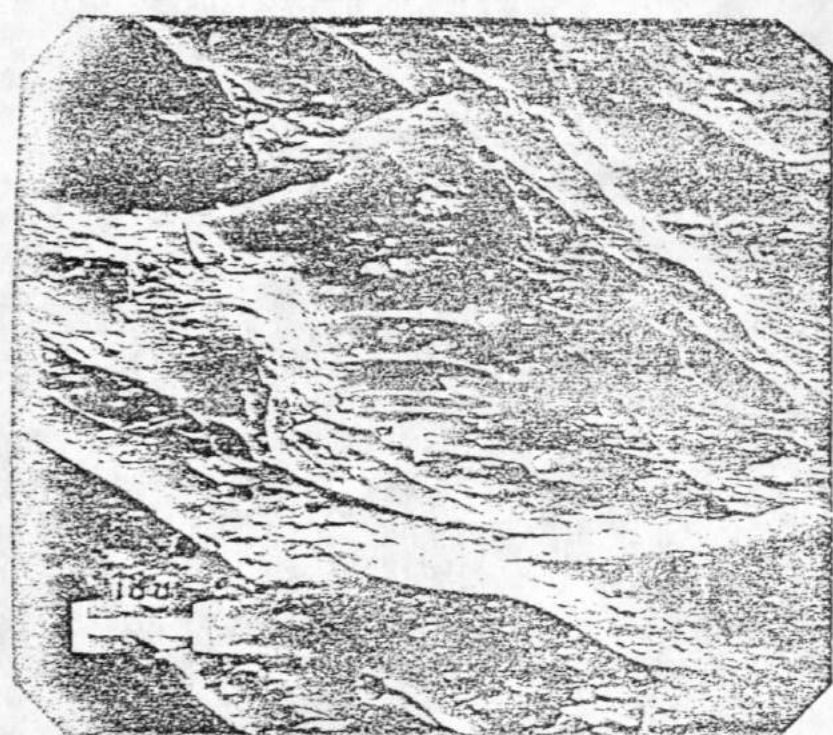
Figure 2. A scanning electron micrograph showing the macro-
porous structure at the surface of a granular
activated carbon particle. Some microparticles
(center) probably generated in the activation
process can be seen as well as several large
surface fissures (upper left and lower right
corners). Scale: 1 cm = 7 microns.

Hemoperfusion[2]

During the last nine years, hemoperfusion over activated carbon
has been used both as an adjunct to conventional hemodialysis and as
a treatment for severe, acute poisoning cases. Yatzidis (1964) did
the pioneering work in applying charcoal hemoperfusion to patients
with chronic renal failure.[3] His perfusion apparatus consisted of
a siliconized glass cylinder containing approximately 200 grams of
activated carbon. After assembly and sterilization, the column of
charcoal was rinsed and primed with heparinized saline. During use,
the patient's heparinized blood flowed from a cannulated artery,
percolated up through the activated carbon, and out the top of the
cartridge. The blood was then returned to the patient via a cannulated
vein. At the end of the hemoperfusion, the blood remaining within
the apparatus was slowly returned to the patient. The duration of
these early clinical hemoperfusions ranged from 30 to 90 minutes and
blood flow rates through the circuit varied from 150 ml/min to 300 ml/min.
Yatzidis reported that at the beginning of a hemoperfusion over charcoal,
plasma creatinine, uric acid, indican, phenolic compounds and guanidine
bases were almost totally removed from the blood which flowed through
the charcoal column. He also reported that clinical hemoperfusions
removed negligible quantities of urea, magnesium, phosphates, sulfates,
potassium, calcium, and water.

From a comparison between charcoal hemoperfusion and hemodialysis
utilizing a Kolff twin coil, Yatzidis concluded that a 60-minute
perfusion of two or three charcoal columns was about as efficient as

a conventional hemodialysis of four to six hours duration. The disadvantages associated with hemoperfusion were limited to high heparin dosage levels, significant platelet drops, fluctuating white cell levels, drops in plasma fibrinogen, and the occurrence of several pyrogenic reactions. Plasma hemoglobin and hematocrit remained normal and in spite of the above limitations, the hemoperfusions usually resulted in an immediate improvement in the patient's general condition.

Dunea and Kolff[4] reported on preliminary clinical experience utilizing charcoal hemoperfusion to treat three uremic patients. Their perfusion apparatus and technique was similar to that reported previously by Yatzidis.[3] The clinical clearance data for creatinine and uric acid was promising. There were no significant changes in blood urea, serum phosphorus, serum electrolytes or white cell count. No pyrogenic reactions were observed. The carbon used had a low ash content and was washed in eight liters of physiological saline before perfusion. The only apparent disadvantages associated with the hemoperfusions were a significant decrease in platelets and blood loss in the column resulting from carbon packing and caking which made complete retransfusion difficult. Because of the low adsorptive capacity of carbon for urea, Dunea and Kolff concluded that charcoal hemoperfusion may be a useful adjunct to hemodialysis since it can do well what dialysis does poorly. For instance, it seems quite feasible to combine charcoal hemoperfusion and hemodialysis into a single artificial

kidney system. Certain undesirable molecules would be removed by adsorption on the activated carbon while water, urea and electrolytes would be removed using a membrane hemodialyzer. The more efficient removal of middle and high molecular weight compounds may possibly cut down on dialysis times or even reduce the number of dialysis sessions required per week. This would not only lower the cost but it would also cut the time required each week for dialysis.

Another aspect of blood perfusion over activated charcoal is the ability of carbon to adsorb considerable amounts of barbiturates, salicylates, and glutethimide from plasma.[3] Yatzidis applied this finding to several patients with severe barbiturate poisoning.[5] He coated the carbon with cellulose acetate to reduce the blood damage which was so prevalent in the earlier clinical trials.[3] Several short-term hemoperfusions were effective in decreasing the plasma barbiturate levels and the general condition of the patients improved considerably. DeMyttenaere[6] evaluated the adsorption capacity of activated carbon for glutethimide (Doriden ®) both in vitro and in vivo, utilizing dogs. He found charcoal hemoperfusion to be an effective method of removing glutethimide from blood and suggested that repeated hemoperfusions utilizing fresh carbon may be necessary for clinical poisoning treatments. DeMyttenaere reported that in vivo glutethimide clearances were superior to those previously reported for hemodialysis utilizing aqueous or lipid dialysate. A comparison of barbiturate removal by conventional hemodialysis, hemoperfusion over an anion exchange resin and hemoperfusion over coated and uncoated

activated carbon was conducted by Rosenbaum, et al. in 1968.[7] They found charcoal hemoperfusion to be superior over hemodialysis and anion exchange resin perfusion for the removal of barbiturate from blood. He also reported that hemoperfusion of charcoal caused a marked hypotension and reduction of platelets and white blood cells. Histopathological tissue samples from dogs previously subjected to hemoperfusions showed charcoal emboli in the lungs and other viscera.

During the last three years, extensive research on hemoperfusion over activated carbon has been conducted by two groups. The first group under the direction of Dr. T. M. S. Chang in Montreal has applied charcoal hemoperfusion on a large scale to the maintenance of patients suffering from chronic renal failure. Chang initiated the concept of 'artificial cells' and the application of microencapsulation technology to medical problems.[8-10]. In the last six years, Chang, et al. have utilized activated carbon coated with several polymeric materials for clinical hemoperfusions. Chang has demonstrated that 300 grams of activated carbon coated with albumin-coated colloidion membranes (ACAC) can remove creatinine and uric acid as effectively as a coil artificial kidney and more efficiently than a plate-type or capillary-type hemodialyzer.[11] Chang also reports that with proper carbon coating, washing and sterilization prior to hemoperfusion no pyrogenic reactions occur and no carbon emboli will escape from the apparatus.[10,11] The presence of the albumin-coated colloidion membrane enhances the blood tolerability of the carbon resulting in only a small drop in blood platelets.

Recently, Chang has reported the results of 55 hemoperfusions conducted on 11 patients utilizing albumin-colloidion activated carbon. The results support his earlier findings and he concludes that the ACAC artificial kidney system is safe and effective for the management of patients with chronic renal failure.[13]

Chang has also evaluted his albumin-coated, colloidion activated carbon in terms of exogenous toxin adsorption. Nembutal and salicylate have been studied and removal from blood via hemoperfusions utilizing dogs seems to be efficient enough to revive the animals after administration of a fatal dose of the exogenous poison.[11] Quite recently, Chang reported that the ACAC artificial kidney has been used to treat a patient with acute glutethimide intoxication.[14] Two hemoperfusions resulted in a marked reduction of blood glutethimide, and the patient regained consciousness.

ACTIVATED CARBON AND THE ARTIFICIAL KIDNEY II*

R. Van Wagenen
J. D. Andrade
Institute for Biomedical Engineering
University of Utah
Salt Lake City, Utah 84112

Research on charcoal hemoperfusion was initiated at the University of Utah in the summer of 1970. At that time the goal of the research was to eliminate the problems which had prevented the hemoperfusion concept from being widely accepted. The major problems were: (1) decreased platelet and white cell levels after hemoperfusion, (2) charcoal caking, packing and clotting which resulted in blood channeling and significantly reduced adsorption efficiency, (3) loss of blood in the column after hemoperfusion, (4) excessively high heparin dosage levels, (5) possible occurrence of pyrogenic reactions, and (6) the microparticle "emboli" problem. It was felt that if these problems could be solved, the simplicity, low cost and efficiency of charcoal hemoperfursion could benefit a large number of dialysis patiets who now rely on two or three hemodialysis treatments each week.

Our approach to these problems was to coat the granular activated carbon with a material that was blood compatible. Acrylic hydrogels with high water content were chosen as coating materials on the basis of previously reported results,[15] and the belief that by minimizing the interfacial energy between a gel-like surface and an aqueous liquid

*Part I was published in this Journal

required to maintain a high concentration difference across the membrane for waste metabolites. Kolobow and Dedrick in 1965 described a new kind of hemodialyzer with a high dialysance at a low dialysate flow rate.[20] The presence of finely powdered activated carbon in the dialysate served as a "sink" for many waste metabolites. The adsorption of these metabolites on the carbon kept the concentration in the dialysate low, maintaining a high concentration gradient. Blaney, Lindan and Sparks applied the concept of a low dialysate volume containing activated carbon to a "wearable" artifical kidney design.[21] They found that creatinine and uric acid are strongly and irreversibly bound to activated carbon but the capacity for urea is low and it binds somewhat reversibly. Blaney, et al. envisioned a small cartridge containing adsorbent for creatinine, uric acid and urea. Since carbon can only remove a relatively small amount of urea, another method would be required for urea removal. The adsorbent plus a low volume of dialysate would be coupled with a small wearable dialyzer and pump to recirculate the dialysate. Periodically dialysate would be replaced and the adsorbent regenerated or replaced. Recently, Dharnidharka, et al. devised an artificial kidney system utilizing isotonic ultrafiltrate as the dialysate, generated by a partial vacuum around the fibers of a hollow-fiber artificial kidney.[22] Water and salt homeostasis can be maintained by removal of the desired amounts of ultrafiltrate and an adsorbent such as charcoal can be used in the dialyzing fluid to remove waste metabolites. Dharnidharka, et. al., concluded that utilization of present hardware and oral doses of anticoagulant make it feasible to develop an artificial kidney based on ultrafiltrate as the dialysate. This eliminates the problems inherent in the use of large volumes of dialysate. Since a blood pump is not required, the weight reduction

During the last two years the research emphasis in this laboratory has been directed toward selection of the optimum grade of carbon and coating material which will give the best hemoperfusion results for the solutes of interest (creatinine, uric acid, salicylates, barbiturates, etc.). Evaluations of most commercially available activated carbons as well as some specialty grades of carbon have been conducted for initial carbon cleanliness (presence of microparticles which could become emboli during hemoperfusion), carbon washability, and resistance to fragmentation.[19] In vitro adsorption evaluations for endogenous and exogenous toxins are conducted on activated carbons which show promising cleanliness and also as an evaluation test for various kinds of polyHEMA coatings.

An ingenious method of encapsulating activated carbon particles is being developed by the group at Southern Research Institute. They are producing polymer fibers loaded with activated carbon particles. The fibers are then wound on a spool and packed in a cartridge for blood perfusion.[24]

The results of clinical hemoperfusion experience reported by Chang and the optimization of carbon selection, washing, hydrogel coating, and in vitro/in vivo evaluations carried out in our laboratories and elsewhere are promising. Hemoperfusion over thoroughly characterized, washed and coated activated carbon deserves serious consideration as a possible adjunct to chronic hemodialysis and as a method for the extracorporeal treatment of severe acute poisoning.

Dialysate Regeneration

One of the limitations to miniaturization of the membrane-type artificial kidney is the extremely large volume of dialysate fluid

(blood), the interactions across the interface (protein adsorption platelet adhesion, etc.) would be minimized.[16, 17] The acrylic hydrogel chosen for coating was polyhydroxyethyl methacrylate (polyHEMA), also call Hydron-S. Much of the emphasis during our early research was oriented toward evaluation of various hydrogel coatings and circuit designs.[16] The evaluations were primarily in vitro stirred batch adsorption sutdies using radiolabeled creatinine and uric acid and in vivo perfusions utilizing sheep and dogs.[16, 18] We found that a combination of proper heparin doses and polyHEMA coatings prevented fibrin buildup, platelet sticking, and subsequent clot formation.[16, 18] This in turn prevented carbon packing and resultant blood channeling during perfusion. The decrease in blood channeling exposed the blood to more activated carbon surface, resulting in an optimal adsorption capacity for the total amount of carbon in the circui

The direction of our research changed during the second year when we realized that the major problem remaining was the possibility of microemboli generation during hemoperfusion. Initial in vitro evaluations showed that some carbons were cleaner and more resistant to fragmentation than others and also that various brands of carbon could be washed cleaner than other brands.[18] In vivo animal experiments were continued and substantiated the in vitro stirred batch adsorption studies with creatinine, uric acid and salicylate. We found that a properly and thoroughly washed carbon which is then encapsulated and contained in a single compartment cartridge will not produce readily detectable carbon emboli. This confirms Chang's histopathological findings for thoroughly washed albumin-colloidion activated carbon.[3-12]

enhances the feasibility of a wearable artificial kidney. Small quantities of charcoal are sufficient for the removal of creatinine and uric acid but for adequate urea removal by adsorption, 20 to 40 times as much activated carbon would be required.[22] This begins to bring weight limitations of a wearable artificial kidney back into the picture.

A commercial approach to dialysate regeneration is the REDY (Recirculating Dialysate) system.[23] The objective of this system is to utilize an appropriate combination of adsorbents to regenerate a small volume of dialysate which is then recirculated through the artificial kidney. A combination of activated carbon, zirconium phosphate, zirconium oxide and urease all contained in a single disposable cartridge effect the removal of waste metabolites from the blood. The sorbent system operates on the principles of ion exchange and physical adsorption. Dialysate from the artificial kidney enters the sorbent pack and urea is converted to ammonium ion and bicarbonate. The ammonium, calcium, magnesium and potassium ions are exchanged for sodium and hydrogen ions on the zirconium phosphate. As the dialysate passes through zirconium oxide, phosphate ion is removed. Organic waste metabolites, creatinine, uric acid, guanidine, etc., are removed by adsorption on activated carbon. Magnesium and calcium ions are infused to the dialysate before it is returned to the dialyzer. The REDY system offers a significant reduction in weight and volume compared to previous designs. It is portable and requires no special electrical or plumbing hook-ups. However, it is not wearable.

Ideally, a wearable artifical kidney would need to be small, light in weight and simple to operate and power.

Summary

Activated carbon has a large capacity for adsorption of nitrogeneous waste products from blood or dialysate by virtue of its high porosity and resulting large surface area. Many of the problems associated with early clinical hemoperfusion attempts have been overcome by proper washing and by coating the granular activated carbon with polymeric materials to improve blood tolerability. The added mechanical strength due to the polymeric coatings also helps prevent the fragmentation and embolization reported in early in vivo animal experiemnts. A number of successful clinical trials have been reported. Activated carbon also finds application in dialysate regeneration schemes. In the future it may serve as a valuable sorbent for removal of waste metabolites in miniaturized wearable artificial kidneys. It is also of great usefulness for the removal of many poisons and drugs in acute poisoning episodes.

REFERENCES

1. Basic Concepts of Adsorption on Activated Carbon, a brochure provided by Pittsburgh Activated Carbon Division of Calgon Corporation, subsidiary of Merck & Co., Inc. Calgon Center, Box 1346, Pittsburgh, Pennsylvania, 15230.

2. Andrade, J. D., Kopp, K., Van Wagenen, R., Chen, C., and Kolff, W. J., "Activated Carbon and Blood Perfusion: A Critical Review," Proc. Europ. Dial. Transplant Assn. 9: 290 (1972).

3. Yatzidis, H., "A Convenient Haemoperfusion Micro-Apparatus over Charcoal for the Treatment of Endogenous and Exogenous Intoxications," Proc. Europ. Dial. Transplant Assn. 1: 83 (1964).

4. Dunea, G. and Kolff, W. J., "Clinical Experience with the Yatzidis Charcoal Artificial Kidney," Trans. Amer. Soc. Artif. Int. Organs 11: 178 (1965).

5. Yatzidis, H., "The Charcoal Artificial Kidney in Clinical Practice," Paper presented at the Cleveland Clinic, Cleveland, Ohio, October 18, 1966.

6. DeMyttenaere, M. H., Maher, J. F. and Schreiner, G. E., "Hemoperfusion Through a Charcoal Column for Glutethimide Poisoning," Trans. Amer. Soc. Artif. Int. Organs 13: 190 (1967).

7. Rosenbaum, J. L., Ronquillo, E. and Argyres, S. N., "Column Hemoperfusion and Hemodialysis Techniques to Treat Barbiturate Intoxication in Dogs," J. Albert Einstein Med. Center 16; 67 (1968).

8. Chang, T. M. S., "Semipermeable Aqueous Microcapsules ('Artificial Cells') with Emphasis on Experiments in an Extracorporeal Shunt System," Trans. Amer. Soc. Artif. Int. Organs 12: 13 (1966).

9. Chang, T. M. S., Pont, A., Johnson, L. J. and Malave, N., "Response to Intermittent Extracorporeal Perfusion Through Shunts Containing Semipermeable Microcapsules," Trans. Amer. Soc. Artif. Int. Organs 14: 163 (1968).

10. Chang, T. M. S., Artifical Cells, Charles C. Thomas, Publisher, 1972.

11. Chang, T. M. S., Gonda, A., Dirks, J. H., and Malave, N.,"Clinical Evaluation of Chronic, Intermittent, and Short-Term Hemoperfusions in Patients with Chronic Renal Failure Using Semipermeable Microcapsules (Artificial Cells) Formed from Membrane-Coated Activated Charcoal," Trans. Amer. Soc. Artif. Int. Organs 16: 246 (1971).

12. Chang, T. M. S. and Malave, N., "The Development and First Clinical Use of Semipermeable Microcapsules (Artificial Cells) as a Compact Artificial Kidney," Trans. Amer. Soc. Artif. Int. Organs 16: 141 (1970).

13. Chang, T. M. S., Gonda, A., Dirks, J. H., Coffey, J. F. and Burns, T. L., "ACAC Microcapsule Artificial Kidney for the Long-Term and Short-Term Management of Eleven Patients with Chronic Renal Failure," Trans. Amer. Soc. Artif. Int. Organs 18: 465 (1972).

14. Chang, T. M. S., Coffey, J. F., Lister, C., Taroy, E., and Stark, A., "Methaqualone, Methyprylon, and Glutethimide Clearance by the ACAC Microcapsule Artificial Kidney: In Vitro and In Patients with Acute Intoxication," Trans. Amer. Soc. Artif. Int. Organs 19: 87 (1973).

15. Levowitz, B. S., et al.,"Biologic Compatibility and Applications of Hydron," Trans. Amer. Soc. Artif. Int. Organs 14: 82 (1968).

16. Andrade, J. D., Kunitomo, K., Van Wagenen, R., Kastigar, B., Gough, D., and Kolff, W. J., "Coated Adsorbents for Direct Blood Perfusion: Hema/Activated Carbon," Trans. Amer. Soc. Artif. Int. Organs 17: 222 (1971).

17. Andrade, J. D., "Interfacial Phenomena and Biomaterials," Med. Inst. 7: 2 (1973).

18. Andrade, J. D., Van Wagenen, R., Chen, C., Ghavamian, M., Volder, J., Kirkham, R., and Kolff, W. J., "Coated Adsorbents for Direct Blood Perfusion II," Trans. Amer. Soc. Artif. Int. Organs 18: 473 (1972).

19. Van Wagenen, R., Lentz, D. and Andrade, J. D., Manuscript in preparation.

20. Kolobow, T. and Dedrick, R. L., "Dialysate Capacity Augmentation at Ultra-Low Flow Rates with Activated Carbon Slurry," Trans. Amer. Soc. Artif. Int. Organs 12: 1 (1965).

21. Blaney, T. L., Lindan, O. and Sparks, R. E., "Adsorption: A Step Toward a Wearable Artificial Kidney," Trans. Amer. Soc. Artif. Int. Organs 12: 7 (1966).

22. Dharnidharka, S. G., Kirkham, R. and Kolff, W. J., "Toward a Wearable Artifical Kidney Using Ultrafiltrate as Dialysate," Trans. Amer. Soc. Artif. Int. Organs 19: 92 (1973).

23. Greenbaum, M. A. and Gordon, A., "A Regenerative Dialysis Supply System," Dialysis and Transplantation, April/May 1972.

24. T. Davis and D. Cowsar, Proc. Artificial Kidney Program Contractors' Meeting, N.I. A.M.D., Bethesda, Md., February, 1973.

Activated Carbons for Medical Applications.
In vitro Microparticle Characterization and Solute Adsorption

R. A. VAN WAGENEN, Ph.D., M. STEGGALL, M.S.,
D. J. LENTZ, Ph.D., and J. D. ANDRADE,* Ph.D.

Department of Materials Science and Engineering and
Institute for Biomedical Engineering
University of Utah
Salt Lake City, Utah 84112

ABSTRACT

Activated carbon is a high surface area adsorbent. Its ability to adsorb nitrogenous metabolic wastes and exogenous poisons from blood has been well documented. Polymeric coatings on activated carbon enhance its biotolerability and make it feasible for use in hemoperfusion devices. The only drawback seems to be the presence of microparticles on the carbon surface. These particles may become emboli during hemoperfusion.

This paper describes a series of in vitro tests used to evaluate many commercially available granular and pelletized activated carbons. The tests were as follows: 1) creatinine adsorption capacity and kinetics, 2) initial cleanliness, 3) washability, 4) attrition resistance, and 5) carbon particle surface morphology.

---

*To whom correspondence concerning this paper should be addressed.

[19] T. M. S. Chang, J. F. Coffey, P. Barre, A. Gonda, J. H. Dirks, M. Levy, and C. Lister, "Microcapsule Artificial Kidney: Treatment of Patients with Acute Drug Intoxication," Can. Med. Assoc. J., 108, 429 (1973).

[20] T. M. S. Chang, J. F. Coffey, C. Lister, E. Taroy, and A. Stark, "Methaqualone, Methyprylon, and Glutethimide Clearance by the ACAC Microcapsule Artificial Kidney: In vitro and in Patients with Acute Intoxication," Trans. Amer. Soc. Art. Int. Org., 19, 87, (1973).

[21] Final Report on Contract #PH-43-68-1027, U.S. Public Health Service, National Institute of Arthritis and Metabolic Diseases, Artificial Kidney-Chronic Uraemia Program, W. J. Kolff, Principal Investigator, March 1973.

[22] K. E. Hagstam, L. E. Larsson, and H. Thysell, "Experimental Studies on Charcoal Hemoperfusion in Phenobarbital Intoxication and Uremia, Including Histopathological Findings," Acta Med. Scand., 180, 593 (1966).

[23] J. D. Andrade, K. Kopp, R. Van Wagenen, C. Chen, and W. J. Kolff, "Activated Carbon and Blood Perfusion: A Critical Review," Proc. Eur. Dial. Transplant Assoc., 9, 290 (1972).

[24] J. P. Merrill, "Treatment of Drug Intoxication by Hemoperfusion," New Eng. J. Med., 284, 911 (1971).

[25] Basic Concepts of Adsorption on Activated Carbon (a brochure), Pittsburgh Activated Carbon Division of Calgon Corporation, subsidiary of Merck & Co., Inc., Calgon Center, Box 1346, Pittsburgh, Pennsylvania 15230.

[26] S. Brunauer, P. H. Emmett, and E. Teller, "Adsorption of Gases in Multimolecular Layers," J. Amer. Chem. Soc., 60, 309 (1938).

Note Added in Proof

Two recent international congresses have discussed activated carbon hemoperfusion in detail. The proceedings of those meetings should be consulted for further information:

C. Giordano, ed., "Uremia," in Kidney International, Supplement No. 3, February 1975.

R. Williams and I. M. Murray-Lyon, eds., Artificial Liver Support, Pittman, 1975.

One grade of activated carbon has been chosen for hemo-
perfusion studies on the basis of the above evaluations.
The nature of the microparticles and the approach used
to remove them from this carbon is described.

I. BACKGROUND

During the last decade granular activated carbon has been utilized
in a number of applications far removed from its intended commer-
cial uses. As a result, problems which would not normally be present
in conventional activated carbon applications may develop. Not only
do unexpected technical difficulties often arise as a result of using a
particular carbon, but problems associated with evaluation and
characterization of candidate carbons for a particular application
can develop. Sometimes these problems are not fully appreciated
or even worse are completely overlooked in picking a particular
kind of activated carbon for a unique specialty application. A case
in point is the use of activated carbon in the treatment of endogenous
and exogenous poisoning cases.

A technique of perfusing blood over granular activated carbon to
remove endogenous waste products and exogenous poisons has been
developed over the past decade. Yatzidis did the pioneering work in
applying charcoal hemoperfusion to the treatment of chronic renal
failure [1]. Yatzidis found that carbon could adsorb considerable
amounts of plasma creatinine, uric acid, indican, phenolic com-
pounds, guanidine bases, and organic acids. He reported that a
60-min hemoperfusion through several columns containing 200 g
of activated carbon had about the same efficiency as a conventional
hemodialysis of 4 to 6 hr duration [1]. Dunea and Kolff employed
a hemoperfusion system comparable to that used by Yatzidis [2].
The results of 18 preliminary clinical hemoperfusions showed
promising removals of serum creatinine and uric acid. There
were no significant changes in blood urea, serum phosphorus, or
serum electrolytes. They observed no pyrogenic reactions, although
Yatzidis had. They confirmed Yatzidis' findings in regard to signifi-
cant destruction of formed blood elements, particularly platelets.
Because of the limited adsorption capacity of carbon for urea, water,
and electrolytes, Dunea and Kolff concluded that "charcoal perfusion
may be a useful adjunct to hemodialysis since it can do well what
dialysis does poorly" [2].

During the last 5 years, extensive research on activated carbon
hemoperfusion has been conducted by several groups. The research

group headed by Dr. T. M. S. Chang in Montreal has done extensive
research and development work on clinical charcoal hemoperfusion.
Chang initiated the concept of "artificial cells" and the application
of microencapsulation technology to medical problems [3-5]. Chang
et al. [6, 7] followed Yatzidis' approach to charcoal hemoperfusion
in that they utilized activated carbon coated with a polymer mem-
brane (heparin-complexed collodion) and showed that this enhanced
the blood tolerability significantly over that of uncoated activated
carbon. Chang et al. were the first to apply hemoperfusion over
charcoal coated with adsorbed albumin collodion membranes to
treat a number of patients suffering from chronic uremia [8].
They have shown that the presence of the membrane not only
reduces damage to the formed blood elements, but also the
mechanical strength provided by the complete encapsulation of
the carbon granules significantly reduces fine particle generation
during hemoperfusion [8, 9]. The coating does not seem to sig-
nificantly compromise the adsorptive capacity of the activated
carbon. In fact, Chang's results with clinical hemoperfusions
seem to indicate that creatinine, uric acid, and guanidine can be
removed from uremic patients with efficiencies comparable to
or greater than conventional hemodialysis [9, 10]. In several
instances, charcoal hemoperfusion supplemented by conventional
coil hemodialysis has reduced the total dialysis time per week
and in some cases dramatically improved the general well being
of the patient [11].

Our initial objectives were to solve several problems which
were preventing the charcoal hemoperfusion concept from
being widely accepted as a safe, cheap, and efficient supplement
to conventional hemodialysis. A marked decrease in platelets
and white blood cells during hemoperfusion, decreased adsorption
capacity due to charcoal caking and packing, loss of red blood
cells in the charcoal column, excessively high anticoagulant
requirements, and pyrogenic reactions all offset the advantages
of low cost, simplicity, and potential high adsorption capacity
for many endogenous and exogenous poisons offered by activated
carbon.

During the last 2 years the previously mentioned problems
have been significantly alleviated or solved completely by coating
the carbon granules with polymeric materials that do not elicit
such a strongly adverse reaction when exposed to blood [12, 13].
Chang et al. have evaluated nylon, collodion, and heparin-complexed
collodion as microencapsulation materials [6]. The approach in our

labs has centered around hydrogel coatings, particularly poly-hydroxyethyl methacrylate (PHEMA) [12, 13] and glutaraldehyde cross-linked albumin [12]. Our results support the findings of other investigators. The use of PHEMA-coated charcoal prevents significant platelet destruction and blood coagulation which pre-viously resulted in carbon packing and caking during hemoperfusion over uncoated charcoal [8]. Also, both in vitro and in vivo adsorption studies utilizing creatinine and uric acid indicate that significant quantities of these solutes can be adsorbed on activated carbon. The presence of the hydrophilic coating may slow down the kinetics of solute removal, but very little total capacity is lost. In fact, coating the carbon actually seems to increase the in vivo adsorption capacity because the coated carbon does not pack and clump together, thus allowing more blood contact and more chance for solute adsorp-tion to occur [13]. Coating the carbon significantly decreases the incidence of microparticles detectable in vitro and histopathologically; however, it does not seem to completely eliminate the microparticle problem as shown by our in vitro studies [13].

Yatzidis was also the first to demonstrate that activated carbon could adsorb significant quantities of exogenous poisons such as the barbiturates, salicylates, and glutethimide in vitro [1, 14]. Prior to this, Yatzidis et al. reported on the successful treatment of two patients suffering from severe barbiturate poisoning [15] and followed this up with treatments of other patients suffering from high blood barbiturate levels. Based on in vitro single pass experiments and in vivo studies utilizing dogs, De Myttenaere et al. concluded that charcoal hemoperfusion is considerably more effective in removal of glutethimide (Doriden) and barbiturate (Veronal) than conventional hemodialysis [16, 17]. Rosenbaum et al. compared the efficacy of hemoperfusion over uncoated charcoal, cellulose-acetate-coated charcoal, and an anion exchange resin to twin-coil hemodialysis for the treatment of sodium pheno-barbital intoxicated dogs [18]. They found that both coated and uncoated carbon were significantly more effective in removing serum barbiturate than either conventional hemodialysis or anion exchange resin techniques. However, they advised against the human application of charcoal hemoperfusion because of the serious reduction in blood pressure, peripheral white blood cell count, blood platelet concentration, and the presence of charcoal emboli in the lung tissues of hemoperfused animals. Refer to Ref. 23 for a critique of these earlier studies.

Chang et al. have done a considerable amount of research on exogenous poison removal utilizing coated activated carbon. They have found that Nembutal (pentobarbital), salicylate, and glutethimide

can all be adsorbed readily on activated carbon [9]. Recently, Chang et al. have reported on the in vitro clearance efficiency of activated carbon for Methaqualone, Methyprylon, and glutethimide and the successful clinical application of charcoal hemoperfusion to remove these exogenous poisons [19, 20]. Work in our labs on adsorption of exogenous poisons by activated carbon confirms the work done by other investigators. It has been found from in vitro stirred batch studies on various commercially available activated carbons that all carbons evaluated are about equal in terms of salicylate and barbiturate adsorption [21]. We have also evaluated the in vivo adsorption of salicylate and barbiturate using coated and uncoated activated carbon.

During the last 2 years we have become aware of the fact that very few commercially available granular activated carbons have been evaluated in regard to use in hemoperfusion applications. Also, many investigators have made only limited mention of the kind of carbon used and how it was treated prior to hemoperfusion. This seems to be a classic example of how one field borrows the technology of another without realizing the limitations or even evaluating all the available options. The fact that uncoated carbon is quite traumatic to the formed elements in blood is one example of a material that first appeared very promising (high adsorption capacity for nitrogenous waste molecules or exogenous poisons) but without extensive modification (washing and encapsulation) proved to be quite bad. Another disadvantage associated with hemoperfusion concerns the presence of minute carbon particles that are attached weakly to the surface of the carbon. These "microparticles" or "fines" are probably generated during activation and shipping of the carbon, and for most industrial applications they are not a problem. However, for a specialty application such as hemoperfusion the fines are a major dis-advantage. If not removed from the surface of the carbon prior to use, it is likely that these microparticles would be carried into the patients body by his own blood during the hemoperfusion. Several investigators have shown that microemboli are a serious problem if the carbon is not adequately washed prior to use, and as a result have questioned the safety of hemoperfusion [18, 22-24]. The cur-rent literature has been critically reviewed in regards to charcoal hemoperfusion, carbon treatment, and the microemboli problem [23].

The work in this laboratory has centered on evaluation of many of the available brands of granular and pelletized activated carbons produced in the United States which could conceivably be used in hemoperfusion. The following characteristics have been evaluated: 1) initial cleanliness, i.e., the amount of microparticles initially

present on the surface; 2) ability to be cleaned, i.e., can the micro-particles be removed completely from the surface of the carbon?; 3) resistance to attrition, i.e., will the carbon resist fragmentation during hemoperfusion?; 4) in vitro adsorption capacity for creatinine; 5) the nature of the carbon particle surface topography; 6) the nature of the carbon emboli in regard to size distribution and geometry; and 7) the optimum cleaning procedure necessary to give a sufficiently clean carbon surface.

II. MATERIAL: ACTIVATED CARBON

Active carbon is a porous material prepared by carbonizing and activating substances of biological origin. The commercial value of an activated carbon depends upon its adsorptive capacity for the particular solutes of interest. Adsorptive capacity in turn is a function of the total surface area and pore structure resulting from the activation of the carbon. Activated carbons usually have surface areas in the range to 500 to 1400 m^2/g.

The production of activated carbon begins with pyrolysis of biological material (wood, coal, peat, shells, petroleum, etc.) in the absence of air or chemical agents. The result of this treatment is a carbonized material with a specific surface area of several square meters per gram. Activation of this carbonized product gives a sorbent with high porosity and a correspondingly high surface area. During carbonization, most of the noncarbon elements are removed in gaseous form, leaving behind irregularly shaped crystallites separated by interstices filled or blocked by tarry substances (amorphous carbon). There is very little pore structure and consequently negligible surface area. Activation by exposure to high-temperature steam or carbon dioxide not only burns out the disorganized amorphous carbon opening up the clogged pores between the crystallites, but also burns out some of the carbon comprising the crystallites as well. Active carbon can also be produced in a one-step process by adding substances (zinc chloride) which prevent the formation of tars during the course of pyrolysis. The net result of either physical or chemical activation is active carbon with a submicroscopic structure of complex, interconnected, irregularly shaped passages of molecular dimensions.

Various grades of activated carbon have been utilized by industry for many years to decolorize and purify gases and organic liquids. The purification process is one of adsorption of solute or gas molecules on the surface of the carbon. The extremely high

adsorption capacity of activated carbon is a result of the large surface area created by the extensive porosity in the carbon substructure. Macropores (channels greater than 1000 Å in diameter) originate at the surface of the carbon particle and penetrate into the interior. The micropores (10 to 1000 Å in diameter) branch off from the macropores; it is these pores which provide the large area necessary for significant solute adsorption. Figure 1 illustrates the micropore structure and the concept of solute competition for available adsorption area. Since the micropores are of molecular

Scale 40A

To Macropore

Micropore

Area available to both adsorbates and solvent

Area available only to solvent and smaller adsorbate
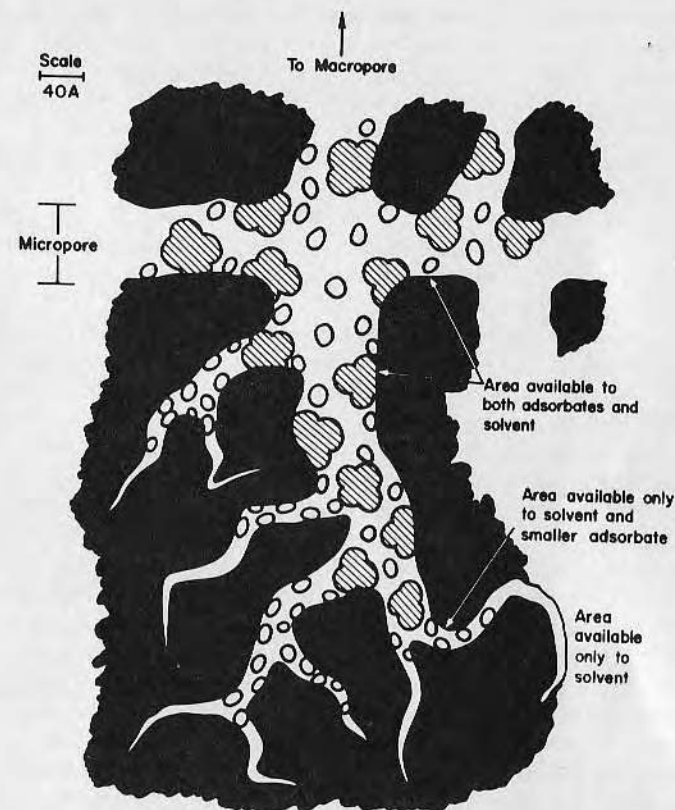
Area available only to solvent

FIG. 1. The microporous structure of activated carbons. Two species of solute molecules are competing for available adsorption surface. The physical size and shape of the larger solute molecule prevents it from gaining access to many micropores. (Redrawn after Ref. 25.)

dimensions, the physical size and shape of the solute molecules will be a factor in determining whether or not they can gain access to the micropores. If more than one species of solute molecule exists, there will be a competition for the available surface area to which these solute molecules have access.

The highly porous structure of the activated carbon particle produces a delicate framework with a much lower mechanical strength than the parent carbonized material. Movement and the resulting mechanical abrasion of the carbon particles against one another results in particle fracture and generation of microparticles.

Table 1 is a summary of the available data concerning the physical properties of the commercial carbons evaluated in our labs. The particle size of the carbon granules refers to the sizes of two screens, either in the U.S. Standard Sieve Series or the Tyler Standard Sieve Series between which the bulk of the carbon sample falls. The relationship between these two sieve standards is shown in Table 2.

Ash refers to the mineral oxide constituents of activated carbon. It is normally quantitated on a weight percent basis after a given amount of sample is reduced to ash. From Table 1 one can see that the petroleum-based activated carbons have the lowest amount of ash.

There are a number of techniques developed by various carbon producers to evaluate the abrasion resistance or hardness of their product. Witco Chemical Corporation uses an NBS abrasion number test. This test measures the percentage reduction in the average particle size resulting from the rotation of a T-bar stirrer in a cylindrical vessel containing a specified amount of carbon. Abrasion numbers and hardness numbers are often quoted by carbon manufacturers. These values are determined by contacting the carbon samples with steel balls in a pan attached to an oscillating machine. The abrasion number is the ratio of the final mean particle diameter to the original mean particle diameter (determined by screen analysis × 100). The hardness number is calculated from the weight of granular carbon retained on a particular sieve after the carbon has been in contact with steel balls as previously described. American Norit Company quantitates its carbon hardness with a test utilizing a cylindrical steel bar rotating inside a steel mesh cylinder. The hardness is expressed as an attrition factor which is the weight of fines produced (dust and fractured carbon) divided by the original weight of carbon and the total test time.

The adsorption characteristics of activated carbon are expressed in a number of standard ways. For instance, the Iodine Number is the number of milligrams of iodine adsorbed by 1 g of carbon at an equilibrium concentration of 0.02 N iodine. The Iodine Number can be correlated with the carbon's ability to adsorb low molecular weight substances. The carbon tetrachloride activity is the steady-state percentage increase in weight of a bed of activated carbon after air saturated with carbon tetrachloride at 0°C is passed through it at 25°C. The Molasses Value (MV) is determined by optical density measurements of a molasses residual filtrate after carbon treatment and subsequently a standard carbon and molasses are used as a base for comparison of adsorbabilities. The Molasses Decolorizing Index (MDI) follows the same lines as MV determinations. The MDI can be correlated with the carbon's ability to adsorb high molecular weight molecules.

Surface area is expressed in square meters per gram of carbon and is usually determined from the nitrogen adsorption isotherm by the Brunauer, Emmett, and Teller (B.E.T.) method [26]. Directly associated with surface area are the pores which produce it. The porosity of an activated carbon is usually quantitated in terms of total pore volume (the volume of all macro- and micropores per unit weight of carbon) and the pore size distribution which is usually expressed on a graph as cumulative pore volume as a function of pore diameter or radius. The derivative of this distribution gives the volume of pores in various size ranges. The micropore distribution can be used to predict the adsorptive capacity of the carbon for molecules of various molecular weights.

ASTM standard procedures are available which describe the following carbon characterizations: apparent density of activated carbon (D 2854-70), particle size distribution of granular activated carbon (D 2862-70), total ash content of activated carbon (D 2866-70), moisture in activated carbon (D 2867-70), and liquid phase evaluation of activated carbon (D 2355-70). At present it would seem that there are no standard tests for establishing the attrition resistance, microparticle content, and cleanability of activated carbons. Even in terms of solute adsorption, each manufacturer seems to have a different approach to quantifying the adsorption capacity of active carbon. Our approach has been to design evaluation procedures where none currently exist and to utilize currently published standard tests (D 2355-70) or modifications of those tests when necessary.

TABLE 1. Physical Characteristics and Specifications of Commercially Available (USA) Granular and Pelletized Activated Carbons Evaluated to Date[a]

Carbon brand and grade[b]	Particle (mesh) size	Raw material	Maximum % ash	Hardness index	Bulk density (g/cc)	Adsorption index	Surface area (m²/g) N₂ B.E.T. Method	Pore size distribution	Cumulative pore volume (cc/g)
Witco 517	12-30 (U.S.)	Petroleum	0.3	NBS abrasion no. 4	0.49	c	1200	~62% of pore volume in 3 to 40 Å range	0.60
Witco 256	4-10 (Tyler)	Petroleum	0.3	NBS abrasion no. 5	0.45	c	1250	c	0.54
Witco 337	12-30 (U.S.)	Petroleum	0.4	NBS abrasion no. 6	0.43	c	1420	c	0.59
Witco 125	12-30 (U.S.)	Petroleum	0.3	NBS abrasion no. 4	0.49	c	1200	c	0.47
Columbia LCK	12-28 (Tyler)	Petroleum	0.5	Abrasion no. 84	0.46	CCl₄ activity 64%	~1300	Similar to Columbia JXC	Similar to Columbia JXC
Columbia JXC	4-10 (Tyler)	Petroleum	2.0	Abrasion no. 95	0.48	CCl₄ activity 60%	~1300	~54% of pore volume in 10 to 40 Å range	0.83
Columbia MBV	4-6 (Tyler)	Coal base	12.0	Abrasion no. 95	0.43	CCl₄ activity 60%	~1100	Fewer pores in the 100 Å range than JXC	c
Pittsburgh SGL	8-30 (U.S.)	Bituminous coal	8.0	Abrasion no. 70	0.48	Iodine no. 900	950-1050	~42% of pore volume in 10 to 40 Å range	0.85
Pittsburgh CAL	12-40 (U.S.)	Bituminous coal	8.5	Abrasion no. 75	0.44	Iodine no. 1000	1000-1100	~48% of pore volume in 10 to 40 Å range	0.94

TABLE 1 (continued)

Carbon brand and grade[b]	Particle (mesh) size	Raw material	Maximum % ash	Hardness index	Bulk density (g/cc)	Adsorption index	Surface area (m^2/g) N_2 B.E.T. Method	Pore size distribution	Cumulative pore volume (cc/g)
Pittsburgh PCB	6-16 (U.S.)	Coconut shells	6.0	Abrasion no. 92	0.44	Iodine no. 1200, CCl_4 activity 60%	1150-1250	~92% of total surface area in 10 to 40 Å pore	0.72
Fisher activated coconut charcoal	6-14 (Tyler)	Coconut shells	10.0	Abrasion no. 95	~0.45	c	1150	Average pore diameter 22 Å	0.62
Darco granular	12-20 (U.S.)	Lignite	Water solubles 1%	c	0.39	c	700	Mean pore radius 29 Å	1.00
Darco LIPT	12-20 (U.S.)	Lignite	Extra low soluble iron and sulfur	c	0.39	c	700	Mean pore radius 29 Å	1.00
Norit granular	8-20 (U.S.)	Wood, peat charcoal, etc.	5-10	Attrition factor 5-1: mg/g/min	0.26-0.30	c	665	~45% of pore volume in 10 to 40 Å range	0.9-1.1
Norit pelletized				Attrition factor, mg/g/min				% of pore volume in 10 to 40 Å range:	
RB I	16-20 (U.S.)	Wood waste products and peat	5-10	0.1-2.0	0.42-0.45	c	900-1000	16	0.95
RB II	8-12 (U.S.)		5-10	0.1-2.0	0.42-0.45	c	900-1000	16	0.95
RB III	6-8 (U.S.)		5-10	0.1-2.0	0.42-0.45	c	900-1000	16	0.95
RB IV	4-6 (U.S.)		5-10	0.1-2.0	0.42-0.45	c	900-1000	16	0.95

(continued)

TABLE 1 (continued)

Carbon brand and grade[b]	Particle (mesh) size	Raw material	Maximum % ash	Hardness index	Bulk density (g/cc)	Adsorption index	Surface area (m^2/g) N_2 B.E.T. Method	Pore size distribution	Cumulative pore volume (cc/g)
Nuchar WV-L	8-30 (U.S.)	Bituminous coal	7.5	Abrasion no. 70	0.48	Minimum iodine no. 950	1000	~29% of pore volume in 10 to 40 Å range	0.58 in 10 to 10^3 Å range
Nuchar WV-G	12-40 (U.S.)	Bituminous coal	8.5	Abrasion no. 75	0.44	Minimum iodine no. 1050	1100	~34% of pore volume in 10 to 40 Å range	0.68 in 10 to 10^3 Å range
Nuchar WV-W	8-30 (U.S.)	Bituminous coal	7.0	Abrasion no. 70	0.57	Minimum iodine no. 850	850	~21% of pore volume in 10 to 40 Å range	0.38 in 10 to 10^3 Å range
Nuchar WV-H	12-30 (U.S.)	Bituminous coal	8.0	Hardness no. 90	0.48	Minimum iodine no. 1100	1000	~38% of pore volume in 10 to 40 Å range	0.53 in 10 to 10^3 Å range
Barnebey Cheney PC	12-30 (Tyler)	Nut shells	10.0	>90% by Ball Abrasion Test	0.46-0.51	c	c	c	c
Barnebey Cheney PA	12-30 (Tyler)	Nut shells	7.0	>90% by Ball Abrasion Test	0.54-0.60	c	c	c	c
Barnebey Cheney FP	12-30 (Tyler)	Mineral carbon	c	>85% by Ball Abrasion Test	0.58-0.65	c	c	c	c
Barnebey Chaney PL	12-30 (Tyler)	Nut shells	5.0	>85% by Ball Abrasion Test	0.37-0.41	CCl$_4$ activity 70% min	c	c	c
Barnebey Cheney PK	12-30 (Tyler)	Pecan shells	5.0	>90% by Ball Abrasion Test	0.47-0.52	c	c	c	c

[a]The carbons and data reported here were obtained from 1970 to
[b]See Acknowledgments.
[c]The information either not readily available or else proprietary

TABLE 2. The Relationship between Standard Mesh Sizes and Particle Dimensions

Standard mesh		Opening	
Tyler	U.S.	mm	Inches
4	4	4.70	0.185
6	6	3.33	0.131
8	8	2.39	0.094
10	12	1.65	0.065
12	14	1.42	0.056
14	16	1.19	0.047
16	18	0.99	0.039
20	20	0.84	0.033
24	25	0.71	0.028
28	30	0.58	0.023
32	35	0.51	0.020
35	40	0.41	0.016
42	45	0.36	0.014
48	50	0.30	0.012
60	60	0.25	0.010
80	80	0.17	0.007
100	100	0.15	0.006
150	140	0.10	0.004
200	200	0.07	0.003
250	230	0.06	0.002
325	325	0.04	0.002
400	400	0.03	0.001

III.   CARBON EVALUATION PROCEDURES

At this time the most important parameters concerning the use of activated carbon for hemoperfusion are adsorption capacity for the solutes of interest and the ease of removal of the previously mentioned microparticles which could become emboli when in contact with blood. When one evaluates the "cleanability" of carbon, it should be understood that this depends on the number of microparticles present on the surface as well as on the ease of their removal. The first evaluation made was concerned with how many particles exist on the various brands of activated carbon, i.e., how "dirty" is the carbon as received from the manufacturer? This was the subject of the initial cleanliness test. A second factor associated with the fine carbon particle problem is removing these potential emboli before the carbon is used in an in vivo experiment. Most investigators report washing the carbon to be used in a series of steps employing running water which thoroughly agitates the carbon and carries away many of the microparticles. This procedure has been used in our laboratory to clean the carbons but with some modifications. The second evaluation performed was concerned with how well the various kinds of carbon could be cleaned by washing and was termed the washability study. All carbons were evaluated in this manner to see if some brands of activated carbon could be washed cleaner than others. The microparticles were removed from the washing solution by filtering, and the qualitative macroscopic and microscopic appearance of these filters was used to determine washability effectiveness.

During the first year of in vivo studies, a fluidized bed was utilized so that the carbon particles agitated freely and at times quite vigorously; carbon particle collisions occurred, resulting in particle fragmentation and creation of particles small enough to escape the restraining screens and be carried in the blood stream as emboli. An attrition test was designed with the goal of measuring the relative attrition strengths of various granular activated carbons. The current effort in our kidney development puts emphasis on a nonfluidized bed of carbon particles. There have been two principal reasons for this. First, the pressure drop across a nonfluidized column is lower than that of a fluidized bed. Second, particle agitation will be almost nil in a nonfluidized bed. This minimizes collisions and possibly fragmentation of the carbon. As a result,

the attrition studies were dropped in favor of other evaluations which would tell us more about the nature and quantity of carbon microparticles which already existed on the carbon surface. The attrition data obtained thus far is included in this report.

In vitro stirred batch solute depletion studies have been used as a means of comparing the relative adsorption capacities of the various granular and pelletized carbons evaluated. The solutes of interest were primarily creatinine, uric acid, salicylates, and barbiturates. Creatinine was chosen as the solute of primary interest with which a comparison between various carbons could be made.

The characterization of the carbon particle surface geometry and the nature of the microparticles on the carbon surface was accomplished using the scanning electron microscope (SEM). The object was to compare the carbon particle surface topography and microparticle content with the previously mentioned tests. The course of the optimal washing procedure and subsequent removal of the microparticles was also followed with SEM.

A. Initial Cleanliness

Twenty grams of the carbon to be evaluated were weighed out in a clean 250 ml polypropylene beaker. One hundred milliliters of phosphate buffered saline (PBS), pH 7.4, were added to the beaker to form a carbon-water slurry. The beaker containing the carbon and PBS was aspirated at room temperature for 30 min. The presence of the ions in the PBS solution may neutralize the static surface charge which exists on the carbon. This static charge seems to enhance the adherence of the microparticles onto the surface of the activated carbon. The aspiration pulled a great deal of the adsorbed and trapped gases from the pores of the carbon particles. As the gas came out in bubble form, it pushed ahead of it many of the carbon microparticles which were lodged in the macropores.

After aspiration the carbon was gently agitated in the polypropylene beaker for 10 sec to get as many microparticles into solution as possible. After another 10 sec the PBS solution containing the microemboli was poured through a 50-mesh stainless steel screen into a clean 100 ml glass beaker. The large granular carbon sample remained behind and was discarded. A 50-ml sample of the solution was taken with a clean syringe and forced through a preweighed Millipore filter (0.22 μm). The filter was then removed from the filter housing and allowed to air dry in a dust-free

environment for 48 hr. It was then reweighed and the weight increase in milligrams over a control was recorded for the particular brand of carbon being tested. Each grade of carbon was evaluated three times.

B. Washability

Twenty grams of the carbon to be tested were weighed out in 250 ml capacity polypropylene beakers. One hundred milliliters of PBS were added to the carbon in the beaker. The carbon-water slurry was aspirated at 24°C for 1 hr. Again, the purpose was to remove as many microparticles from the surface of the carbon as possible. After aspiration the PBS solution containing many microparticles was poured off, leaving the granular carbon behind in the beaker. One hundred milliliters of distilled water were then added to the carbon and the carbon-water slurry was agitated for 30 sec to suspend as many remaining microparticles as possible in the fluid. The distilled water containing microparticles was then poured through a 50-mesh stainless steel screen into a clean 250 ml glass beaker. A 20-ml sample of this wash solution was taken via a clean plastic syringe after thorough mixing and forced through a preweighed Millipore filter (pore size, 0.22 μm). The initial sample represents the fines content present at the beginning of a dynamic wash with tap water.

The carbon sample was then placed in a washing cylinder where it was restrained by 50 mesh stainless steel screens at both inflow and outflow ends. Tap water flowed via a roller pump through the cylinder at 400 ml/min and vigorously agitated the carbon particles. This washing continued for 90 min. At 30 min intervals the wash water flow was shut off and 100 ml of the wash water present in the cylinder at that time was allowed to drain into a clean glass beaker. A 20-ml sample of the wash water was taken via a clean syringe and forced through another preweighed Millipore filter. The flow was reestablished through the wash cylinder for another 30 min. Second and third samples were taken in the same way. At the conclusion of the test the four filters were air dried in a dust-free environment for 24 hr and reweighed. They were photographed macroscopically and microscopically. A qualitative comparison was then made between the initial amount of microparticles on the first filter and the presence of microparticles on the subsequent filters obtained during water washing. Originally, we had hoped to quantitate the progressive decrease in the number of emboli washed from the carbon by weighing the filters. However,

this was not feasible for all the carbons because of the exceedingly small filter weight increases (less than 10 μg) in the latter washing stages (60 and 90 min samples).

C. Attrition Resistance

The carbon to be tested was removed from its bulk container and sieved to 12 × 24 Tyler mesh in approximately 50 g quantities. When about 250 g of sized carbon was processed, it was spread thinly over a sheet of absorbent paper and allowed to equilibrate with the water vapor in the atmosphere for 24 hr. At the end of this time, 20 g quantities of the carbon were weighed out and placed in the attrition test apparatus shown in Fig. 2. Air from a compressed air source was admitted to the chamber at an inflow pressure of 20 psi and a flow rate of 30 liter/min. The flow rate remained constant for 20 min and was sufficiently strong to project all the carbon particles against the upper stainless steel restraining screen several times a minute. The force of the repeated impacts fragmented some particles. The degree of fragmentation was a function of the particular brand and grade of carbon being tested; all other factors were held constant.

After a 20-min exposure to the air flow, the carbon was removed from the test cartridge and resized to 12 × 24 Tyler mesh. The particles which had fragmented were reduced enough in size to fall through the screen and were discarded. The carbon which remained was placed on absorbent paper and allowed to reequilibrate with the atmosphere for 24 hr. After equilibration the carbon was reweighed and the loss in weight recorded as the percent reduction due to particle fragmentation. This procedure was repeated for four to ten samples of each particular carbon tested.

D. In vitro Adsorption of Creatinine

The carbon to be tested for creatinine adsorption capacity was dried thoroughly by aspiration in a vacuum oven at 40°C for 30 min. Five grams of this carbon were placed in a glass beaker containing 50 ml of PBS solution (pH 7.4). This solution was aspirated for 15 min at room temperature. Following this the PBS solution was poured off and discarded. The carbon in the glass beaker was placed in a water bath at 37°C and an automatic stirrer with a Teflon tip was inserted. One milliliter of radiolabeled creatinine (1 μCi) was diluted in 200 ml of PBS solution to give a creatinine
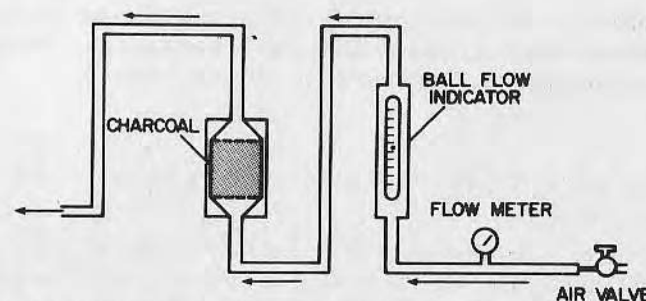
FIG. 2. Apparatus for determining the attrition resistance of granular activated carbon.

concentration in PBS of 100 mg% initially. This solution with isotope was added to the carbon in the beaker at 37°C with stirring. One milliliter samples were taken at 15 and 30 sec and 1, 2, 5, 30, and 60 min.

Ten milliliters of Aquasol (New England Nuclear Corp.) counting solution were added to each sample. The samples were then counted (±1% at a 95% confidence level) in a liquid scintillation counter to determine the activity of each sample. From that data the creatinine concentration in solution could be determined. The result was a curve of creatinine solution concentration versus time for each particular brand and grade of carbon evaluated.

E. Carbon Particle Surface Morphology

Carbon samples were gently poured out of the bulk container onto an aluminum specimen stub previously coated with a thin layer of silver print paint. In this way the carbon particles were not handled or subjected to any more structural trauma than necessary. After drying, the silver print paint served the dual purpose of enhancing electron conductivity and mechanically securing the particles to the specimen stub. The stubs containing the granular and pelletized carbon samples were then coated with a layer of gold (<100 Å thick) in a vapor deposition apparatus. The specimens were observed in a Cambridge Stereoscan SEM at low magnification (~100×) to show total particle geometry and at a higher magnification (~1000×) to show surface morphology (macropores, microparticles, cracks, etc.).

SEM observations on carbon particles subjected to the current washing procedure were carried out in exactly the same manner

with one addition to the procedure; all carbon was thoroughly dried overnight before mounting, and again it was transferred as carefully as possible to prevent any fragmentation and generation of microparticles.

F. Characterization of Carbon Microparticles

Microparticles from granular Witco 517 carbon were collected by adding 100 ml of PBS solution to 20 g of bulk carbon, followed by aspiration at room temperature for 30 min. The PBS solution was poured off and replaced by 100 ml of distilled water. The carbon-water slurry was agitated so that larger quantities of microparticles were suspended in solution and this was poured into a clean glass beaker. Twenty milliliters of the solution were forced through a 0.22-μm Millipore filter (25 mm diameter), leaving the microparticles behind on the filter. The filter was allowed to air dry in a dust-free environment for 24 hr. A portion of this filter was then mounted on an aluminum specimen stub, coated with vapor deposited gold, and observed in the SEM at a magnification of 1000×. Four pictures were taken of random areas on the filter surface. The microparticles were measured along their longest dimension and the number of particles in various size ranges from 0.5 μm on up was determined.

IV. RESULTS OF CARBON EVALUATIONS

A. Initial Cleanliness

The initial cleanliness data are shown in Table 3. The carbons are listed in order of increasing microparticle content on the filter. The average filter weight increase in milligrams indicated that there was quite a wide spread in initial microparticle content. Several of the Witco grades, particularly 517 and 256, seemed especially clean. In contrast, grades of Darco, Pittsburgh (Grades CAL and SGL) and Barnebey Cheney (Grades PA and PC) tend to be the dirtiest in regard to initial microparticle content. The pelletized Columbia carbons (LCK, MBV, and JXC) all seemed promising in terms of initial cleanliness. Norit pelletized carbon RBI, Norit Granular carbon, Witco 337 and 125, and Barnebey Cheney FP and PK were all fairly clean. Most of the Nuchar grades of carbon as well as Fisher Coconut carbon were moderately dirty. This data correlated fairly well with other published data which was more qualitative in

TABLE 3. Results of Test for Initial Carbon Cleanliness

Carbon brand and grade	Mesh size range	Average filter weight increase (mg) ±1 standard deviation
Witco 517	12-30	1.9 ± 0.5
Witco 256	4-10	3.3 ± 0.7
Columbia JXC	4-10	3.3 ± 0.3
Columbia LCK	12-28	3.7 ± 1.3
Barnebey Cheney FP	12-30	3.8 ± 0.6
Norit RBI	16-20	4.8 ± 1.5
Columbia MBV	4-10	4.9 ± 0.1
Norit Granular	8-20	5.2 ± 0.0
Barnebey Cheney PK	12-30	5.5 ± 0.2
Witco 337	12-30	5.8 ± 3.8
Witco 125	12-30	6.0 ± 1.6
Nuchar WV-W	8-30	9.3 ± 3.0
Nuchar WV-L	8-30	9.4 ± 2.8
Norit RB II	8-12	9.9 ± 5.9
Barnebey Cheney PL	12-30	10.2 ± 0.8
Norit RB III	6-8	10.3 ± 6.2
Pittsburgh PCB	6-16	11.2 ± 0.7
Nuchar WV-G	12-40	12.0 ± 0.1
Fisher Coconut	6-14	12.3 ± 1.9
Darco LIPT	12-20	12.9 ± 0.7
Barnebey Cheney PA	12-30	14.7 ± 1.3
Pittsburgh SGL	8-30	15.3 ± 3.0
Nuchar WV-H	12-30	15.4 ± 0.5
Norit RB IV	4-6	16.0 ± 0.0
Barnebey Cheney PC	12-30	20.0 ± 1.1
Pittsburgh CAL	12-40	23.2 ± 4.2
Darco Granular	12-20	31.1 ± 4.6

nature [13]. It can now be stated definitively that Witco carbons, particularly grades 517 and 256, and Columbia LCK and JXC tend to be the cleanest whereas carbons such as Pittsburgh and Darco are the dirtiest in the "as received" condition. Most of the other carbons, such as Norit, Nuchar, Fisher, and Barnebey Cheney, are intermediate in cleanliness.

B.   Washability

The results of the washability sequences for 12 representative grades of carbon are shown in Figs. 3 and 4. These particular carbons were picked because they represented the two extremes of carbon washing efficacy. For instance, Witco carbon 517 (refer to Fig. 3) was one of the cleanest carbons in terms of the initial sample and it also washed quite clean over a period of 90 min. On the other hand, Darco LIPT was extremely dirty initially, and in the 90-min wash sample there were still many emboli evident. The washing sequences not shown were intermediate between these two samples.

Pittsburgh SGL was initially one of the dirtiest carbons evaluated. The sequential washing samples were unusual in respect to the extremely large size of some of the microparticles. It is possible that these are microparticle aggregates. Barnebey Cheney PL was also quite dirty initially, but water washing seemed to be successful in removing a large number of the fines. Barnebey Cheney PC was not as dirty as PL, but water washing after 30 min was not successful in removing any more microparticles. This is a good example of how water washing can clean some carbons which are quite dirty initially but for other carbon grades washing rapidly loses its effectiveness. The reason for this may be that some carbons are relatively more attrition-resistant than others. Water washing a strong carbon cleans it by carrying away the microparticles. Collisions between carbon granules are not sufficient to produce more microparticles. On the other hand, washing a weaker carbon under the same conditions may be sufficient to produce a sizable number of microparticles from collisions. A point of diminishing returns is reached and the carbon does not get any cleaner. Carbons differ from grade to grade in terms of their ability to be cleaned.

Norit pelletized RB III was also quite dirty initially and continued water washing did not effectively remove any extraneous particulates after 30 min. Two kinds of particulate contaminants have been found to be associated with the pelletized Norit carbons.

In addition to the regular carbon microparticles, there are also large numbers of slender transparent fibers several hundred micrometers in length. The composition and source of these fibers remains unknown. It is possible that they are polymeric binding fibers used to hold the pelletized particle together.

From Fig. 4 it can be seen that the initial samples of Nuchar WV-L, Fisher Coconut, granular Norit, and Pittsburgh PCB were all extremely dirty. Water washing for 60 min was quite effective in cleaning these carbons, but continued washing after this produced only minimal improvement at best. Columbia LCK, Witco 256, and Witco 337 (not shown) were all relatively clean in terms of the initial sample. Water washing for 30 min was sufficient to remove the greatest part of the microparticles, and after 90 min of washing there were no microparticles visible on the filters corresponding to Columbia LCK and Witco 256.

Some of the washing sequences for various carbons not shown here were quite promising. For instance, Barnebey Cheney FP was quite clean initially and a 30-min water wash was sufficient to clean the carbon to a point of diminishing returns. The pelletized carbons Norit RB IV and Columbia JXC and MBV washed completely clean in 60 to 90 min. Witco 337 granular carbon was one of the cleanest carbons evaluated in the initial state, and the filter sequence indicated that it could be washed cleaner than most carbons evaluated in only 30 min.

C.   Attrition Resistance

The attrition test data are shown in Table 4. The average weight loss due to particle fragmentation is a measure of the resistance to fracture for each of the seven carbons evaluated. A small weight loss like that exhibited for Witco 517, Columbia LCK, Witco 337, and Witco 125 implies that these carbons are more resistant to fragmentation during perfusion than is granular Darco carbon which had the highest weight loss of those carbons tested. There seems to be a correlation between the initial cleanliness test and the attrition test in that Witco 517 and Columbia LCK were the cleanest carbons as received and these same two carbons have been found to be the most resistant to attrition. On the other hand, granular Darco was the dirtiest carbon found in the initial cleanliness test and it was also the carbon most susceptible to fragmentation. Witco 337 and Witco 125 were comparable in resistance to attrition, and they seem to be comparable in terms of initial microparticle content (see Table 3). Pittsburgh SGL and granular Norit carbons
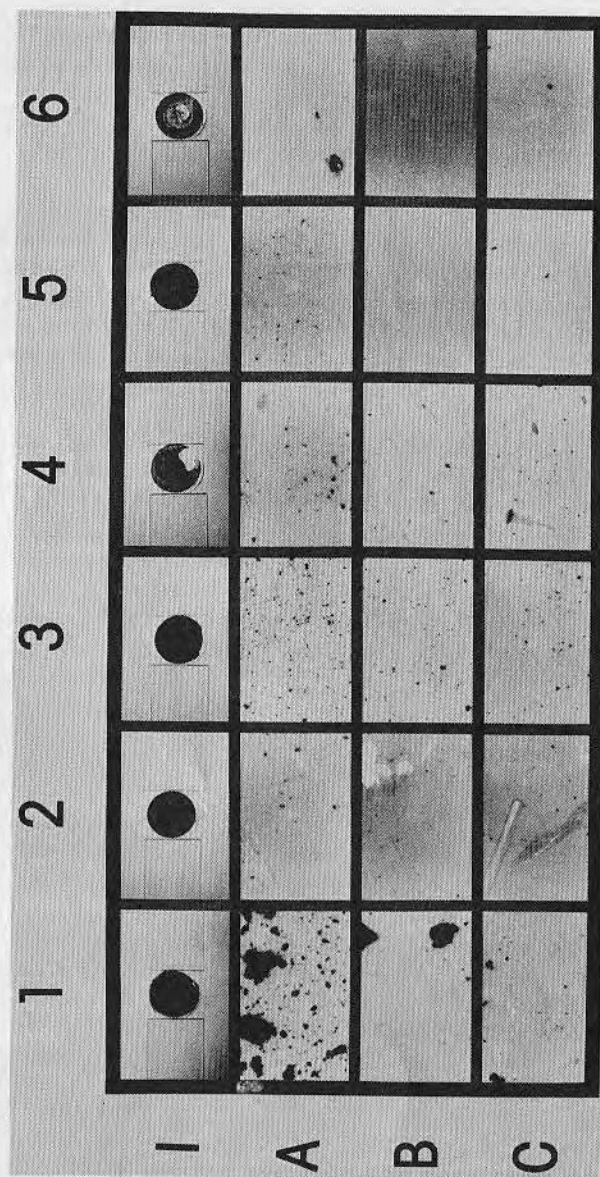
FIG. 3. Washing sequences for activated carbons. Numbers represent the following: (1) Pittsburgh SGL, (2) Norit RB III, (3) Darco LIPT, (4) Barnebey Cheney PC, (5) Barnebey Cheney PL, and (6) Witco 517. The letters signify the following washing stages: (I) Initial wash sample; (A), (B), and (C) are 30, 60, and 90 min samples, respectively.
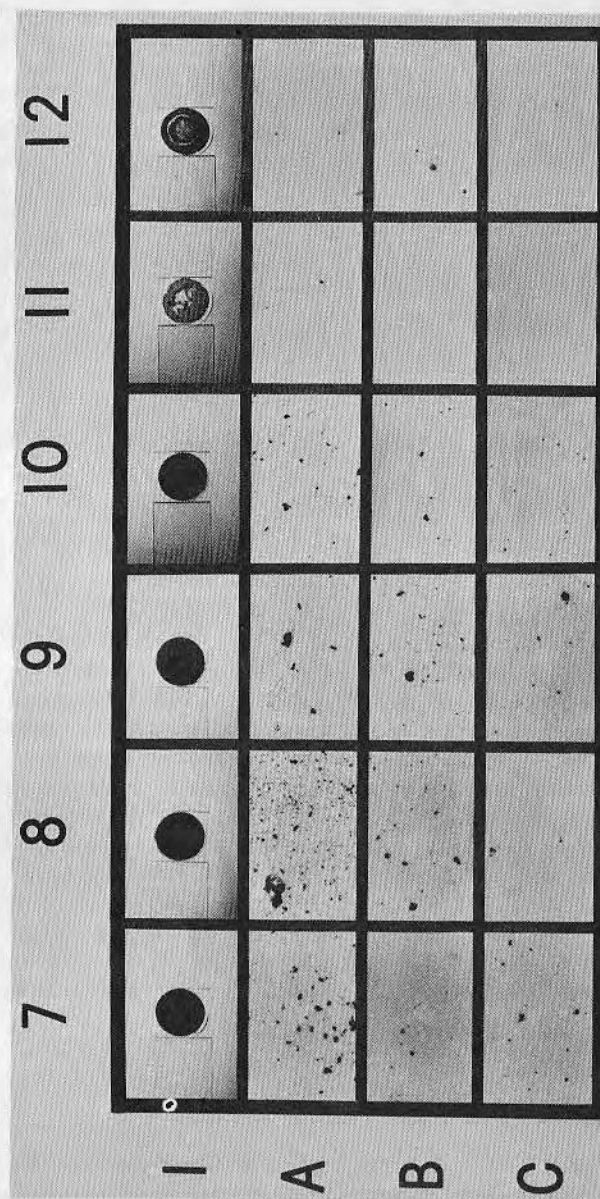
FIG. 4. Washing sequences for activated carbons. Numbers represent the following: (7) Nuchar WV-L, (8) Fisher Coconut, (9) Norit Granular, (10) Pittsburgh PCB, (11) Columbia LCK, and (12) Witco 256. The letters signify the following washing stages: (I) Initial wash sample; (A), (B), and (C) are 30, 60, and 90 min samples, respectively.

TABLE 4. Attrition Test Data

Carbon brand and grade	Mesh size (Tyler)	Average weight loss (g) ± 1 standard deviation	Average weight loss (%)	No. of trials
Witco 517	12 × 24	2.52 ± 0.31	12.6	10
Columbia LCK	12 × 24	3.14 ± 0.21	15.7	9
Witco 337	12 × 24	3.53 ± 0.21	17.6	9
Witco 125	12 × 24	3.97 ± 0.44	19.8	9
Pittsburgh SGL	12 × 24	4.55 ± 0.79	22.7	7
Norit	12 × 20	7.42 ± 0.37	37.1	7
Darco	12 × 24	11.92 ± 0.21	59.6	4

were intermediate in attrition resistance. It is possible that this correlation between attrition resistance and initial microparticle content exists because of brand and grade variations in resistance to fragmentation during processing, packaging, and shipping.

One reason for only evaluating seven carbons was related to the standard test size of 12-24 Tyler mesh. Many of the pelletized and large granular carbons did not fit in this size range and could not be evaluated. This applies primarily to the Norit RB series, Columbia JXC and MBV, and Fisher 6-14.

There is now available a National Bureau of Standards analytical test for determining the abrasion resistance of granular carbons. Information concerning this test can be obtained from Atlas Chemical Industries, Inc.

D. In vitro Creatinine Adsorption

Figures 5 through 9 show solution depletion of creatinine as a function of time for the various grades of activated carbons evaluated. From these figures it can be seen that the best carbons for creatinine adsorption were Witco 517, Columbia LCK, Pittsburgh SGL, Witco 337, Nuchar WV-G, Pittsburgh carbons PCB and CAL, and Barnebey Cheney PL. The carbons with the poorest adsorption capacity for
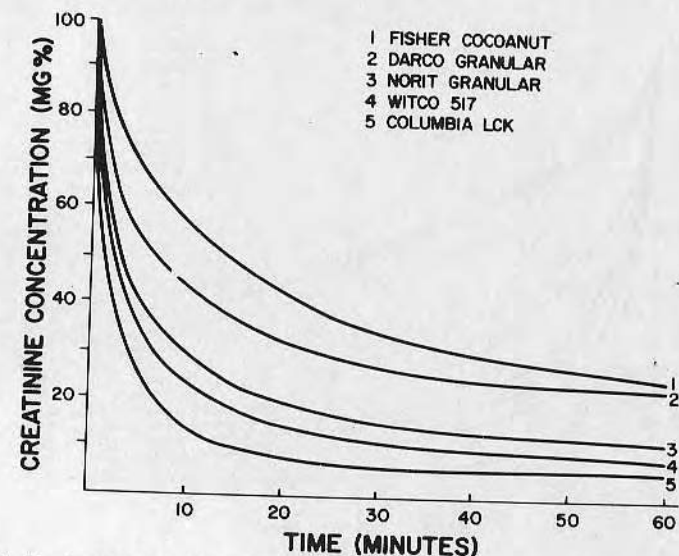
FIG. 5. Radiolabeled creatinine solute depletion from aqueous solution by various grades of granular activated carbon as a function of time.
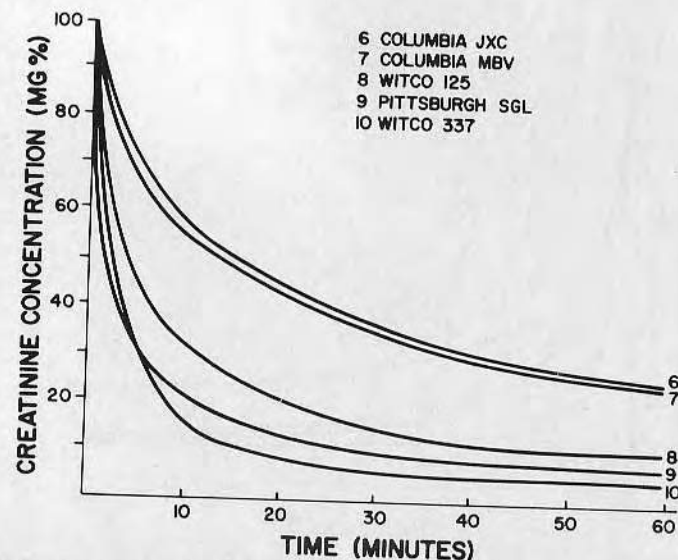

FIG. 6. Radiolabeled creatinine solute depletion from aqueous solution by various grades of granular and pelletized activated carbon as a function of time.
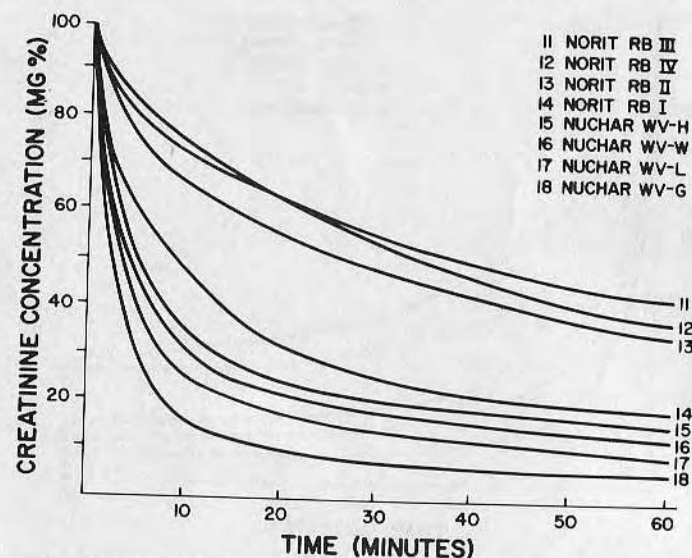
FIG. 7. Radiolabeled creatinine solute depletion from aqueous solution by various grades of granular and pelletized activated carbon as a function of time.
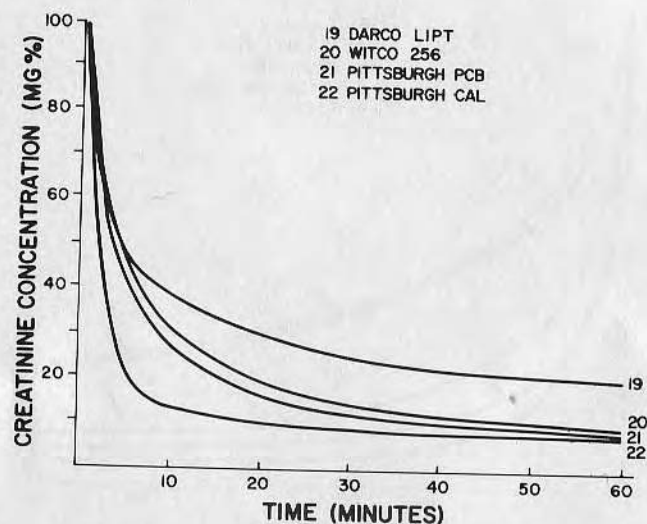

FIG. 8. Radiolabeled creatinine solute depletion from aqueous solution by various grades of granular activated carbon as a function of time.
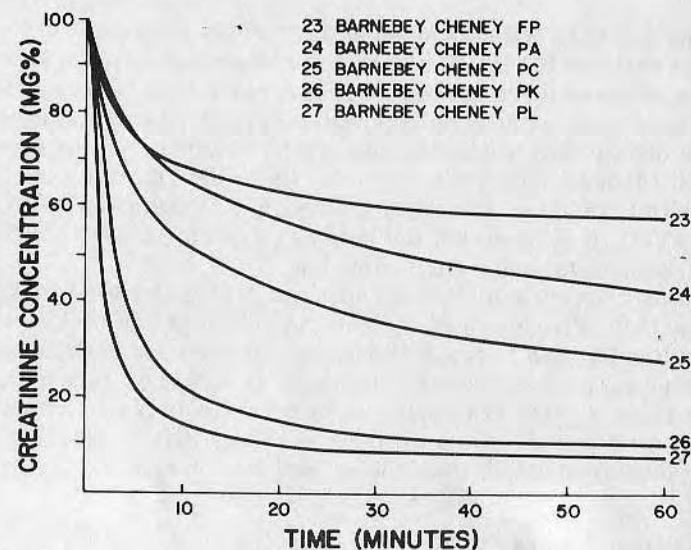
FIG. 9. Radiolabeled creatinine solute depletion from aqueous solution by various grades of granular activated carbon as a function of time.

creatinine were Fisher Coconut; granular Darco; the pelletized Columbia carbons JXC and MBV; the pelletized Norit carbons RB II, RB III, and RB IB; Darco LIPT; and the Barnebey Cheney carbons FP, PA, and PC. All other grades of carbon evaluated were intermediate in terms of creatinine adsorption.

The low adsorption characteristics of the Columbia and Norit pelletized carbons probably results from hindered solute diffusion into the bulk of the pellets. These pellets are quite large (with the exception of Norit RBI, which had fair adsorption characteristics for creatinine) and most of the carbon mass in the interior of the pellet has a limited exposure to the solute molecules. Consequently, the diffusion of solute molecules into the interior of these carbons is quite slow and total solute adsorption for a limited amount of time is relatively low. On the other hand, there is much less opposition to solute diffusion in the case of the granular carbons and so the adsorption is faster. Both total adsorption capacity and kinetics must be considered when one is evaluating activated carbon. As an example, consider Fig. 7. Nuchar WV-G has very high kinetics as evidenced by the rapidly decreasing solute concentration in the first 10 min. Total adsorption capacity for

creatinine solute is reached in about 25 min. In contrast, the Norit pelletized carbons RB II, III, and IV have slower adsorption kinetics. The slope of these three curves is considerably less, and even after 60 min these carbons have not reached complete adsorption capacity. Norit pelletized RBI has better adsorption kinetics than the other pelletized carbons, and it reaches total adsorption capacity in approximately 60 min. However, if Norit RBI is compared with Nuchar WV-G, it is seen that the latter is superior both in terms of kinetics and total adsorption capacity.

Based on kinetics and ultimate adsorption capacity for creatinine, Columbia LCK; Pittsburgh SGL, CAL, and PCB; Nuchar WV-G and WV-L; Witco 337 and 517; and Barnebey Cheney PL are superior to the other carbons evaluated. However, it should be kept in mind that this is an in vitro evaluation carried out for only one solute. In actual blood perfusion where there is competitive adsorption by many molecular species, this comparison may not hold.

E. Carbon Surface Morphology

The results of SEM analysis for representative grades of each brand of activated carbon are shown in Figs. 10 through 13. It should be kept in mind that all carbons studied exhibit a heterogeneous surface in regard to microparticle distribution, macropores, cracks, etc. The areas shown in the micrographs are representative of the surface of each particular carbon studied. The bar in each SEM micrograph represents length in either 20 or 200 μm as specified.

The surface of Witco 517 shown in Fig. 10 (a and b) shows a granular particle with a large number of surface cracks. One would think that this extensively fractured surface would be quite susceptible to fragmentation. However, Witco 517 was the cleanest carbon in the as-received condition, and it was also the most attrition-resistant of the carbons tested. The macroporous nature of this carbon as well as the presence of a moderate amount of microparticles is evident. The surface of Fisher Coconut carbon is completely devoid of any extensive surface fractures. From Fig. 10 (c and d) it can be seen that the most outstanding feature of this particular carbon is the extensive and quite uniform surface porosity. At many times these macropores are occluded with microparticles, and as a rule there seem to be more microparticles on this surface than on the Witco 517. This would tend to confirm the initial cleanliness studies in that Witco 517 was considerably cleaner than Fisher Coconut.
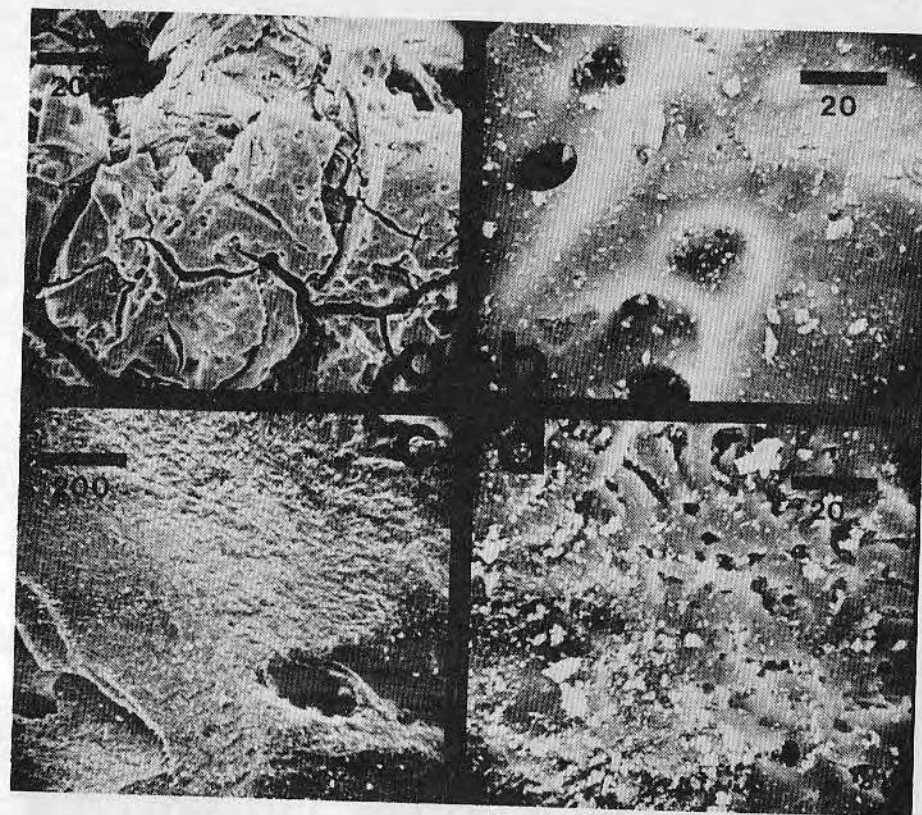
FIG. 10. SEM micrographs of Witco 517 (a and b) and Fisher Coconut (c and d) activated carbons.

Micrographs of Columbia LCK are shown in Fig. 11 (a and b). The low magnification picture shows a rough surface which suggests the particle microstructure is completely free of well-defined macropores or extensive microparticles deposits. This also confirms the cleanliness data in that Columbia LCK was one of the cleanest carbons studied (Table 3).

Figure 11 also includes micrographs of the Darco granular carbon surface. At low magnification the Darco surface is devoid of macroporosity or crack formation; however, microparticles can easily be discerned. The high magnification micrograph indicates that the surface of the particle is quite uniform and homogeneous and that it is covered with large amounts of
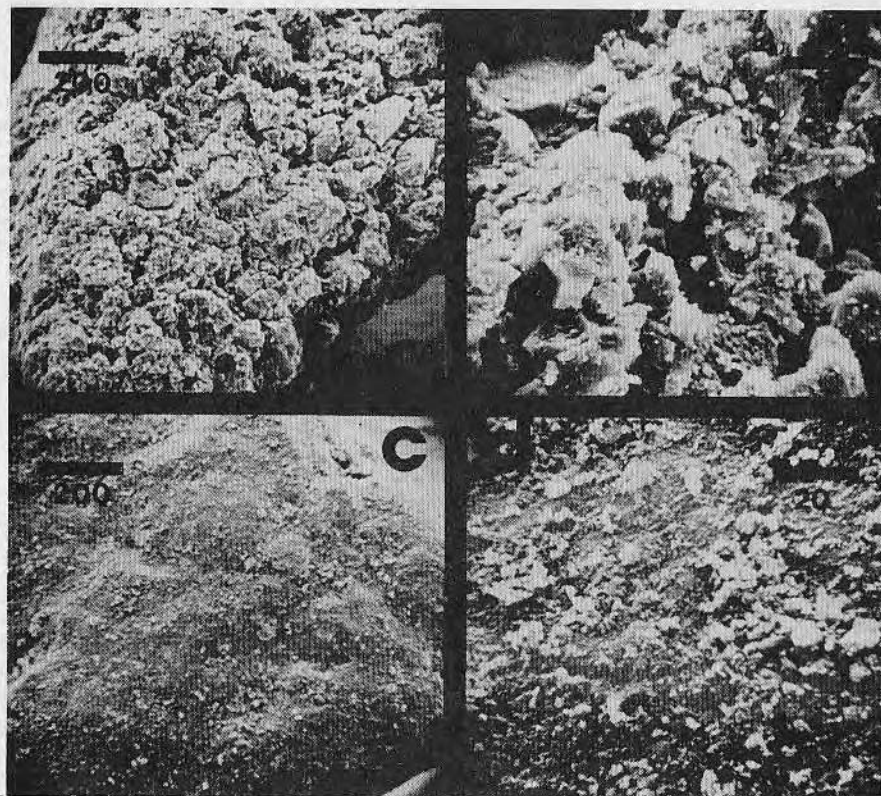
FIG. 11. SEM micrographs of Columbia LCK (a and b) and granular Darco (c and d) activated carbons.

FIG. 12. SEM micrographs of Nuchar WV-W (a and b) and Barnebey Cheney FP (c and d) activated carbons.

microparticles. Of all the carbons evaluated in terms of surface morphology, Darco granular seems to be the dirtiest in regard to microparticles. The initial cleanliness data confirm this since Darco is the dirtiest of all 27 grades evaluated.

Nuchar WV-W has a considerable amount of surface heterogeneity as shown in Fig. 12 (a and b). There are several fissures visible in the low magnification micrograph as well as many large macroparticles. Very few pores are visible. The high magnification micrograph indicates that there are a moderate number of surface microparticles, many of which are quite large.

Barnebey Cheney FP has a surface which is quite extensively covered with surface fissures; however, it does not appear that
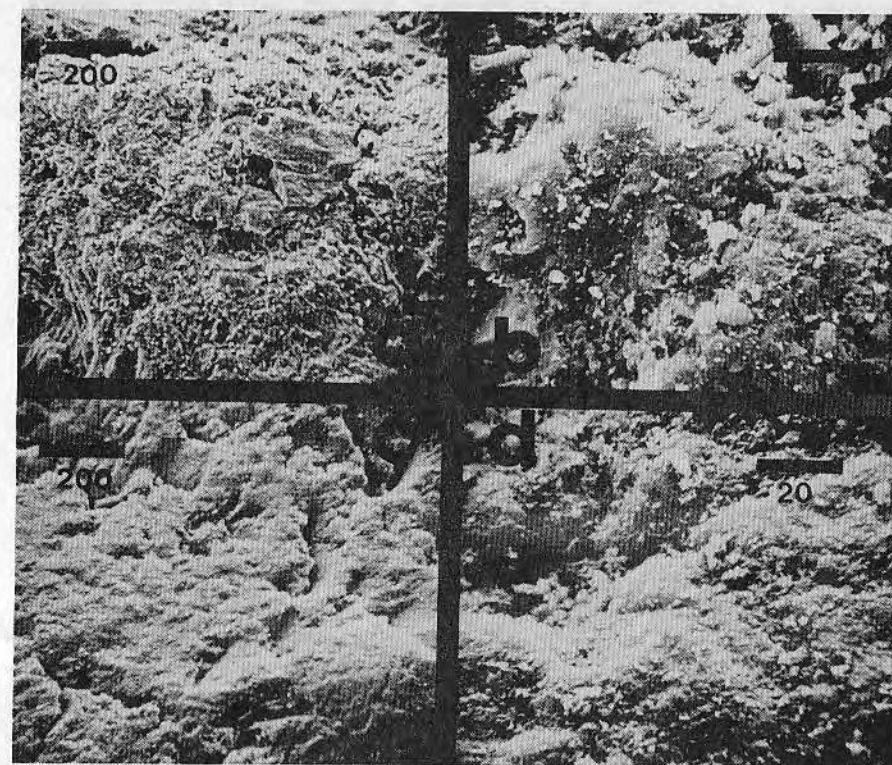
they penetrate very deeply into the particle substructure. These fissures give the appearance of having been worn or etched out in a rather smooth shape and not formed as the result of material fracture. The micrographs in Fig. 12 (c and d) also show a surface quite extensively covered with microparticles, but very few macropores are visible. In many instances, microparticles are situated in the fissures and surface depressions. This applies to a number of different grades of carbon evaluated that had rough surfaces.

The surface of Norit granular carbon appears to be somewhat fibrous or spongy as shown in Fig. 13 (a and b). There is a well-developed surface macroporosity that seems to arise from the fibrous structure but there is no extensive microparticle distribution. This carbon was one of the cleaner carbons evaluated
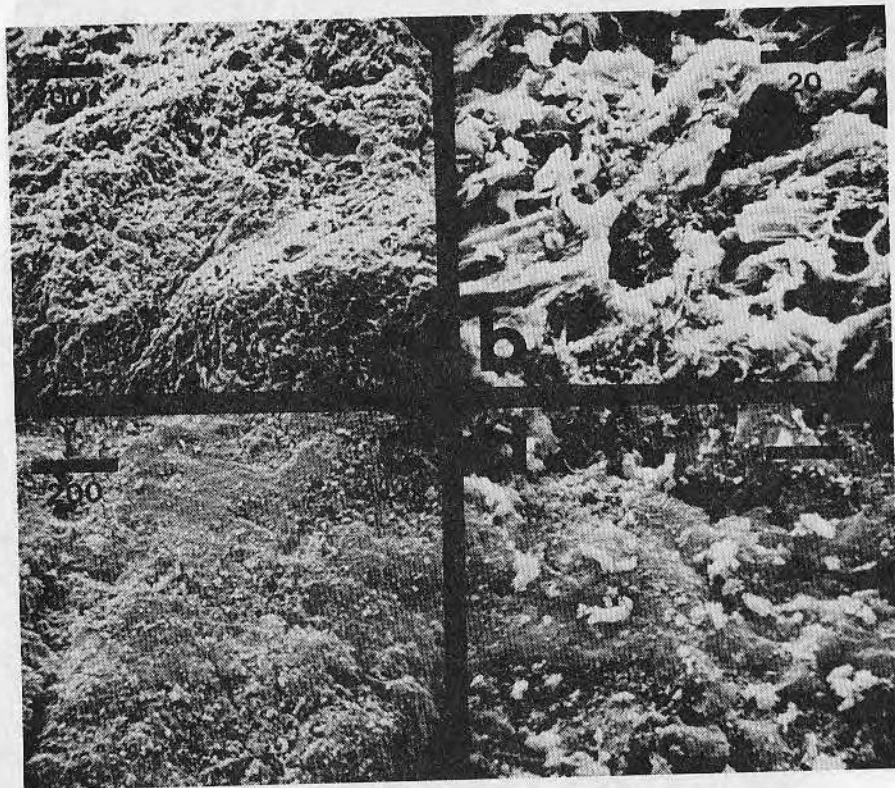
FIG. 13. SEM micrographs of Norit granular (a and b) and
Pittsburgh SGL (c and d) activated carbons.

at high magnification. These fibrous structures appear quite fragile
and one may imagine that mechanical trauma to the surface could
cause fragmentation and generation of microparticles. Indeed, it
appears that some of the delicate fibrous structure has been
destroyed. This is clearly shown in Fig. 13(b). It is impossible
to determine whether or not this mechanical trauma to the surface
occurred during manufacture, shipping or sampling. The fibrous
nature of the surface may have originated from the starting
material in the manufacturing sequence.

Micrographs of Pittsburgh SGL are also shown in Fig. 13. At
low magnification the surface seems quite homogeneous with the
exception of several surface fissures and large microparticles.
At higher magnification it appears that the surface cracks are

quite narrow and long and they probably penetrate into the particle a
considerable distance. Perhaps they help substitute for macropores
which tend to be very rare in this particular grade of carbon. There
are a considerable number of microparticles of various sizes
present, with a high percentage being quite large (greater than
10 μm in longest dimension). This is also in keeping with the
initial cleanliness data. Pittsburgh SGL was one of the carbons
with a high initial content of microparticles.

F. Carbon Microparticles

Based on the results from the previously described evaluations,
Witco 517 was chosen as the optimum carbon for our in vivo hemo-
perfusion studies. Even though it was considered the optimum,
microparticles were still present in large numbers. We wanted
some idea of the size distribution and shape of these microparticles.
The shape of the majority of the microparticles was found to be
quite irregular for the larger particle sizes (>20 μm), but as the
greatest measured dimension of the particles decreased (<10 μm)
the shape of the particles became more uniformly ellipsoidal. The
results of the microparticle size distribution are shown in Fig. 14.
Almost 35% of all the microparticles obtained from the carbon
surface are in the 2 to 3 μm size range. The great majority of
the microparticles (94%) are in the 1 to 7 μm size range. Less
than 5% of all the microparticles are larger than 10 μm, and
there were essentially no microparticles larger than 20 μm.

The small size and large number of these microparticles means
that it will be extremely difficult to remove all of them. The use
of line filters during hemoperfusion would not be successful owing
to the extremely small size of the particles. Our approach has
been to wash the granular carbon free of the majority of the
microparticles by utilizing water and ultrasound. It is then coated
with a synthetic hydrogel which serves to mechanically restrain
the remaining particulate matter on the surface and enhances the
biocompatibility during hemoperfusion [12].

V. PRESENT CARBON CLEANING PROCEDURE

A. Procedure

Carbon is taken through the washing sequence in 100 g quantities.
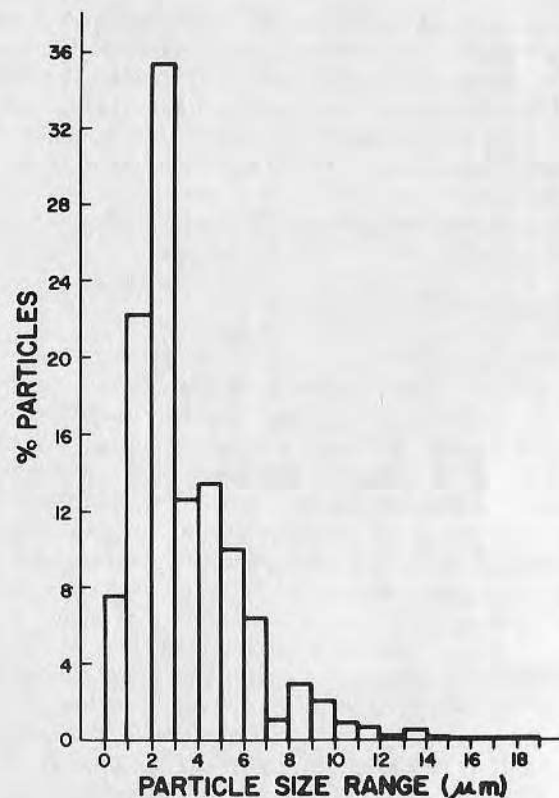Wash water samples are taken at various stages and passed through

FIG. 14. Size distribution of microparticles removed from granular Witco 517.

Millipore filters. The quantity of microparticles on the filter surface is indicated by a filter weight increase, SEM, and light microscopy. A few granules of carbon are obtained at the same time for SEM analysis of microparticle content and distribution on the carbon surface.

The carbon is placed in a 1-liter capacity polypropylene beaker. In the dry state many of the carbon microparticles are pulled off the granular carbon and tightly held to the walls of the beaker by electrostatic forces. Distilled water (200 ml) is added to the carbon and the carbon-water slurry is subjected to a negative pressure of 25 in. Hg for 30 min. As previously noted, the negative pressure above the solution helps to pull out air and

microparticles which are trapped in the porous carbon substructure. Once in solution, these particulates can be washed away. For sampling purposes the microparticles suspended in the solution after aspiration are poured into a clean glass beaker. A 100-ml sample of this initial wash solution is obtained with a syringe and passed through a Millipore filter. A few carbon granules are set aside for SEM analysis.

The carbon is then placed in a 4-liter capacity polyethylene wash bottle. Tap water is admitted at the spigot in the bottom of the bottle at a flow rate of 3 liters/min. Fluid flows in an antigravity direction and thoroughly agitates the carbon granules. The effluent flows out the top which is screened (#50 mesh stainless steel) to prevent carbon particle escape. This water washing continues for 30 min. After this the carbon is transferred back to the 1-liter polypropylene beaker and 200 ml of distilled water is added. The carbon-water slurry is gently agitated for 1 min and the water containing micro-particles is poured off into a clean glass beaker. Samples for Millipore filter analysis and SEM are taken as previously described.

The carbon is then transferred to a Buchner porcelain funnel. Tap water flows in an antigravity direction up through the funnel over the funnel rim and is discarded. The flow rate is 3 liters/min. An ultrasonic probe (Branson Sonic Power model No. 975) is positioned in the carbon-water slurry and turned on at low power density. The current in the tuned state is 0.6 A. This ultrasound effectively knocks many of the microparticles off the surface which were not removed by water washing. Caution must be exercised during the ultrasonication step. If the power density is set too high in the tuned condition, the carbon will be pulverized to dust in a matter of seconds. Usually 5 or 10 min of ultrasonication is sufficient. The carbon is transferred back to the polypropylene beaker and samples are taken as previously described.

The final carbon wash is carried out in distilled water. The carbon is transferred back to the Buchner funnel and 15 liters of distilled water flows through the carbon supported in the funnel in an anti-gravity direction at a flow rate of approximately 3 liters/min driven by a gravity feed. This flow is sufficient to gently suspend and agitate the carbon particles but not so high that the granular carbon is washed out the top of the funnel. Following this final water wash the carbon is transferred back to the 1-liter beaker and final samples for Millipore and SEM analysis are taken. The carbon is then ready to be coated with polymeric materials which improve blood compatibility.

It should be made clear that this approach is adequate for cleaning bulk Witco 517; however, different grades of carbon are quite variable in regard to initial cleanliness, washability, and attrition resistance. In practice an optimal washing procedure should be devised for each particular carbon under study.

B. Results

The results of the carbon washing procedure are shown as a series of sequential Millipore filter samples and SEM micrographs in Fig. 15. The numerically labeled bars on the SEM micrographs denote distance in micrometers (μm).

1. Filters

The filter photos in Fig. 15 show a decreasing content of carbon microparticles as the wash sequence proceeds. The initial sample (1, post-aspiration) was covered with a thick coat of carbon dust. Washing with tap water was effective in removing some microparticles but many more are still present (2, post-tap water wash sample). This is to be expected because the tap water wash caused a great deal of agitation and carbon attrition, and so eventually a point of diminishing returns is reached where just as many emboli are created by attrition as are washed away. Ultrasonication reduces the number of microparticles considerably (3, post-ultrasonication); however, there are still a significant number of microparticles present on the filter. An antigravity distilled water wash through a Buchner funnel further reduces the number of microparticles. However, as can be seen from the filter sample (4, final sample after distilled water wash), carbon microparticles are still present (as compared with a control filter C). A second wash with another 15 liters of distilled water produced a filter sample (not shown) exactly like sample 4, indicating that again a point of diminishing returns is being reached where further water washing is ineffective in removing microparticles.

2. SEM

The corresponding SEM micrographs also show a progressively decreasing number of surface microparticles as washing progresses. Initially, the carbon surface is covered with microparticles, most of which are smaller than 10 μm in longest dimension (control C). In some areas on the surface it seems that these microparticles are concentrated in crevices, cracks, and pores. Perhaps this is where they originated during activation of the carbon. In any event, a
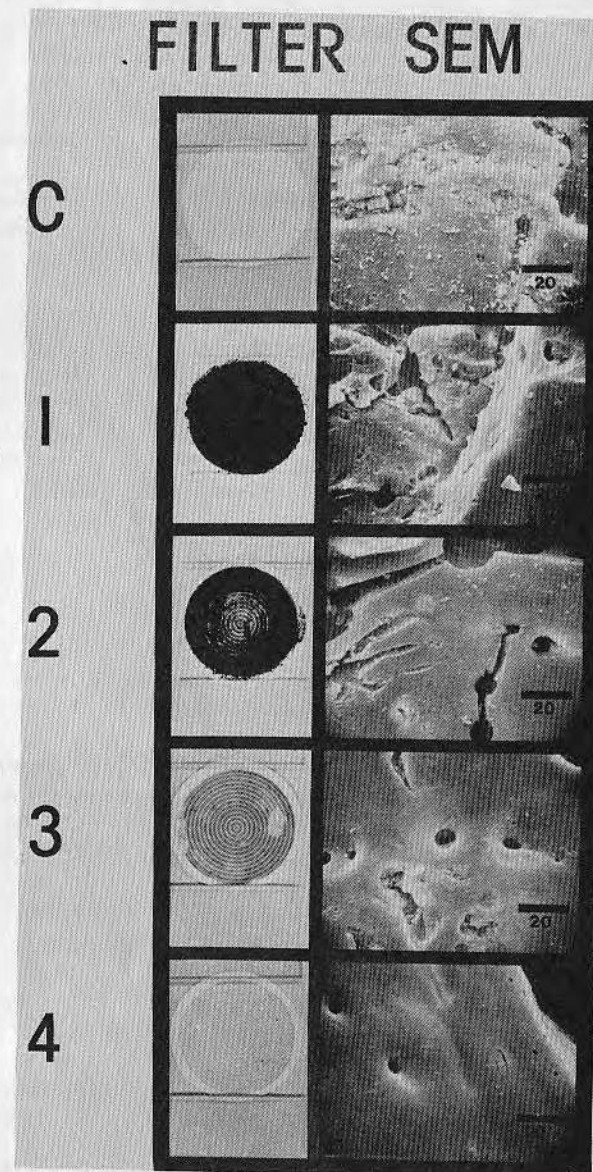
FIG. 15. Sequential samples of Millipore filters and particle surfaces (SEM) at various stages of washing. Samples are as follows: (c) control, (1) post-aspiration, (2) following tap water wash, (3) following ultrasonication, and (4) following distilled water wash. Horizontal bar represents 20 μm.

combination of aspiration, running tap water, ultrasonication, and a final wash with distilled water reduces the number of surface microparticles to a very minimal value. It should be understood, however, that this minimal value is not zero. These residual microparticles seem to be localized in pores and fissures where they are very difficult to remove.

At this stage of the process the carbon is ready to be coated with polymeric materials which will significantly enhance blood compatibility and help to restrain physically any remaining microparticles.

This paper has only considered microparticles, washing, and in vitro creatinine adsorption characteristics in the selection of an activated carbon for hemoperfusion applications. One must also consider the chemical nature of the carbon with respect to extractables and leachable components, and the toxicity, pyrogenicity, and sterilizability of the carbons. Carbon coating techniques have only been mentioned in passing, but they also play a significant role in optimizing activated carbon hemoperfusion for subsequent clinical use.

VI.   CONCLUSIONS

The following observations are made on the basis of our experience with activated carbon and its utilization for hemoperfusion.

1. Commercially available granular and pelletized activated carbons vary widely in terms of initial microparticle content. Witco carbons 517 and 256; Columbia carbons JXC, LCK, and MBV; Barnebey Cheney FP; and pelletized Norit RBI were the cleanest carbons in the as received state.

2. Various carbons differ in terms of efficacy of water washing. Some carbons can be effectively cleaned using this approach while other carbons cannot. The Witco carbons 517, 256, and 337 as well as the Columbia carbons JXC, MBV, and LCK were all effectively cleaned by water washing. Darco granular and LIPT, Barnebey Cheney PC, Pittsburgh SGL, and Nuchar WV-W carbons were cleaned least effectively using a water wash approach. All other grades of carbon were intermediate between these extremes.

3. Witco carbons 517, 125, and 337 and Columbia LCK were all more resistant to attrition than Norit, Darco, and Pittsburgh SGL granular activated carbons.

4. There seems to be a good correlation between the initial cleanliness, washability, and attrition resistance of the various carbons evaluated. Carbons such as Witco 517 and Columbia LCK are consistently superior in all of the previously mentioned tests while granular Darco rated consistently low in those same evaluations.

5. There were a number of carbons which had very good in vitro adsorption characteristics for creatinine. Witco 517 and Columbia LCK were quite good in this regard. Fisher Coconut granular activated carbon was quite poor both in terms of in vitro creatinine adsorption and the two previously mentioned tests concerned with microparticle evaluation. Most of the pelletized carbons were relatively poor in terms of creatinine adsorption.

6. The surface morphology of various grades of activated carbon was markedly different for each carbon evaluated. This observation was made on the basis of SEM evaluations carried out on a number of samples of each grade of carbon tested. There seems to be a rough correlation between the number of microparticles on the surface and the initial cleanliness test. Witco 517 and Columbia LCK seemed to have surfaces which were relatively free of microparticles in comparison to the other carbons.

7. A large percentage (94%) of the microparticles obtained from thoroughly washed Witco 517 are in the 1 to 7 μm range.

8. The present carbon washing procedure utilizing Witco 517 is quite adequate for removal of the great majority of microparticles from the carbon surface. However, not all the microparticles on the carbon surface can be removed by washing.

9. Witco 517 granular activated carbon has been chosen for utilization in our hemoperfusion studies because it is superior to all others in terms of initial cleanliness and attrition resistance, and it is comparable to other activated carbons in terms of optimal water washing and in vitro creatinine adsorption (fairly rapid kinetics and acceptable ultimate adsorption capacity).

ACKNOWLEDGMENTS

REFERENCES

[1] H. Yatzidis, "A Convenient Haemoperfusion Micro-Apparatus Over Charcoal for the Treatment of Endogenous and Exogenous Intoxications," Proc. Eur. Dial. Transplant Assoc., 1, 83 (1964).

[2] G. Dunea and W. J. Kolff, "Clinical Experience With the Yatzidis Charcoal Artificial Kidney," Trans. Amer. Soc. Art. Int. Org., 11, 178 (1965).

[3] T. M. S. Chang, "Semipermeable Microcapsules," Science, 146, 524 (1964).

[4] T. M. S. Chang, Artificial Cells, Thomas, Springfield, Illinois, 1972.

[5] T. M. S. Chang, "Semipermeable Aqueous Microcapsules (Artificial Cells): With Emphasis on Experiments in an Extracorporeal Shunt System," Trans. Amer. Soc. Art. Int. Org., 12, 13 (1966).

[6] T. M. S. Chang, A. Pont, L. J. Johnson, and N. Malave, "Response to Intermittent Extracorporeal Perfusion through Shunts Containing Semipermeable Microcapsules," Ibid., 14, 163 (1968).

[7] T. M. S. Chang, L. J. Johnson, and O. J. Ransome, "Semipermeable Aqueous Microcapsules. IV. Nonthrombogenic Microcapsules with Heparin-Complexed Membranes," Can. J. Physiol. Pharmacol., 45, 705 (1967).

[8] T. M. S. Chang and N. Malave, "The Development and First Clinical Use of Semipermeable Microcapsules (Artificial Cells) as a Compact Artificial Kidney," Trans. Amer. Soc. Art. Int. Org., 16, 141 (1970).

[9] T. M. S. Chang, A. Gonda, J. H. Dirks, and N. Malave, "Clinical Evaluation of Chronic, Intermittent, and Short Term Hemoperfusions in Patients with Chronic Renal Failure Using Semipermeable Microcapsules (Artificial Cells) Formed from Membrane-Coated Activated Charcoal," Ibid., 17, 246 (1971).

[10] T. M. S. Chang, A. Gonda, J. H. Dirks, J. F. Coffey, and T. L. Burns, "ACAC Microcapsule Artificial Kidney for the Long Term and Short Term Management of Eleven Patients With Chronic Renal Failure," Ibid., 18, 465 (1972).

[11] T. M. S. Chang, "Microcapsule Artificial Kidney and Medium Molecular Weight Clearance," Proc. Eur. Dial. Transplant Assoc., 8, 568 (1972).

[12] J. D. Andrade, K. Kunitomo, R. Van Wagenen, B. Kastigar, D. Gough, and W. J. Kolff, "Coated Adsorbents for Direct Blood Perfusion: Hema/Activated Carbon," Trans. Amer. Soc. Art. Int. Org., 17, 222 (1971).

[13] J. D. Andrade, R. Van Wagenen, C. Chen, M. Ghavamian, J. G. R. Volder, R. Kirkham, and W. J. Kolff, "Coated Adsorbents for Direct Blood Perfusion II," Ibid., 18, 473 (1972).

[14] H. Yatzidis, "The Charcoal Kidney in Clinical Practice," a Paper Presented at the Cleveland Clinic, Cleveland, Ohio, October 18, 1966.

[15] H. Yatzidis, D. Oreopoulos, D. Triantaphyllidis, S. Vaudiclari, N. Tsaparas, G. Gavras, and A. Stavrovlakis, "Treatment of Severe Barbiturate Poisoning," Lancet, 2, 216 (1965).

[16] M. H. De Myttenaere, J. F. Maher, and G. E. Schreiner, "Hemoperfusion through a Charcoal Column for Glutethimide Poisoning," Trans. Amer. Soc. Art. Int. Org., 13, 190 (1967).

[17] M. De Myttenaere, "Haemoperfusion through a Charcoal Column for Treatment of Poisoning," Proc. Eur. Dial. Transplant Assoc., 5, 320 (1968).

[18] J. L. Rosenbaum, E. Ronquillo, and S. N. Argyres, "Column Hemoperfusion and Hemodialysis Techniques to Treat Barbiturate Intoxication in Dogs," J. Albert Einstein Med. Cent., 16, 67 (1968).

Adsorbent hemoperfusion: Nonbiological particulate matter

R. Van Wagenen, D. L. Coleman and J. D. Andrade

*Department of Materials Science and Engineering and Institute for Biomedical Engineering,
University of Utah, Salt Lake City, Utah*

Adsorbent hemoperfusion generally consists of passing blood over a column of sorbent granules constrained within a suitable extracorporeal circuit. Certain solutes are adsorbed on the surface of the granules and thereby removed from the blood. In many cases the physical adsorption process is strong enough to remove normally protein-bound substances [1]. The three generally utilized classes of sorbents are: *1*) ion-exchange resins; *2*) polymeric, nonionic adsorbents, in particular the Amberlite XAD series (Rohm and Haas Corp.); and *3*) activated carbon. The last is a broad-spectrum adsorbent suitable for removing a variety of exogeneous and endogeneous toxins [1], including some of interest in uremia [2-4]. Of the three classes noted, only activated carbon has been shown effective and useful in the partial treatment of uremia [2].

The great bulk of the work on activated carbon hemoperfusion has utilized granules or pellets; however, work on hydrophilic fibers containing powdered activated carbon [5] and on dialysis membranes containing activated carbon is in progress.

Sorbent hemoperfusion for acute application is becoming generally recognized and accepted. Polymeric adsorbents have been applied by Rosenbaum for acute poison treatment [6]. Activated carbon has been extensively used for the treatment of acute poisoning and acute hepatic failures [1, 7]. An activated carbon cartridge (300 g, hydrophilic polymer coated) is now commercially available in limited quantities [8].

There are, however, two problems associated with sorbent hemoperfusion, particularly for chronic applications: *1*) blood compatibility of the system; and *2*) particle release from the extracorporeal circuit.

Blood compatibility has been considered in a number of publications [9-11]. Generally the problem is solved by coating or encapsulating the adsorbent with a blood-tolerable material. Aqueous gels (cellulose, polyhydroxyethyl methacrylate and others) and albumin coatings have been widely used [11].

In this brief paper we consider only the particulate problem.

Particulates

There are a number of ways in which particulate matter is delivered to an organism: *1*) by direct respiration of particulate-laden air; *2*) by surgery; *3*) by intravenous solutions; *4*) orally; and *5*) by extracorporeal therapy.

We are concerned only with the last category. The particles produced by extracorporeal circuits can be divided into two classes; biological (clots, platelet aggregates, cellular emboli, micellar aggregates and so on) and nonbiological. Biological particulate matter is potentially reversible, and in the case of clots an efficient mechanism exists for their dispersal and removal. Nonbiological particulate matter is generally treated as foreign matter and processed into the reticuloendothelial system for breakdown (if possible) and for sequestration.

We are concerned here only with nonbiological particulate matter which is due largely to two major sources: roller pump tubing debris, and sorbent particles or fragments which escape the restraining elements in the circuits (generally screens or filters).

Sorbent micro particles

The sorbent fragments arise from two sources: microparticles present in and on the sorbent granules, and particles formed by granule/granule or granule/container collision and attrition.

As received, activated carbon granules generally contain large quantities of fines or microparticles on their surfaces [11, 12]. The appearance of the carbons is greatly affected by proper washing [12]. The particulate

release observed as a function of washing time and conditions can be quantitated and greatly affected by the nature of the washing treatment [12, 13]. With almost all washing procedures a point of diminishing returns is reached, which is probably due to collisions and attrition, where further washing is not helpful. Attrition tests are available for the evaluation of various carbons [12]. The effect of attrition due to granule movement and collisions can be greatly decreased by the use of a totally fixed bed column [8] or by immobilizing the particles in some manner.

Our work has shown that a column of well-cleaned, strong activated carbon (up to 200 g) perfused at a flow rate of 150 to 200 ml/min for three hours generates 200 to 500 μg of carbon particles, with most of the particles in the 1 to 2 μ diameter range [12, 13]. These data were obtained in a closed *in vitro* circuit where the perfusate was passed through a 0.22 μm pore diameter Millipore filter.

The particulate release can be decreased significantly by coating the carbon; some coatings are obviously much more effective than others in reducing the particulate release [11]. Although studies are available comparing a wide range of carbons and preparation treatments for particle release [12], no such study is available for carbons coated with the various available and readily prepared coatings [11]—and such a study is needed before extensive commercial development leads us to one coating type.

Polymeric adsorbents, originally believed to be considerably cleaner than activated carbon hemoperfusion [14], also suffer from microparticle problems [6].

Do such particles have histopathological significance? The studies by Hagstam, Larsson and Thysell [15], in which considerable quantities of carbon particles were infused into rabbits by activated carbon (uncoated) hemoperfusion, showed relatively little tissue reaction. Activated carbon particles deposited in tissues show little evidence of tissue reaction.

In order to semiquantitate the sensitivity of histological methods for detecting carbon particulate matter, we conducted a preliminary double-blind study injecting controlled quantities of carbon particulates into the tail veins of Swiss Webster mice.

We assumed a 70 kg patient would receive up to 700 μg of carbon particles per perfusion, or up to 0.01 mg/kg. We then injected μ-sized carbon particles into the tail veins of Swiss Webster mice at doses of 0.01, 0.1, 2 and 10 mg/kg, i.e., up to three orders of magnitude greater than we would expect in a clinical hemoperfusion using our systems. No acute effects were noted in any of the mice. The animals were sacrificed at 1, 7 and 24 hr, and lung, liver, spleen and kidney were examined histologically. The samples were coded so the person doing the histological evaluation did not know the particulate dose or survival time of the tissues examined. The results are given in Table 1. It is clear that particles are readily seen only with the 10 mg/kg dose. Thus, particle loadings on the order of over 200 times higher than that produced by a single perfusion are required before such particles can be readily detected histopathologically. It is evident that nonhistological methods are required to detect particulate release. Such methods are readily available [8, 12]. Another tentative conclusion, if these preliminary data can be extrapolated to the clinical situation, is that several years of daily sorbent hemoperfusion would be required before particles could be *readily* detected on histological examination.

Particle loading can perhaps be decreased by a factor of 10 to 100 or more times what we have currently achieved by selective coating treatments [2, 8] or by column design and packing [8].
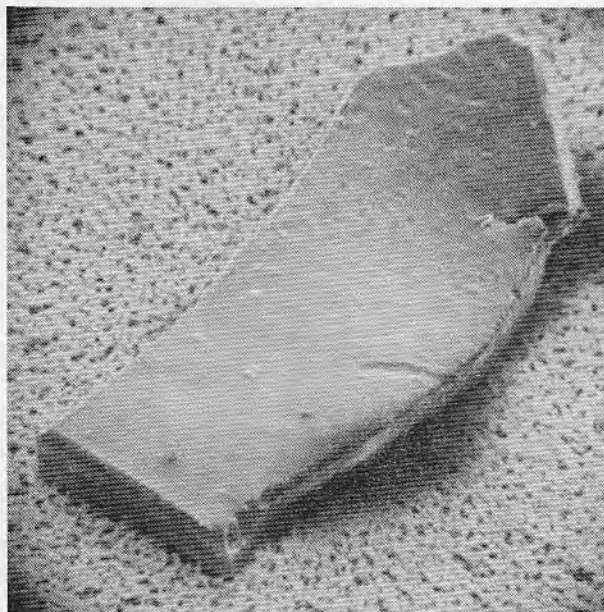
Roller pump tubing particles

Particle release from activated carbon hemoperfusion circuits may be a relatively minor part, by weight, of the

Table 1. The histological evaluation of activated carbon particles injected into the tail vein of Swiss Webster mice.
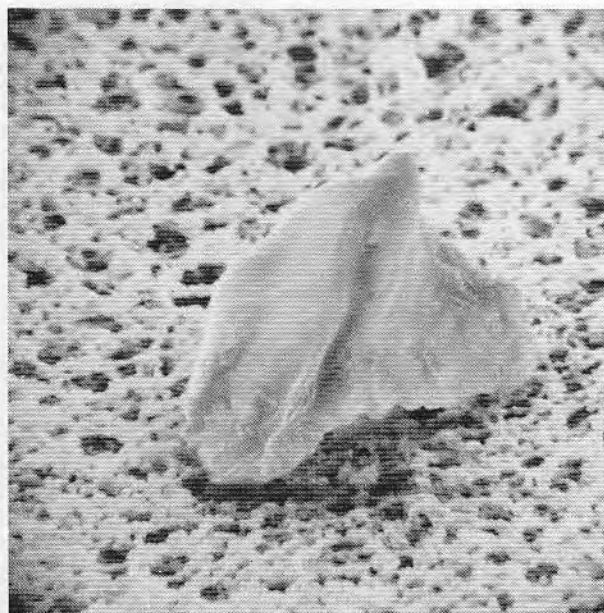
Time, hr	Organ	Dose, mg/kg			
		10	2	0.1	0.01
1	Lung	+	+	0	0
	Liver	±	0	0	0
	Spleen	++a	±	0	0
	Kidney	0	0	0	0
7	Lung	++	+	0	0
	Liver	++a	0	0	0
	Spleen	±a	0	0	0
	Kidney	±a	0	0	0
24	Lung	++	0	0	0
	Liver	−	0	0	0
	Spleen	++a	0	0	0
	Kidney	±a	0	0	0
Control not injected	Lung	0			
	Liver	0			
	Spleen	0			
	Kidney	0			

aCarbon particles were smaller than those seen in the lung.
Tissue sections were graded on a 0 to + 4 scale as follows: 0, no carbon particles per high power field (hpf, 400 ×) in 10 fields of view (F.V.); ±, 1 or 2 particles seen in 1 or 2 of the 10 F.V.; +, 1 or 2 particles in 5 of the 10 F.V.; ++, 1 or 2 particles in 9 or 10 of the 10 F.V.; +++, 2 or 3 particles in 9 or 10 of the 10 F.V.; ++++, more than 3 particles in 10 of the 10 F.V.

total particulate loading to which a chronic hemodialysis patient is subjected. This statement results from *in vitro* control studies of sorbent hemoperfusion circuits containing *no* sorbent. In such studies we found mg quantities of large particulate matter, readily observable on scanning electron microscopy of Millipore filters. We conducted a preliminary study of particles released by polyvinyl chloride (PVC) arterial hemodialysis tubing sets from

A

B

Fig. 1. *Scanning electron micrograph of particles on Millipore filter (0.22 μpores) produced during an* in vitro *study of particle release by polyvinyl chloride hemodialysis arterial tubing sets. A), The particle dimensions are approximately 10 × 80 × 200 μ, B), particle length dimension is about 30 μ.*

three main U.S.A. suppliers. The pump tubing segment was placed in a Sarns Model 5500 roller pump adjusted to the "just occlusive" mode [16]. Particle release was measured by total weight change of the filter and varied by two orders of magnitude (from about .01 to over 2 mg), depending primarily on the tubing set supplier. The filters were examined by scanning electron microscopy and the particles clearly seen (Fig. 1). Energy dispersive x-ray analysis in the scanning electron microscope indicated that some of the particles were very rich in chlorine, leading us to suspect that they are polyvinyl chloride.

It, thus, appears from these preliminary studies that patients placed on extracorporeal circuits utilizing roller pumps with PVC pump segments may be receiving PVC particles.

Similar results were obtained by Boretos and Wagner [17] in an *in vitro* study of particulate production by pump tubing segments utilized for cardiopulmonary bypass.

If all the particles are as large as indicated in Fig. 1, they might be filterable by blood line filters or by a fixed bed of adsorbent particles. However, it is probable that much smaller particles are also generated and infused by the circuit. Our activated carbon work shows that a major number of the carbon particles released are in the 1 to 2 μ range (for Witco 517 uncoated activated carbon, see [12]). Such particles could not be removed by conventional filtration methods.

Discussion and conclusions

The preliminary work reported here indicates: *1)* polymer particulate matter is released from at least some PVC roller pump tubing segments when pumped with a "just occlusive" roller pump; *2)* particle release by well-washed, well-prepared and properly selected activated carbon is about 200 to 1000 times below the level required for routine histological detection and a factor of 1 to 100 (by weight) less than that generated by PVC pump tubing segments; *3)* particle release by coated carbon is considerably lower than that for uncoated carbon, and is greatly dependent on the type of coating.

In addition, we know that PVC contains 30 to 50% plasticizer, commonly dioctylphthalate [18]. The dioctylphthalate is readily leached and released into the organism, and there is growing evidence that dioctylphthalate is relatively toxic [19]. Thus, one can suspect that PVC particles released into an organism will function as a local "drug" release system, releasing dioctylphthalate to the organism. It is thus possible that PVC particles may have physical and chemical effects on the organism. If we insist on composing a list of potential uremic toxins, PVC particles and dioctylphthalate should at least be considered.

It is imperative that particle release by extracorporeal circuits be quantitated and minimized.

References

1. In *Artificial Support Systems for Acute Hepatic Failure,* edited by Williams RS, London, Pittman, 1974, in press
2. Chang TMS: *Artificial Cells.* Springfield, Illinois, Thomas, 1972
3. Yatzidis H: A convenient haemoperfusion microapparatus over charcoal in the treatment of endogenous and exogenous intoxications. *Proc Eur Dial Transpl Assoc* 1:83–4, 1964
4. Andrade JD, Kopp K, Van Wagenen R, Chen C, Kolff WJ: Activated carbon and blood perfusion: A critical review. *Proc Eur Dial Transpl Assoc* 9:290–301, 1972
5. Davis TA: Activated carbon fibers in hemoperfusion devices. *Kidney Int* (Suppl. No. 3) 7:406–408, 1975.
6. Rosenbaum JL: Biocompatibility of resin haemoperfusion, in *Artificial Support Systems for Acute Hepatic Failure,* edited by Williams RS, London, Pittman, 1974, in press
7. Chang TMS, Coffey JF, Barre P, Gonda A, Dirks JH, Levy M, Lister C: Microcapsule artificial kidney: Treatment of patients with acute drug intoxication. *Can Med Assoc J* 108:429–433, 1973
8. Fennimore J: Design and development of Smith and Nephew Column, in *Artificial Support Systems for Acute Hepatic Failure,* edited by Williams RS, London, Pittman, 1974, in press
9. Chang TMS: Recent trends in biocompatible materials and microcapsular absorbents for kidney function replacement, in *Perspectives in Biomedical Engineering,* edited by Kenedi RM, London, University Park Press, 1972, pp. 39–43
10. Chang TMS: Platelet-surface interaction: Effect of albumin coating or heparin complexing on thrombogenic surfaces. *Can J Physiol Pharmacol* 52:275–285, 1974
11. Andrade JD, Coleman DL, Kim SW, Lentz DJ: Activated carbon coatings for optimal blood compatibility, in *Artificial Support Systems for Acute Hepatic Failure,* edited by Williams RS, London, Pittman, 1974, in press
12. Van Wagenen R, Stegall M, Lentz DJ, Andrade JD: Activated carbons for medical applications. I. *In vitro* microparticle characterization and solute adsorption, submitted
13. Andrade JD, Van Wagenen R, Chen C, Ghavamian M, Volder JGR, Kirkham R, Kolff WJ: Coated adsorbents for direct blood perfusion. II. *Trans Am Soc Artif Intern Organs* 18:473–483, 1972
14. Merrill JP: Treatment of drug intoxication. *N Engl J Med* 284:911–912, 1971
15. Hagstam KE, Larsson LE, Thysell H: Experimental studies on charcoal haemoperfusion in phenobarbital intoxication and uremia including histopathological findings. *Acta Med Scand* 180:593–603, 1966
16. Meyer MM: Blood pump occulsion. *J Extracorporeal Tech,* Fall, 1973, pp. 8–15
17. Boretos JW, Wagner FR: Particle fragmentation generated in pump sets. *J Biomed Mater Res* 5:411–413, 1971
18. Geertz W, Dyer K, Johnson D, Miller B, Taylor B, Sharp W: Polyvinyl chloride biomedical products. *Trans Am Soc Artif Intern Organs* 20: 1974, in press
19. Peterson RV: Toxicology of plastic devices having contact with blood. U.S. Government Report PB 224558, Sept., 1973

Adsorbent hemoperfusion: Nonbiological particulate matter

R. Van Wagenen, D. L. Coleman and J. D. Andrade

Department of Materials Science and Engineering and Institute for Biomedical Engineering,
University of Utah, Salt Lake City, Utah

Adsorbent hemoperfusion generally consists of passing blood over a column of sorbent granules constrained within a suitable extracorporeal circuit. Certain solutes are adsorbed on the surface of the granules and thereby removed from the blood. In many cases the physical adsorption process is strong enough to remove normally protein-bound substances [1]. The three generally utilized classes of sorbents are: *1*) ion-exchange resins; *2*) polymeric, nonionic adsorbents, in particular the Amberlite XAD series (Rohm and Haas Corp.); and *3*) activated carbon. The last is a broad-spectrum adsorbent suitable for removing a variety of exogeneous and endogeneous toxins [1], including some of interest in uremia [2-4]. Of the three classes noted, only activated carbon has been shown effective and useful in the partial treatment of uremia [2].

The great bulk of the work on activated carbon hemoperfusion has utilized granules or pellets; however, work on hydrophilic fibers containing powdered activated carbon [5] and on dialysis membranes containing activated carbon is in progress.

Sorbent hemoperfusion for acute application is becoming generally recognized and accepted. Polymeric adsorbents have been applied by Rosenbaum for acute poison treatment [6]. Activated carbon has been extensively used for the treatment of acute poisoning and acute hepatic failures [1, 7]. An activated carbon cartridge (300 g, hydrophilic polymer coated) is now commercially available in limited quantities [8].

There are, however, two problems associated with sorbent hemoperfusion, particularly for chronic applications: *1*) blood compatibility of the system; and *2*) particle release from the extracorporeal circuit.

Blood compatibility has been considered in a number of publications [9-11]. Generally the problem is solved by coating or encapsulating the adsorbent with a blood-tolerable material. Aqueous gels (cellulose, polyhydroxyethyl methacrylate and others) and albumin coatings have been widely used [11].

In this brief paper we consider only the particulate problem.

Particulates

There are a number of ways in which particulate matter is delivered to an organism: *1*) by direct respiration of particulate-laden air; *2*) by surgery; *3*) by intravenous solutions; *4*) orally; and *5*) by extracorporeal therapy.

We are concerned only with the last category. The particles produced by extracorporeal circuits can be divided into two classes; biological (clots, platelet aggregates, cellular emboli, micellar aggregates and so on) and nonbiological. Biological particulate matter is potentially reversible, and in the case of clots an efficient mechanism exists for their dispersal and removal. Nonbiological particulate matter is generally treated as foreign matter and processed into the reticuloendothelial system for breakdown (if possible) and for sequestration.

We are concerned here only with nonbiological particulate matter which is due largely to two major sources: roller pump tubing debris, and sorbent particles or fragments which escape the restraining elements in the circuits (generally screens or filters).

Sorbent micro particles

The sorbent fragments arise from two sources: microparticles present in and on the sorbent granules, and particles formed by granule/granule or granule/container collision and attrition.

As received, activated carbon granules generally contain large quantities of fines or microparticles on their surfaces [11, 12]. The appearance of the carbons is greatly affected by proper washing [12]. The particulate

release observed as a function of washing time and conditions can be quantitated and greatly affected by the nature of the washing treatment [12, 13]. With almost all washing procedures a point of diminishing returns is reached, which is probably due to collisions and attrition, where further washing is not helpful. Attrition tests are available for the evaluation of various carbons [12]. The effect of attrition due to granule movement and collisions can be greatly decreased by the use of a totally fixed bed column [8] or by immobilizing the particles in some manner.

Our work has shown that a column of well-cleaned, strong activated carbon (up to 200 g) perfused at a flow rate of 150 to 200 ml/min for three hours generates 200 to 500 μg of carbon particles, with most of the particles in the 1 to 2 μ diameter range [12, 13]. These data were obtained in a closed *in vitro* circuit where the perfusate was passed through a 0.22 μm pore diameter Millipore filter.

The particulate release can be decreased significantly by coating the carbon; some coatings are obviously much more effective than others in reducing the particulate release [11]. Although studies are available comparing a wide range of carbons and preparation treatments for particle release [12], no such study is available for carbons coated with the various available and readily prepared coatings [11]—and such a study is needed before extensive commercial development leads us to one coating type.

Polymeric adsorbents, originally believed to be considerably cleaner than activated carbon hemoperfusion [14], also suffer from microparticle problems [6].

Do such particles have histopathological significance? The studies by Hagstam, Larsson and Thysell [15], in which considerable quantities of carbon particles were infused into rabbits by activated carbon (uncoated) hemoperfusion, showed relatively little tissue reaction. Activated carbon particles deposited in tissues show little evidence of tissue reaction.

In order to semiquantitate the sensitivity of histological methods for detecting carbon particulate matter, we conducted a preliminary double-blind study injecting controlled quantities of carbon particulates into the tail veins of Swiss Webster mice.

We assumed a 70 kg patient would receive up to 700 μg of carbon particles per perfusion, or up to 0.01 mg/kg. We then injected μ-sized carbon particles into the tail veins of Swiss Webster mice at doses of 0.01, 0.1, 2 and 10 mg/kg, i.e., up to three orders of magnitude greater than we would expect in a clinical hemoperfusion using our systems. No acute effects were noted in any of the mice. The animals were sacrificed at 1, 7 and 24 hr, and lung, liver, spleen and kidney were examined histologically. The samples were coded so the person doing the histological evaluation did not know the particulate dose or survival time of the tissues examined. The results are given in Table 1. It is clear that particles are readily seen only with the 10 mg/kg dose. Thus, particle loadings on the order of over 200 times higher than that produced by a single perfusion are required before such particles can be readily detected histopathologically. It is evident that nonhistological methods are required to detect particulate release. Such methods are readily available [8, 12]. Another tentative conclusion, if these preliminary data can be extrapolated to the clinical situation, is that several years of daily sorbent hemoperfusion would be required before particles could be *readily* detected on histological examination.

Particle loading can perhaps be decreased by a factor of 10 to 100 or more times what we have currently achieved by selective coating treatments [2, 8] or by column design and packing [8].
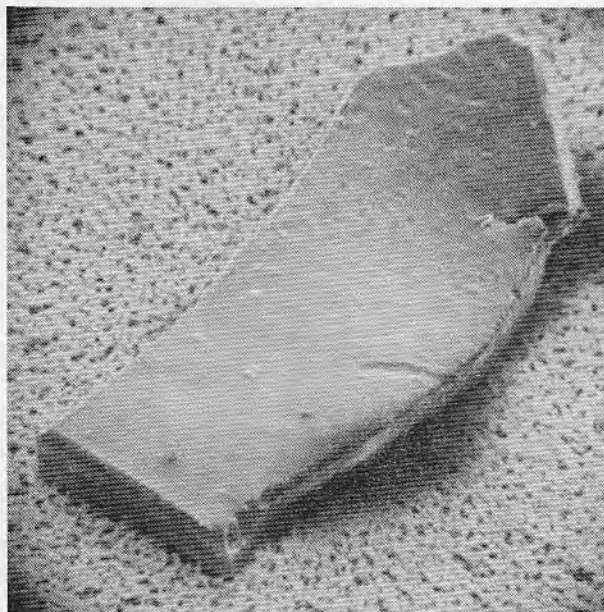
Roller pump tubing particles

Particle release from activated carbon hemoperfusion circuits may be a relatively minor part, by weight, of the

Table 1. The histological evaluation of activated carbon particles injected into the tail vein of Swiss Webster mice.
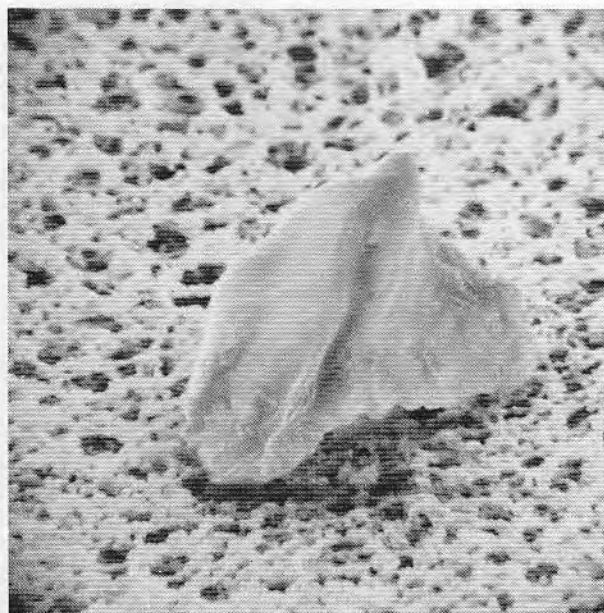
Time, hr	Organ	Dose, mg/kg			
		10	2	0.1	0.01
1	Lung	+	+	0	0
	Liver	±	0	0	0
	Spleen	++a	±	0	0
	Kidney	0	0	0	0
7	Lung	++	+	0	0
	Liver	++a	0	0	0
	Spleen	±a	0	0	0
	Kidney	±a	0	0	0
24	Lung	++	0	0	0
	Liver	−	0	0	0
	Spleen	++a	0	0	0
	Kidney	±a	0	0	0
Control not injected	Lung	0			
	Liver	0			
	Spleen	0			
	Kidney	0			

aCarbon particles were smaller than those seen in the lung.
Tissue sections were graded on a 0 to + 4 scale as follows: 0, no carbon particles per high power field (hpf, 400 ×) in 10 fields of view (F.V.); ±, 1 or 2 particles seen in 1 or 2 of the 10 F.V.; +, 1 or 2 particles in 5 of the 10 F.V.; ++, 1 or 2 particles in 9 or 10 of the 10 F.V.; +++, 2 or 3 particles in 9 or 10 of the 10 F.V.; ++++, more than 3 particles in 10 of the 10 F.V.

total particulate loading to which a chronic hemodialysis patient is subjected. This statement results from *in vitro* control studies of sorbent hemoperfusion circuits containing *no* sorbent. In such studies we found mg quantities of large particulate matter, readily observable on scanning electron microscopy of Millipore filters. We conducted a preliminary study of particles released by polyvinyl chloride (PVC) arterial hemodialysis tubing sets from

A

B

Fig. 1. *Scanning electron micrograph of particles on Millipore filter (0.22 μpores) produced during an* in vitro *study of particle release by polyvinyl chloride hemodialysis arterial tubing sets. A), The particle dimensions are approximately 10 × 80 × 200 μ, B), particle length dimension is about 30 μ.*

three main U.S.A. suppliers. The pump tubing segment was placed in a Sarns Model 5500 roller pump adjusted to the "just occlusive" mode [16]. Particle release was measured by total weight change of the filter and varied by two orders of magnitude (from about .01 to over 2 mg), depending primarily on the tubing set supplier. The filters were examined by scanning electron microscopy and the particles clearly seen (Fig. 1). Energy dispersive x-ray analysis in the scanning electron microscope indicated that some of the particles were very rich in chlorine, leading us to suspect that they are polyvinyl chloride.

It, thus, appears from these preliminary studies that patients placed on extracorporeal circuits utilizing roller pumps with PVC pump segments may be receiving PVC particles.

Similar results were obtained by Boretos and Wagner [17] in an *in vitro* study of particulate production by pump tubing segments utilized for cardiopulmonary bypass.

If all the particles are as large as indicated in Fig. 1, they might be filterable by blood line filters or by a fixed bed of adsorbent particles. However, it is probable that much smaller particles are also generated and infused by the circuit. Our activated carbon work shows that a major number of the carbon particles released are in the 1 to 2 μ range (for Witco 517 uncoated activated carbon, see [12]). Such particles could not be removed by conventional filtration methods.

Discussion and conclusions

The preliminary work reported here indicates: *1)* polymer particulate matter is released from at least some PVC roller pump tubing segments when pumped with a "just occlusive" roller pump; *2)* particle release by well-washed, well-prepared and properly selected activated carbon is about 200 to 1000 times below the level required for routine histological detection and a factor of 1 to 100 (by weight) less than that generated by PVC pump tubing segments; *3)* particle release by coated carbon is considerably lower than that for uncoated carbon, and is greatly dependent on the type of coating.

In addition, we know that PVC contains 30 to 50% plasticizer, commonly dioctylphthalate [18]. The dioctylphthalate is readily leached and released into the organism, and there is growing evidence that dioctylphthalate is relatively toxic [19]. Thus, one can suspect that PVC particles released into an organism will function as a local "drug" release system, releasing dioctylphthalate to the organism. It is thus possible that PVC particles may have physical and chemical effects on the organism. If we insist on composing a list of potential uremic toxins, PVC particles and dioctylphthalate should at least be considered.

It is imperative that particle release by extracorporeal circuits be quantitated and minimized.

References

1. In *Artificial Support Systems for Acute Hepatic Failure*, edited by Williams RS, London, Pittman, 1974, in press
2. Chang TMS: *Artificial Cells*. Springfield, Illinois, Thomas, 1972
3. Yatzidis H: A convenient haemoperfusion microapparatus over charcoal in the treatment of endogenous and exogenous intoxications. *Proc Eur Dial Transpl Assoc* 1:83–4, 1964
4. Andrade JD, Kopp K, Van Wagenen R, Chen C, Kolff WJ: Activated carbon and blood perfusion: A critical review. *Proc Eur Dial Transpl Assoc* 9:290–301, 1972
5. Davis TA: Activated carbon fibers in hemoperfusion devices. *Kidney Int* (Suppl. No. 3) 7:406–408, 1975.
6. Rosenbaum JL: Biocompatibility of resin haemoperfusion, in *Artificial Support Systems for Acute Hepatic Failure*, edited by Williams RS, London, Pittman, 1974, in press
7. Chang TMS, Coffey JF, Barre P, Gonda A, Dirks JH, Levy M, Lister C: Microcapsule artificial kidney: Treatment of patients with acute drug intoxication. *Can Med Assoc J* 108:429–433, 1973
8. Fennimore J: Design and development of Smith and Nephew Column, in *Artificial Support Systems for Acute Hepatic Failure*, edited by Williams RS, London, Pittman, 1974, in press
9. Chang TMS: Recent trends in biocompatible materials and microcapsular absorbents for kidney function replacement, in *Perspectives in Biomedical Engineering*, edited by Kenedi RM, London, University Park Press, 1972, pp. 39–43
10. Chang TMS: Platelet-surface interaction: Effect of albumin coating or heparin complexing on thrombogenic surfaces. *Can J Physiol Pharmacol* 52:275–285, 1974
11. Andrade JD, Coleman DL, Kim SW, Lentz DJ: Activated carbon coatings for optimal blood compatibility, in *Artificial Support Systems for Acute Hepatic Failure*, edited by Williams RS, London, Pittman, 1974, in press
12. Van Wagenen R, Stegall M, Lentz DJ, Andrade JD: Activated carbons for medical applications. I. *In vitro* microparticle characterization and solute adsorption, submitted
13. Andrade JD, Van Wagenen R, Chen C, Ghavamian M, Volder JGR, Kirkham R, Kolff WJ: Coated adsorbents for direct blood perfusion. II. *Trans Am Soc Artif Intern Organs* 18:473–483, 1972
14. Merrill JP: Treatment of drug intoxication. *N Engl J Med* 284:911–912, 1971
15. Hagstam KE, Larsson LE, Thysell H: Experimental studies on charcoal haemoperfusion in phenobarbital intoxication and uremia including histopathological findings. *Acta Med Scand* 180:593–603, 1966
16. Meyer MM: Blood pump occulsion. *J Extracorporeal Tech*, Fall, 1973, pp. 8–15
17. Boretos JW, Wagner FR: Particle fragmentation generated in pump sets. *J Biomed Mater Res* 5:411–413, 1971
18. Geertz W, Dyer K, Johnson D, Miller B, Taylor B, Sharp W: Polyvinyl chloride biomedical products. *Trans Am Soc Artif Intern Organs* 20: 1974, in press
19. Peterson RV: Toxicology of plastic devices having contact with blood. U.S. Government Report PB 224558, Sept., 1973

Streaming Potential Measurements of Biosurfaces

R. A. Van Wagenen and J. D. Andrade

Department of Material Science and Engineering, University of Utah, Salt Lake City, Utah 84112

and J. B. Hibbs, Jr.

*Veterans Administration Hospital and Department of Medicine, University of Utah Medical Center,
Salt Lake City, Utah 84132*

Streaming Potential Measurements of Biosurfaces

R. A. Van Wagenen and J. D. Andrade

Department of Material Science and Engineering, University of Utah, Salt Lake City, Utah 84112

and J. B. Hibbs, Jr.

Veterans Administration Hospital and Department of Medicine, University of Utah Medical Center, Salt Lake City, Utah 84132

ABSTRACT

A technique based on the measurement of streaming potentials has been developed to evaluate the electrokinetic region of the cell periphery. This approach is feasible for cell lines propagated in *in vitro* cell culture in monolayer form. The advantage of this system is that cells may be evaluated in the living state attached to a substrate. Thus it is not necessary to subject the cells to enzymatic, chemical, or mechanical trauma required to obtain monodisperse suspensions which are then normally evaluated by microelectrophoresis. In this manner it should be possible to study the influence of substrate and environmental factors on the charge density and potential at the cell periphery. The apparatus and procedure are described as well as some results concerning the electrokinetic (ζ) potential of borosilicate capillaries as a function of ionic strength, pH, and temperature. The effect that turbulence and entrance flow conditions have on accurate streaming potential measurements is discussed. The ζ-potential of BALB/c 3T12 fibroblasts has been quantitated as a function of pH, ionic strength, glutaraldehyde fixation, and Giemsa staining.

The electrokinetic properties of monodisperse suspensions of blood cells have been comprehensively investigated. Electrokinetic studies have been carried out on erythrocytes as a function of pH, ionic strength, and anion binding (1), various chemical treatments (2, 3), and proteolytic enzyme exposure (4). Similar studies have been conducted on lymphocytes (5), leukocytes (6, 7), and platelets (8). Seaman and Heard (9) have modified a microelectrophoresis apparatus originally designed by Bangham *et al.* (10) for analysis of biological materials in monodisperse form.

However, the great majority of cell types are not free and monodispersed in their natural state but, rather, are intimately associated in tissues. Investigators have attempted to characterize cells from *in vivo* sources (11) and cells from *in vitro* tissue cultures (12) using the microelectrophoresis technique. This usually necessitates a dissolution of the tissue or cell monolayer by mechanical, chemical, or enzymatic means to yield a monodispersed suspension. The assumption that such treatments do not significantly alter the peripheral region of the cells and thus their electrokinetic behavior is unsound. Ponder (13) and Seaman and Heard (14) have shown that trypsinization significantly reduces the electrophoretic mobility of human erythrocytes. Seaman and Uhlenbruck (4) extended this analysis to a number of proteolytic enzymes and erythrocytes derived from a variety of species. In most instances there was a significant alteration in measured electrophoretic mobility. Also, it is possible that the association of cells in tissues or monolayers in *in vitro* culture results in profound alterations in their electrokinetic properties compared to those commonly observed in suspension microelectrophoresis.

The initial objective of this research was to develop an apparatus and experimental technique which could directly measure the electrokinetic properties of cells grown in *in vitro* tissue culture. The approach chosen was based on the streaming potential phenomena originally quantitated by Helmholtz and Smoluchowski (15) and explained in some detail by Davies and Rideal (16).

The relationship between the measured streaming potential and the potential at the hydrodynamic shear plane, the zeta (ζ)-potential is given as

$$\zeta = \frac{4\pi\eta}{\epsilon} \frac{Estr}{P} \left[K_B + \frac{2K_s}{a} \right] \qquad [1]$$

where η and ϵ are viscosity and dielectric constant, respectively, in the diffuse double layer, $Estr$ is the streaming potential measured across the streaming capillary, P is the pressure difference across the capillary responsible for the flow of electrolyte, a is the radius of the capillary, and K_B and K_s are the specific bulk and surface conductance. The ζ-potential can be calculated from measurements of streaming potential and driving pressure if surface conductance is accounted for. This is accomplished by utilizing Eq. [2]

$$\zeta = \frac{4\pi\eta}{\epsilon} \frac{Estr}{P} \frac{C}{R} \qquad [2]$$

Here C is a predetermined system constant and R is the measured a-c resistance of the capillary-electrolyte system.

Normally Eq. [2] is utilized when ionic strength is so low that surface conductance comprises a significant proportion of the total conductance. At high ionic strengths, *i.e.*, physiological electrolyte concentrations, surface conductance is negligible compared to the total conductance, and Eq. [1] simplifies to Eq. [3]

$$\zeta = \frac{4\pi\eta K_B}{\epsilon} \frac{Estr}{P} \qquad [3]$$

K_B can then be determined in a standard conductivity cell utilizing platinized gray platinum electrodes. Viscosity and dielectric constant in the diffuse layer are assumed to be equal to bulk values; however, this is probably incorrect according to Hayden (17).

Ball and Fuerstenau (18) have reviewed the streaming potential literature in regard to $Estr/P$ data. They have concluded that, due to as yet unexplained flow and asymmetry potentials common to a wide variety of electrode types, the slope of the loci of $Estr$ data at a number of driving pressures in opposite flow directions ($\Delta Estr/\Delta P$) should be utilized in Eq. [1], [2], and [3]. This has been the case in this research where the loci of streaming potential data as a function of driving pressure in both flow directions have been fitted to a

linear regression best fit straight line using a Hewlett Packard (Model 9820A) programmable calculator.

Apparatus

The streaming potential apparatus is illustrated in Fig. 1. It is composed entirely of borosilicate (Corning 7740) glass with the exception of two sections of Silastic (Dow Corning polydimethyl siloxane medical grade) tubing (F) used to connect the streaming capillary (E) to the electrode chambers (C). The electrodes are of the silver, silver chloride type and are prepared by the anodic electrolytic deposition of an AgCl coating on a silver wire (A. D. Mackay, New York). The wire electrodes are in the form of a spiral and are epoxied into 7/15 $\overline{\textrm{S}}$ glass joints which mate with the electrode chambers. Two 200 ml reservoirs (A) serve as containers for the streaming fluid and are connected to the electrode chambers (C) and an N_2 pressure source via section B. Section D is a dip tube extending to the bottom of each reservoir. Sections A, B, C, and D are connected together via 7/15 and 19/22 $\overline{\textrm{S}}$ glass joints and were made small enough to be rf glow discharged prior to each streaming experiment.

The reservoirs are positioned in a constant temperature bath and stirring can be accomplished with a magnetic stirrer. The system pH (Corning Model 12 pH meter and glass electrode combination) and temperature (0-100°C, accurate to 0.1°C) can be monitored continuously. Purified N_2 gas (99.999% pure) serves as a pressure source utilized to drive the streaming fluid through the capillary. The four-way ball valve (V) (Whitey Model B-43YF2) simultaneously exposes one reservoir to N_2 driving pressure and the other to atmospheric pressure. A 90° rotation of the valve applies pressure to the opposite reservoir and reverses the electrolyte flow. Pressure is adjusted with a two-stage oxygen regulator (Matheson Gas Products Model 3104) with an adaptor for N_2 and a Tycos pressure gauge (T) (0-300 mm Hg, accurate to 1 mm Hg). The components of the pressure drive system are connected to the streaming apparatus via Silastic tubing. The streaming potential is measured with a high input impedance digital electrometer (Keithley Model 616), and the resistance or conductance of the streaming fluid is measured with an a-c bridge at a frequency of 1 kHz (General Radio Model 1650B). The streaming apparatus is electrically isolated from extraneous electrical signals by a Faraday cage (copper screen 50 mesh/in.) (FC).

Procedure

Streaming potential data were obtained by measuring streaming potentials at a driving pressure of 2 cm Hg, then reversing the flow direction and repeating the measurement. The driving pressure was increased by 2 cm Hg and streaming potentials were again measured in both flow directions. This process was repeated until the driving pressure reached 12-14 cm Hg. The slope, $\Delta Estr/\Delta P$, of the best fit straight line was utilized in Eq. [3]. Solution specific conductance was determined in a precalibrated cell with platinized platinum electrodes. The cell constant, C, of the streaming capillary and the conductivity cell were predetermined using a 0.1N KCl solution of known specific conductance (19). Following streaming measurements, the resistance of the capillary electrode system was measured with the a-c bridge. In most instances where ionic strength was high, solution conductance masked surface conductance and K_B was determined in a conventional conductivity cell. Equation [3] was then utilized. This was the case for all data reported here.

Radio frequency glow discharge (RFGD) of the streaming cell components was carried out to eliminate problems with surface contamination which occasionally developed. RFGD (Commercial Plasmod System, Tegal Corporation, Richmond, California) in argon gas at 100 μm Hg and an rf power density of 50W for 5 min was highly effective in removing surface contamination.

All chemicals utilized were analytical reagent grade (Fisher Scientific Company, Fairlawn, New Jersey). Water used in this study was twice distilled over Pyrex glass (Corning Still Model AG-11) and had a conductivity of 1 ± 0.1 μmho/cm. Phosphate buffered saline (PBS) was made up as 0.145M NaCl, 2×10^{-4}M KH_2PO_4, and 8×10^{-4}M Na_2HPO_4 using twice distilled water. Glutaraldehyde was employed as a fixative in a 2% (v/v) solution in PBS (obtained in purified form as an 8% (v/v) unbuffered aqueous solution sealed under pure N_2 from Polysciences, Incorporated, Warrington, Massachusetts). Giemsa biological stain (Fisher Scientific Company, Fairlawn, New Jersey) was utilized at 10% (v/v) in twice distilled water. Nigrosin (Eastman Organic Chemicals, Rochester, New York) dye exclusion was used as a test of membrane viability at a concentration of 1% (wt/v) in PBS. Dulbecos modified Eagle Medium (Grand Island Biological Labs) supplemented with penicillin (100 units/ml), streptomycin (100 mg/ml), and 20 mM HEPES (N-2-hydroxyethyl piperazine-N-2-ethane sulfonic acid, ICN Pharmaceuticals, Cleveland, Ohio) buffer was utilized as the cell culture medium and will be referred to as DMM. Fetal bovine serum (fbs) was added as specified.

An established line of BALB/c 3T12 mouse fibroblasts (noncontact-inhibited, tumorigenic cells) were cultured to confluency in borosilicate capillaries 600 ± 20 μm ID. The cells were harvested from milk dilution bottles by trypsinization [6 ml of 0.25% (v/v) trypsin], resuspended in DMM supplemented with 10% (v/v) fbs, and centrifuged at 200g for 5 min. The cells were then resuspended in DMM, counted in a hemocytometer, washed in DMM twice, and resuspended at a seeding concentration of 1×10^6 cell/ml in DMM. The cells were seeded by drawing the cell suspension into the capillary using a 1 cm^3 syringe. Both ends of the capillary were capped with Silastic tubing and clamps; the capillary was placed in an incubator at 37°C, 90% humidity, and 95% air/5% CO_2 for 20-30 min. This was sufficient time to allow the cells to contact and form an adhesive bond with the glass surface. Fresh DMM supplemented with 10% (v/v) fbs was then drawn into the capillary. After approximately 5-10 hr the capillary was removed from the incubator and reseeded in another position on the internal circumference in the same manner. Four to five cell seedings over a 24-36 hr period were sufficient to get a uniform distribution of cells on the interior of the capillary. Glass syringes of 30 ml capacity were attached to each end of the capillary via Silastic rubber tubing. Supplemented medium (DMM, 10% fbs) was continuously perfused through the capillary at a flow rate of 0.5 ml/hr using a Sage syringe pump (Sage Instruments Model 341). This was sufficient to keep the cells metabolically and mitotically
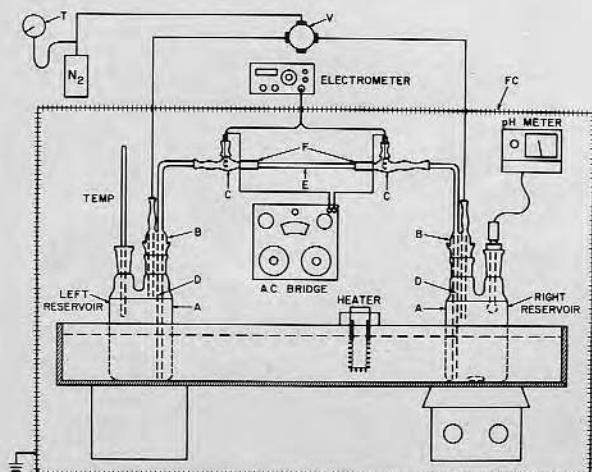

Fig. 1. A schematic diagram of the streaming potential apparatus

Table I. Composition of aqueous electrolyte utilized in electrokinetic evaluation of living cells

Component	Millimoles/L of component
NaCl	133.00
CaCl$_2$	1.80
KCl	5.36
MgSO$_4$ · 7H$_2$O	0.81
KH$_2$PO$_4$	0.20
Na$_2$HPO$_4$	0.80
D-glucose (anhydrous)	5.55

active, and after 24-36 hr the cells had proliferated to monolayer density.

The capillary was removed from the perfusion apparatus and rinsed in 5 ml of cell streaming solution (Table I) at 5 ml/min. It was then inserted into the streaming apparatus and evaluated within 10-15 min. Following this, the cells in the capillary were fixed in a 2% (v/v) glutaraldehyde PBS solution for 30 min at 37°C. After fixation the electrokinetic properties of the cells were evaluated as a function of *pH* and ionic strength. When the electrokinetic evaluations were completed, the cells were stained in a 10% Giemsa solution in distilled water, reevaluated electrokinetically, and photographed in both transmitted light and the scanning electron microscope. The cells on glass substrates were post fixed in 1% osmium tetroxide PBS solution at 37°C for 15 min, dehydrated in a graded series of ethanol water solutions, critical point dried in liquid CO$_2$, mounted, coated with carbon and gold, and observed in a Cambridge stereoscan scanning electron microscope.

For streaming studies on glass and cell monolayers as a function of *pH*, *pH* was adjusted with solutions of NaOH or KOH and HCl having the same ionic strength as the streaming solution. In all studies where *pH* was maintained constant, phosphate buffer (2 × 10^{-5}M KH$_2$PO$_4$, 8 × 10^{-5}M Na$_2$HPO$_4$) was added to the streaming electrolyte. The temperature was maintained constant at 24°C in all studies.

Results and Discussion

Preliminary investigations concerning the effect of capillary geometry on measured streaming potential indicated a linear decrease in $\Delta Estr/\Delta P$ as the length of the capillary decreased. This was at odds with the conclusion inherent in the derivation of the streaming potential equation in that capillary geometry should not affect the streaming potential. An analysis of flow turbulence and entrance effects on streaming potential was carried out to determine the cause of the discrepancy.

Figure 2 is an *Estr vs. P* plot for two streaming tubes. Tube A is 600 μm ID and 30 cm in length, while tube
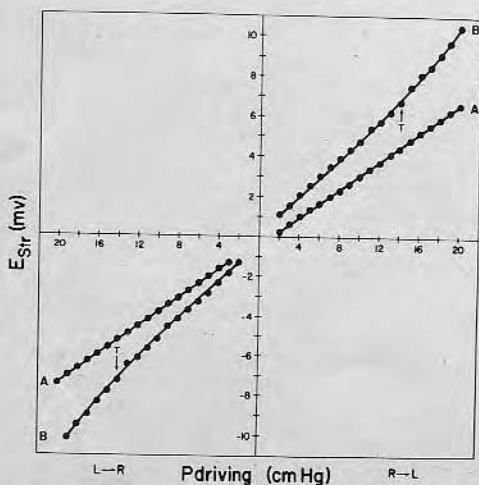
B is 1250 μm ID and 30 cm long. In the case of tube A the data is linear and the slope ($\Delta Estr$ vs. ΔP) is equal in both flow directions. Measured flow rates and subsequently calculated Reynolds numbers indicated laminar flow throughout the measured pressure range for tube A. In the case of the larger tube (B), the data at low driving pressures is linear and the slopes are equal in both flow directions; however, at a pressure of 14 cm Hg the flow becomes turbulent ($R > 2000$) and the data becomes nonlinear at higher driving pressures. This seems to indicate a marked deviation in the $\Delta Estr/\Delta P$ data obtained if the flow changes from laminar to turbulent. This is at odds with data published by others (19) for turbulent flow in aqueous systems. One can also see a difference in $\Delta Estr/\Delta P$ for tubes A and B which would seem to indicate that turbulent flow is not the only cause of deviations in the calculated ζ-potential for tubes of various sizes.

The results of streaming potential studies on borosilicate capillaries as a function of length and internal diameter are shown in Fig. 3. Each tube was evaluated at its greatest length and then successive portions were removed and it was reevaluated. This was continued until no tube remained. The only variable was length since η and ϵ are assumed constant and K_B greatly predominated over K_s at this high ionic strength (0.01 g ions/L). Capillaries B (1284 ± 34 μm ID) and C (595 ± 15 μm ID) were commercial borosilicate; there was no significant variation in ID along the length. Both capillaries exhibited a constant $\Delta Estr/\Delta P$ value until a critical length was reached whereupon there was a marked drop in $\Delta Estr/\Delta P$. The critical length (L_c) at which this occurred was 58 cm for tube B and 20 cm for tube C. Capillary A was hand drawn from a larger tube. There were significant variations in ID along its length. Points 1 and 2 shown in Fig. 3 were obtained when the capillary was 190 ± 12 μm ID, while equivalent lengths taken from the center of the tube gave lower $\Delta Estr/\Delta P$ values and had an ID of 160 ± 5 μm. This would seem to indicate that at lengths less than some critical length the diameter and length of the streaming capillary markedly affect the measured streaming potential, while at lengths greater than L_c minor variations in diameter and length have no measurable effect.

The onset of turbulent flow does not seem to cause this behavior since flow was laminar in all cases for tubes A and C and there seemed to be no significant effect due to turbulent flow for tube B. If one compares the measured flow rates, Q_m, in the three tubes with the theoretical flow rates, Q_t, calculated using Poiseuille's law as expressed in Eq. [4]

$$Q_t = \frac{\pi}{8} \frac{r^4}{\eta} \frac{dP}{dX} \qquad [4]$$

Fig. 2. *Estr vs. Pdriving* for two borosilicate capillaries A and B. The streaming solution was 0.01M KCl buffered to a *pH* of 7.
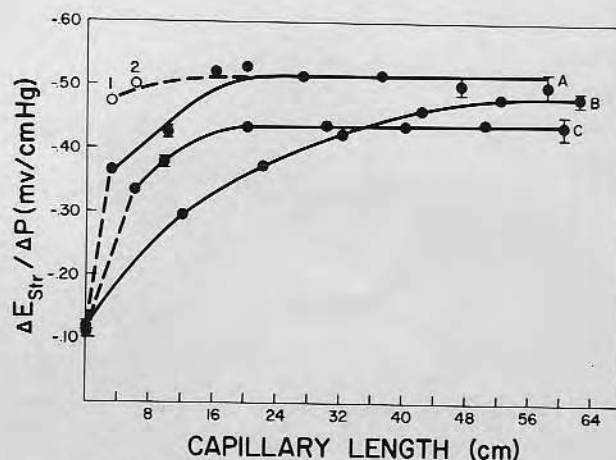
Fig. 3. $\Delta Estr/\Delta P$ vs. streaming tube length for three borosilicate tubes A, B, and C. The streaming solution was 0.01M KCl buffered to a *pH* of 7. Error ranges correspond to one standard deviation.

where r is the tube radius, η is the fluid viscosity, and dP is the pressure drop across a flow length dX, it is found that Q_t and Q_m are equal until the critical length, L_c, is reached, *i.e.*, 20 cm for tube C and 58 cm for tube B. It can be concluded from this that the streaming data and calculated ζ-potential are independent of capillary geometry (the variations in plateau values of $\Delta Estr/\Delta P$ are expected since the tubes were from different sources and most probably had different surface histories) as long as Poiseuille flow exists. This is what Helmholtz predicted as Bocquet has pointed out (20). Poiseuille flow actually requires that four basic conditions exist, *i.e.*, the flow is steady, incompressible, laminar, and established.

Many investigators have simply ignored the established flow criteria. It takes a certain length, L_e, past the entrance of a cylindrical flow system, to establish a parabolic velocity profile during steady laminar flow of an incompressible fluid. The value of L_e has been found both experimentally (21) and theoretically (22) to be given by Eq. [5]

$$L_e \simeq 0.06RD \qquad [5]$$

Here R is the Reynolds number and D is the diameter. On the basis of this analysis, it seems that if L_e is greater than $10 \pm 1\%$ of the total streaming tube length, the $\Delta Estr/\Delta P$ ratio and subsequently calculated ζ-potential will be anomalously low.

Electrode asymmetry at high ionic strength can develop, particularly if the electrodes have aged appreciably over the course of several months' use, and if they have been exposed to protein or other adsorbable solutes. This is illustrated in Fig. 4. Curves 8B through 12B were obtained utilizing silver, silver chloride electrodes which had previously been exposed to a streaming capillary with a surface of adsorbed fetal bovine serum. The asymmetry developed at that time. It was absent in earlier experiments at high ionic strength (0.1 g ions/L) where protein was not present (not shown). The asymmetry diminished with continuous streaming of electrolye in approximately 30 min (8B-10B). As long as streaming continued, the slope $\Delta Estr/\Delta P$ (10B-12B) remained constant.

If flow ceased for any length of time, asymmetry reappeared and it required another 30-40 min of streaming to obtain good linearity and reproducibility. At lower ionic strength (0.01 g ions/L) the asymmetry was not evident (1B and 4B, Fig. 4). When fresh electrodes were prepared and protein contamination was absent, there was no deviation from linearity at low ionic strength (0.01 g ions/L) or high ionic strength (0.1 g ions/L) as shown in Fig. 5.

The asymmetry exhibited by aged silver, silver chloride electrodes at high ionic strength may be due
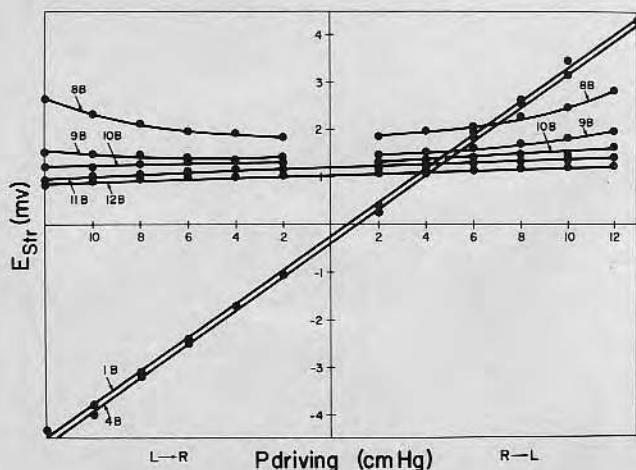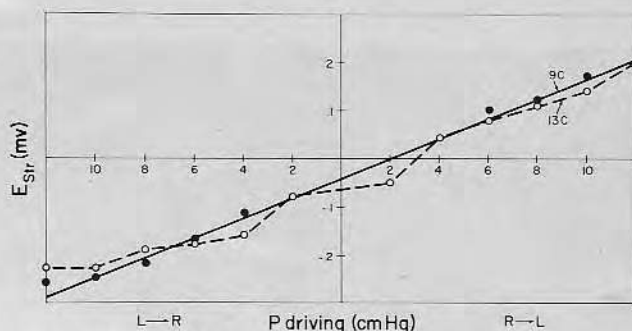
Fig. 5. *Estr vs. Pdriving for a borosilicate capillary.* The streaming solution was 0.1M KCl. 13C was immediately after chloridization while 9C was after equilibration and short-circuiting in streaming solution for 30 min.

to protein adsorption in the pores of the AgCl coating. Janz and Ives (23) maintain that silver may form stable complexes with amino and sulfhydryl groups of organic molecules which can compete with the insolubility of the AgCl thus negating the proper functioning of the electrodes. It has also been suggested (23) that 10-25% of the silver should be chloridized to AgCl to produce electrodes having good reproducibility and stability. The electrodes exhibiting asymmetry problems had only 1% conversion (assuming 100% current efficiency) of Ag to AgCl. Srinivasan (24) has recommended that silver, silver chloride electrodes be prepared in a slowly alternating a-c fashion utilizing anodic deposition of AgCl and cathodic current to increase surface area by enhanced pore formation. The above recommendations were followed. Silver, silver chloride electrodes were prepared electrolytically with a slowly alternating current (5 min anodic, 2 min cathodic, etc.); the gross surface area per electrode was 1 cm^2 and the net anodic current density time product was 6.9 A-sec/cm^2. There was a theoretical conversion of silver to silver chloride of 16%. Electrodes freshly prepared in this fashion are stable and have never shown prolonged asymmetry at high ionic strength even upon protein adsorption.

Figure 6 comprises 4 SEM micrographs of silver, silver chloride electrode surfaces. The general shape of the electrodes used in this study are shown in Fig. 6a. They consist of silver wire coils 6 mm long and 3.8 mm OD. The gross surface area is 1 cm^2. Figure 6b illustrates the AgCl surface of a freshly prepared electrode (anodic 5 mA/cm^2 for 4 min, 1% conversion of Ag to AgCl). A number of pores can be seen as well as some microgranularity on a cobblestone surface. Figure 6c is the same electrode after approximately 3 months use. This was the same electrode which developed asymmetry at high ionic strength and protein exposure. The cobblestone appearance is still partially evident; however, much of the pore structure and all of the microtexture are lost. The pores between the cobblestones are now replaced by smaller pores in an incomplete cobblestone structure. Figure 6d is the surface of a freshly prepared electrode employing the alternating anodic and cathodic deposition of AgCl previously described. The highly porous structure obviously increases the surface area available for current transport. Electrodes prepared in this manner have not exhibited asymmetry at high ionic strength and exposure to protein solutions as long as they are equilibrated several hours prior to use.

The calculated ζ-potential of borosilicate glass as a function of temperature is shown in Fig. 7. The standard deviations at both ionic strengths are rather large, particularly for 0.1M NaCl. This is due primarily to the variation in $\Delta Estr/\Delta P$ slopes obtained at various temperatures and not so much to the inability to get accurate slopes at constant equilibrium temperatures. Due to the wide standard deviations it can only be con-

Fig. 4. *Estr vs. Pdriving for a borosilicate capillary.* The streaming solution was 0.1M KCl (unbuffered) for curves 8B-12B and 0.01M KCl (unbuffered) for curves 1B and 4B.
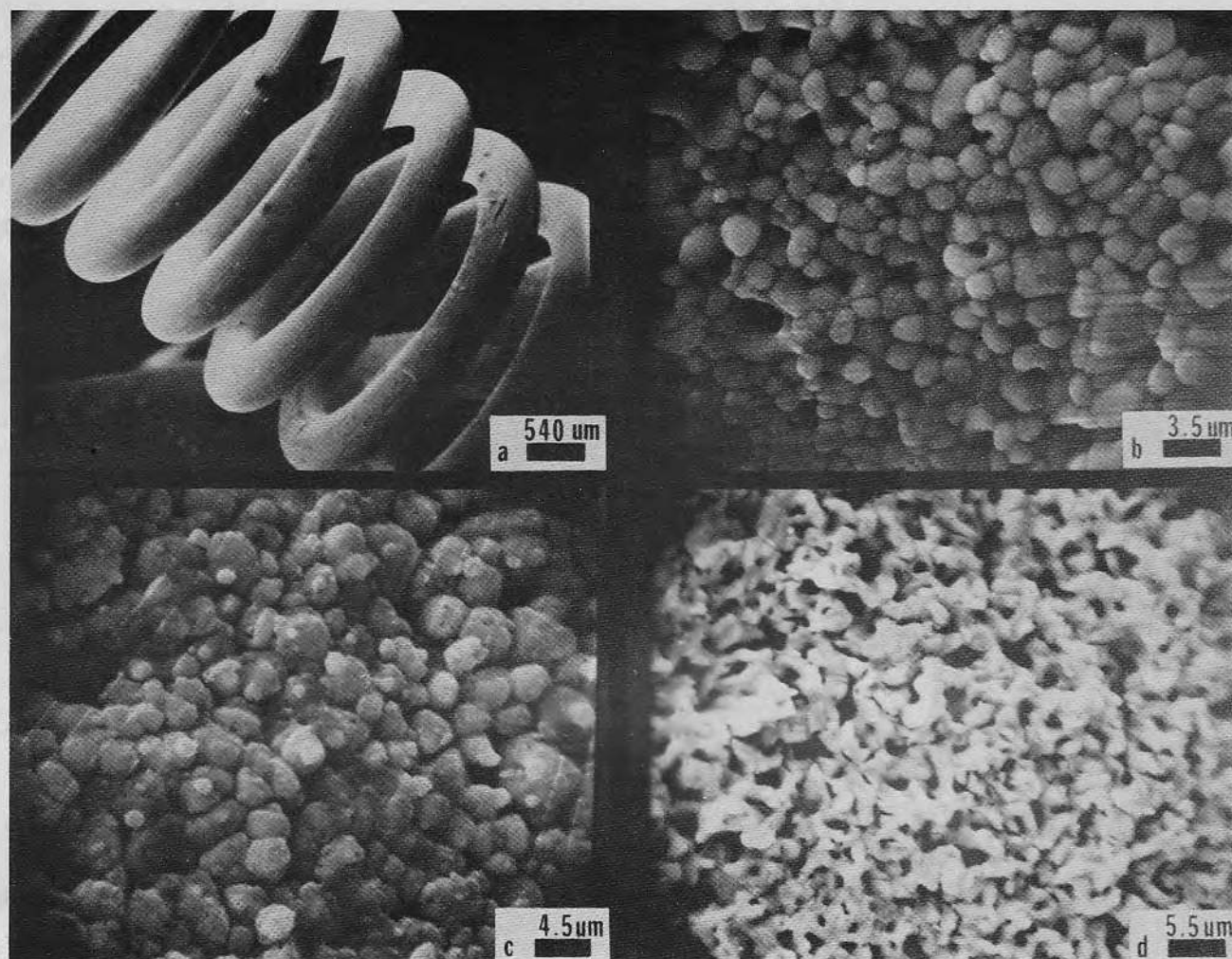
Fig. 6. SEM micrographs of silver, silver chloride electrode surfaces

cluded that there is no statistically significant variation in ζ as a function of temperature.

The variation in ζ-potential with pH for borosilicate glass is shown in Fig. 8. The data indicates that borosilicate has a pKa of ~ 5.7 assuming that all the surface charge is due to the ionization of ionogenic $\equiv$ Si-OH (silanol) groups in the hydrated region of the glass. This is at variance with the data of Hair and Hertl (25) and Marshall *et al.* (26) which suggests a pKa for surface silanol groups of 7.1-7.2. However, it is quite prob-

able that high concentrations of hydronium ions exist in the hydrated surface region of the glass due to cation exchange. If this were the case, the ζ-potential at acidic pH could be considerably less than that occurring as a result of charge generation purely by ionogenic silanol groups. The result would be an apparent shift in pKa. A second cause of the discrepancy may be due to the presence of boranol groups ($\equiv$ B-OH) in significant numbers at the hydrated surface of borosilicate glass. The proportion of boron to silicon in the porous surface may be as high as 1:3 rather than 1:18
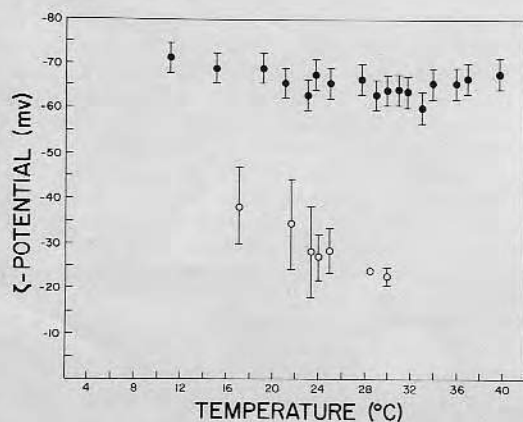
Fig. 7. Calculated ζ-potential of borosilicate glass as a function of temperature. Streaming solution was 0.01M KCl ($\bullet$) and 0.1M NaCl ($\bigcirc$); both solutions were buffered to a pH of 7.0. Error ranges correspond to one standard deviation.

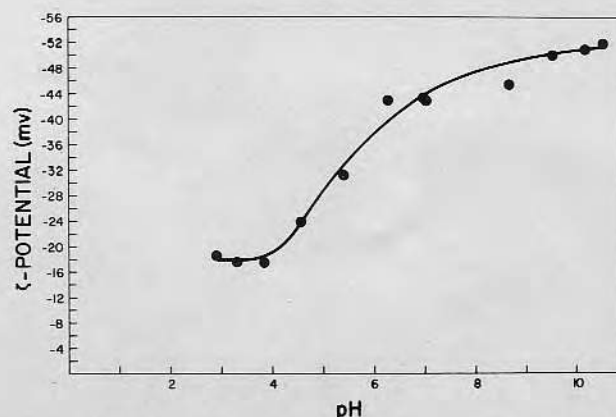**Fig. 8.** Calculated ζ-potential of borosilicate glass as a function of pH. Streaming solution is 0.01 KCl. The pH was altered with KOH and HCl solutions of the same ionic strength.

as expected in the bulk (27). The pKa of boranol groups is 5.1 and this would also tend to shift the resultant surface pKa to a more acidic region.

Figure 9 illustrates the increase in ζ-potential with decreasing ionic strength (KCl) at constant pH (7.1) and temperature (24°C). The linear portion of the curve corresponds to the expansion of the electrical double layer as ionic strength decreases. At an ionic strength of less than 3×10^{-4} g ions/L there is a deviation from linearity due to the onset of surface conductance which was not accounted for in the calculation of ζ. This is in agreement with the detailed analysis of surface conductance made by Rutgers and DeSmet (28) and Li and DeBruyn (29).

Streaming potential studies on living 3T12 cells were carried out using cell streaming solution as described in Table I. It was necessary to incorporate divalent cations and glucose in the electrolyte to maintain good cell substrate adhesion during streaming since the high flow rates (typically 10 cm³/min) are sufficient to shear off cells with altered adhesive properties. Even in the solution used, the cells begin to lose adhesiveness after approximately 20 min. For this reason streaming evaluations on living cells were limited to 10-12 min. Nigrosin staining (30) of 3T12 cells indicated that their membranes retained semipermeability for more than 60 min in streaming solution, even though most cells had retracted off the surface in monolayer sheets. Apparently, the cells sacrifice cell-substrate bonds rather than cell-cell bonds and retain membrane function and viability even after 60 min of exposure to streaming solution at room temperature. The ζ-potential of living cells was −28.8 ± 2.5 mV (streaming solution Table I, ionic strength 0.145, pH 7.3, temperature 24°C). Following 2% glutaraldehyde fixation, the ζ-potential dropped to −17.6 ± 2.6 mV under the same conditions. The decrease in electrokinetic potential following glutaraldehyde fixation may be due to a loss of free draining volume in the cell periphery, that is, the region of hydrodynamic slip containing a portion of the peripheral charge is eliminated due to glutaraldehyde cross-linking of membrane protein, thus preventing the detection of this charge by electrokinetic techniques. Following fixation the cells were evaluated as a function of ionic strength and pH.

The effect of pH on fixed 3T12 cells is shown in Fig. 10. Ionic strength was constant at 0.01 g ions/L (NaCl). In a qualitative sense the data is similar to that of Vassar et al. (3) for fixed human erythrocytes. In the plateau region from pH 7 to 10 there is no variation in ζ-potential; however, there is a precipitous and quite linear decrease in ζ-potential below pH 6 indicating the presence of an ionogenic molecular type(s) with an acidic pKa of 4.5 or less. There is no indication of an
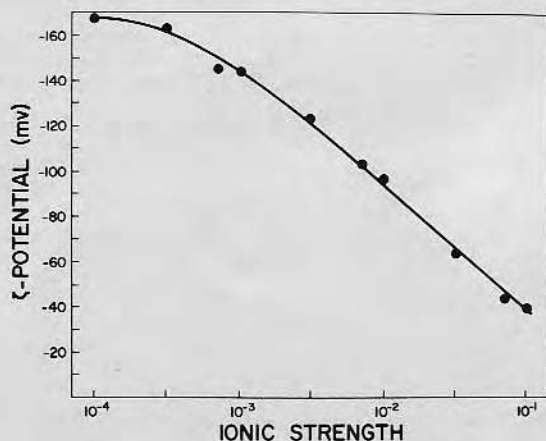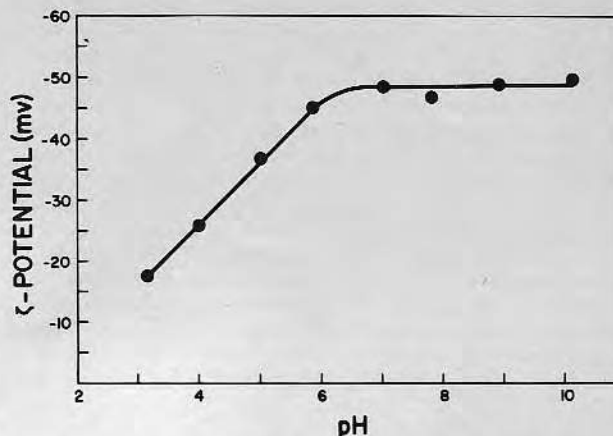

Fig. 10. Calculated ζ-potential of 3T12 cells cultured in borosilicate capillaries following fixation in glutaraldehyde. The streaming solution was 0.01M NaCl. The pH was altered with NaOH and HCl solutions of equal ionic strength.

ionogenic species of pKa ∼ 6.5 due to glutaraldehyde fixation as reported by Vassar et al. (3). This discrepancy is further accentuated when it is realized that glutaraldehyde fixation caused a 38% decrease in the ζ-potential of 3T12 fibroblasts, while it resulted in about a 10% increase in electrophoretic mobility of human erythrocytes. However, when making comparisons of this sort and attempting to see relationships, it should be kept in mind that at least two variables could and probably do invalidate any present attempt at comparison. (i) Different electrolyte components, ionic strengths, and buffers were utilized. (ii) Cell types evaluated were different.

The ζ-potential as a function of ionic strength (NaCl) relationship for fixed 3T12 cells is shown in Fig. 11. The expansion of the double layer at lower ionic strength results in a higher ζ-potential. The increase is quite linear, and there is no indication of the predominance of surface conductance at low ionic strengths $(1 \times 10^{-3}$ g ions/L). This data is similar to that of Heard and Seaman (1) for unfixed human erythrocytes; however, in the case of 3T12 cells, the slope over the ionic strength range 0.1-0.01 g ions/L is not as steep as is the case for the erythrocytes. Here again the differences between cell type, fixation, and the presence of sorbital during microelectrophoresis prevents direct comparison.

Following the evaluation of the 3T12 electrokinetic surface, i.e., that region of the cell periphery within ∼ 10A of the hydrodynamic shear region, several

Fig. 9. Calculated ζ-potential of borosilicate glass as a function of ionic strength. The streaming solution is KCl buffered to a pH of 7.1.
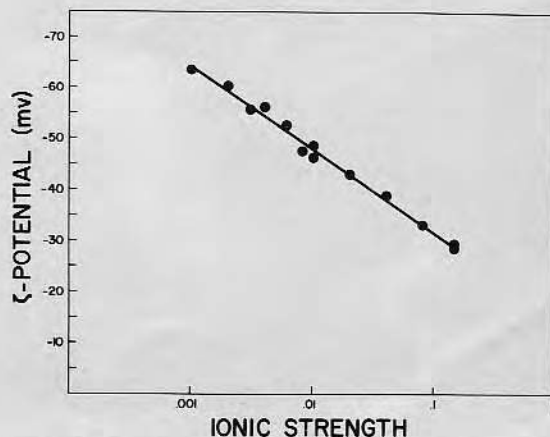

Fig. 11. Calculated ζ-potential of 3T12 cells following fixation in glutaraldehyde as a function of ionic strength. Streaming solution was NaCl buffered to a pH of 7.3.

streaming experiments were repeated under identical conditions of ionic strength and pH. There was no significant deviation from original data after 5 days storage in PBS. This would seem to substantiate the assumption that glutaraldehyde fixation produces a stable cell membrane in the electrokinetic sense. The cells were stained in Giemsa to enhance microscopic evaluation of the uniformity of the 3T12 cell layer. Giemsa staining at 25°C for 8 min resulted in a 20% reduction in calculated ζ-potential, *i.e.*, -46.2 ± 1.3 mV to -36.7 ± 0.8 mV (0.01M NaCl, phosphate buffer, 25°C, pH 7.2).

Comparative scanning electron micrographs of stained and unstained 3T12 monolayers indicated that Giemsa-stained cells were altered morphologically. Nonstained cells were well spread and in contact with the substrate, while stained cells had a more rounded appearance and had lost some contact with the glass. The decrease in ζ-potential may have been due to the effect of Giemsa stain on the cell periphery or the altered morphology of the cells. Giemsa is composed of Azure II, Eosin, glycerin, and methanol and any of these may have been the cause of the decrease in ζ.

Recently, a technique of evaluating cells cultured in capillary tubes utilizing electroosmosis has been reported by Fike and Van Oss (31). The advantage of this approach is that the cells may be evaluated for long times in the living state; however, the disadvantage is that the ionic strength must be an order of magnitude lower than physiological to obtain accurate measurements.

In conclusion, a streaming potential apparatus and technique have been developed which make it possible to evaluate the electrokinetic properties of cells grown in *in vitro* cell culture. The results for borosilicate glass substrate and 3T12 mouse fibroblasts cultured to confluency on this substrate attest to the feasibility of the approach. The usefulness of various electrokinetic techniques applied to investigations of cell membranes has been established. Microelectrophoresis, streaming potential, and electroosmosis have all been utilized on various cell types, but no single technique seems feasible for a detailed study of a wide variety of cells under all conditions. Rather, the three mentioned techniques must be utilized in conjunction to gain a more complete understanding of the similarities and differences in cell membranes over a wider range of cell types.

Acknowledgments

LIST OF SYMBOLS

ζ	zeta potential (mV)
η	viscosity in double layer (poise)
ϵ	dielectric in double layer
E_{str}	measured streaming potential (mV)
P	pressure difference driving electrolyte through capillary (cm Hg)
a	capillary radius (cm)
K_B	specific bulk conductance (mho/cm)
K_s	surface conductance (mho)
R	resistance (Ω)

REFERENCES

1. D. H. Heard and G. V. F. Seaman, *J. Gen. Physiol.*, **43**, 635 (1960).
2. D. A. Haydon and G. V. F. Seaman, *Arch. Biochem. Biophys.*, **122**, 126 (1967).
3. P. S. Vassar, J. M. Hards, D. E. Brooks, B. Hagenberger, and G. V. F. Seaman, *J. Cell Biol.*, **53**, 809 (1972).
4. G. V. F. Seaman and G. Uhlenbruck, *Arch. Biochem. Biophys.*, **100**, 493 (1963).
5. P. S. Vassar, J. M. Hards, and G. V. F. Seaman, *Biochim. Biophys. Acta*, **291**, 107 (1973).
6. P. S. Vassar, M. J. Kendall, and G. V. F. Seaman, *Arch. Biochem. Biophys.*, **135**, 350 (1969).
7. G. V. F. Seaman, P. S. Vassar, and M. J. Kendall, *ibid.*, **135**, 356 (1969).
8. G. V. F. Seaman and P. S. Vassar, *ibid.*, **117**, 10 (1966).
9. G. V. F. Seaman and D. H. Heard, *Blood*, **18**, 599 (1961).
10. A. D. Bangham, D. H. Heard, R. Flemans, and G. V. F. Seaman, *Nature (London)*, **182**, 642 (1958).
11. I. Simon-Reuss, G. M. W. Gook, G. V. F. Seaman, and D. H. Heard, *Cancer Res.*, **24**, 2038 (1964).
12. T. Yamada, T. Takaoka, H. Katsuta, M. Namba, and J. Sato, *Jpn. J. Exp. Med.*, **42**, 377 (1972).
13. E. Ponder, *Blood*, **6**, 350 (1957).
14. G. V. F. Seaman and D. H. J. Heard, *J. Gen. Physiol.*, **44**, 251 (1960).
15. M. Helmholtz, *Wied. Ann.*, **7**, 337 (1879); M. Smoluchowski, "Handbuch der Elektrizitat und des Magnetismus," Vol. 11, Graetz, Editor, p. 366, Barth, Leipzig (1921).
16. J. T. Davies and E. K. Rideal, "Interfacial Phenomena," 2nd ed., p. 108, Academic Press, New York (1963).
17. D. A. Haydon, *Recent Prog. Surf. Sci.*, **1**, 94 (1964).
18. B. Ball and D. W. Fuerstenau, *Miner. Sci. Eng.*, **5**, 267 (1973).
19. G. Jones and B. C. Bradshaw, *J. Am. Chem. Soc*, **55**, 1780 (1933).
20. P. E. Bocquet, Ph.D. Thesis, University of Michigan (1952).
21. L. Prandtl and O. G. Tietjens, "Applied Hydro- and Aeromechanics," p. 22, McGraw-Hill Book Co., New York (1934).
22. H. L. Langhaar, *Trans. Am. Soc. Mech. Eng.*, **64**, A55 (1942).
23. G. T. Janz and D. J. C. Ives, *Ann. N. Y. Acad. Sci*, **148**, 210 (1968).
24. S. Srinivasan, Personal communication.
25. M. L. Hair and W. J. Hertl, *J. Phys. Chem.*, **74**, 91 (1970).
26. K. Marshall, G. L. Ridgewell, C. H. Rochester, and J. Simpson, *Chem. Ind. (London)*, **19**, 775 (1974).
27. F. M. Ernsberger, *Annu. Rev. Mater. Sci.*, **2**, 529 (1972).
28. A. J. Rutgers and M. DeSmet, *Trans. Faraday Soc.*, **43**, 102 (1947).
29. H. C. Li and P. L. DeBruyn, *Surf. Sci.*, **5**, 203 (1966).
30. J. P. Kaltenbach, M. H. Kaltenbach, and W. B. Lyons, *Exp. Cell Res.*, **15**, 112 (1958).
31. R. M. Fike and C. J. Van Oss, Personal communication.

Flat Plate Streaming Potential Investigations: Hydrodynamics and Electrokinetic Equivalency

R. A. VAN WAGENEN AND J. D. ANDRADE

Department of Bioengineering, College of Engineering, University of Utah, Salt Lake City, Utah 84112

The accurate measurement of streaming potentials in either capillaries or flat plate systems requires Poiseuille flow, i.e., flow must be steady, incompressible, laminar, and established. The established flow stipulation is rarely addressed yet it is of critical importance. Our findings suggest that while the onset of turbulence causes no abrupt change in the streaming potential, flow must be established throughout at least 90% of the flow field for accurate streaming potential measurement. The development of a flat plate flow system based on $(1 \times 25 \times 75)$ mm plates is discussed in light of the hydrodynamic requirements. The electrokinetic equivalency between plates and capillaries of the same material is discussed and the small discrepancy is attributed to surface roughness and possible differences in surface chemical composition. The flat plate system offers substantial advantages over capillaries in that both surface treatments and analyses via a variety of quantitative techniques are greatly facilitated.

INTRODUCTION

The measurement of a streaming potential across a porous plug or capillary can provide information concerning both the zeta-potential, ψ_ζ, and the net charge density, σ_ζ, at the hydrodynamic shear plane. Such electrical parameters may be important factors governing the biocompatibility of prosthetic devices exposed to blood or tissue (1). The streaming potential and thus ψ_ζ is valid and independent of flow geometry only if certain hydrodynamic stipulations are met, i.e., fluid flow must be steady, incompressible, laminar, and established (2). The last two conditions generally limit the applicability of streaming measurements to long capillary tubes or porous plugs of compacted particles or fibers. Consequently, the surface under investigation cannot be easily probed by various other quantitative surface techniques.

Our approach to this impasse has been to develop a streaming cell configuration based on flow between two flat, parallel plates. This simplifies substrate preparation involving macroscopic plates rather than capil-laries or small particles. However, the major advantage is the greatly facilitated utilization of a variety of quantitative surface analysis techniques to study the same surface, i.e., streaming potential, ellipsometry, total internal reflectance fluorescence, light and electron microscopy, and X-ray photoelectron spectroscopy (XPS). Such a plate approach has recently been utilized by DePalma to study the adsorption of fibrinogen on germanium substrates (3).

This paper describes a streaming cell system designed for the electrokinetic analysis of both capillaries and flat plate samples. Hydrodynamic limitations and results for both capillary and flat plate systems are discussed and some comparative analyses of similar glass substrates in capillary and plate form are presented.

STREAMING POTENTIAL EQUATION: FLAT PLATE GEOMETRY

The following derivation of the streaming potential equation is based on that of a

cylindrical conduit (4) (see also Ref. 3). The flow system consists of two parallel plates of length L and width C separated by a distance $2b$ where $L > C \gg 2b$ (Fig. 1a). Poiseuille conditions prevail throughout the system, i.e., the flow is steady, incompressible, laminar, and established.

The following equation describes the parabolic velocity profile between the plates as derived by Eskinazi (5)

$$V = \frac{P}{2\eta L}(y^2 - b^2) \qquad [1]$$

where P is the driving pressure across the conduit of length L; bulk electrolyte viscosity is η and y is the vertical coordinate. Differentiation gives the velocity gradient close to the wall as
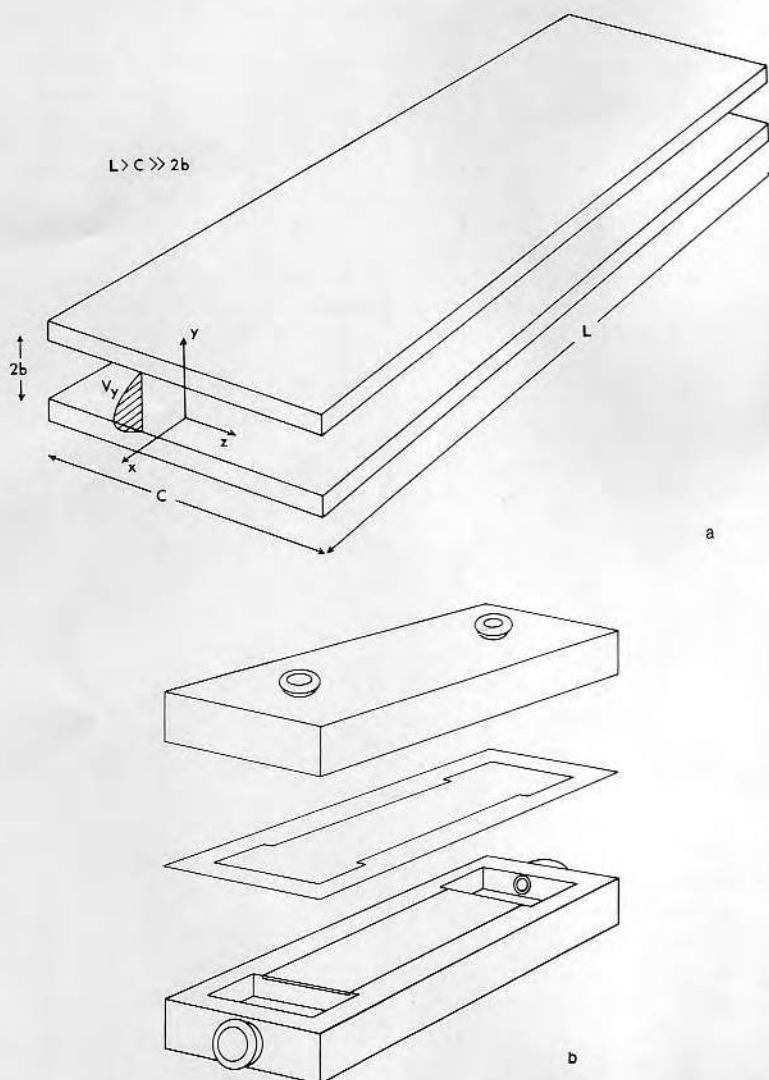

FIG. 1. (a) Coordinate system schematically depicting established laminar flow between two parallel plates of length L, width C, and spacing $2b$. (b) Block cell design for parallel plate streaming potential measurements showing electrode ports, flow ports, and a Teflon gasket which serves as a plate spacer.

$$\left(\frac{dV}{dy}\right)_{y=b} = \frac{yP}{\eta L} = \frac{bP}{\eta L} . \qquad [2]$$

Ordinarily, the effective thickness of the diffuse ionic atmosphere, κ^{-1}, is much thinner than the macroscopic thickness of the conduit and the velocity, V, at any distance, s, away from the wall ($s = b - y$) is obtained by integrating Eq. [2] over s,

$$V = \int_0^s \left(\frac{dV}{dy}\right)_{y=b} ds = \frac{bPs}{\eta L} . \qquad [3]$$

The charge transported by the flowing electrolyte is the streaming current, I_{str}.

$$I_{str} = 2C \int_{s=0}^{s=b} \rho_s V ds. \qquad [4]$$

Since $C \gg 2b$, the perimeter is approximated by $2C$. The volume charge density in the mobile lamina close to the wall, ρ_s, is given by the Poisson equation

$$\nabla^2 \Psi = \frac{-4\pi\rho_s}{\epsilon} ; \qquad [5]$$

ϵ is the dielectric constant. Substitution of Eqs. [5] and [3] into Eq. [4] gives Eq. [6] assuming that the dielectric constant and viscosity are invariant with s in the mobile charge region.

$$I_{str} = -\frac{P\epsilon bC}{2\pi\eta L} \int_{s=0}^{s=b} sds \frac{d^2\Psi}{ds^2} . \qquad [6]$$

Integration by parts gives,

$$I_{str} = -\frac{P\epsilon bC}{2\pi\eta L} \left\{ \left[s \frac{d\Psi}{ds} \right]_{s=0}^{s=b} - [\Psi]_{s=0}^{s=b} \right\} . \qquad [7]$$

Two boundary conditions are invoked for the solution of Eq. [7]. When b is much greater than κ^{-1} the potential, ψ, and gradient, $d\psi/ds$, are zero at $y = 0$. Also, the potential at the hydrodynamic shear plane near the wall is termed the zeta-potential, ψ_ζ. Equation [7] becomes

$$I_{str} = -\frac{P\epsilon bC\psi_\zeta}{2\pi\eta L} . \qquad [8]$$

This streaming current generates a stream-ing potential, E_{str}. At equilibrium the streaming current is balanced by a back current, I_b, having both bulk and surface con-ductance components, K_B and K_S, re-spectively.

$$I_b = \frac{2bCK_B E_{str}}{L} + \frac{2CK_S E_{str}}{L} . \qquad [9]$$

Equating Eqs. [8] and [9] and solving for ψ_ζ gives

$$\psi_\zeta = \frac{4\pi\eta E_{str}}{P\epsilon} \left[K_B + \frac{K_s}{b} \right] . \qquad [10]$$

Surface conductance is generally insignif-icant except in electrolytes of extremely low ionic strength, i.e., $\Gamma < 10^{-3}$ g ions liter^{-1} (6, 7). Ball and Fuerstenau (8) have re-viewed much of the pertinent streaming po-tential literature and conclude that an "asymmetry," E_a, or "flow" potential often causes an unpredictable deviation in the in-tercept of the E_{str} versus P data from a zero value. This may be a function of both elec-trode age and preparation. They recom-mend that the slope, $\Delta E_{str}/\Delta P$, of the best fit line for E_{str} vs P data be used to calculate ψ_ζ. Equation [10] then becomes

$$\psi_\zeta = \frac{4\pi\eta K_B \Delta E_{str}}{\epsilon \Delta P} . \qquad [11]$$

Equation [11] is found to be identical to that derived for tubular conduits (4), i.e., ψ_ζ is independent of geometry as long as the hy-drodynamic assumptions and boundary con-ditions are fulfilled.

Steady, incompressible, laminar flow is easy to attain during the streaming of an aqueous electrolyte. Established flow is of equal importance yet rarely addressed in contemporary literature. Fluid flow in a con-duit requires a length L_e to develop an equi-librium parabolic flow profile. For laminar flow between two plates separated by a distance $2b$, that development length is given (9) as

$$L_e = 0.026bRe \qquad [12]$$
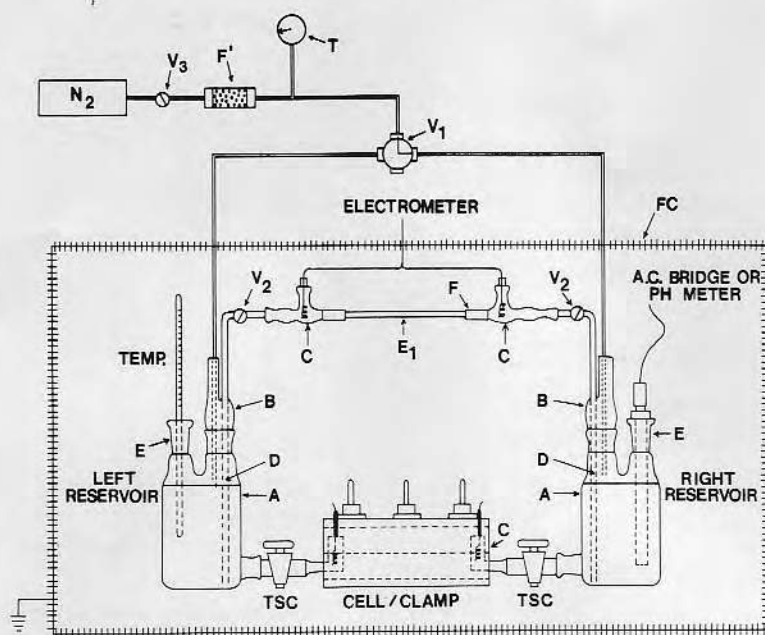
where Re is the Reynolds number.

FIG. 2. Schematic illustration of the dual streaming potential system capable of analyzing plate systems or capillaries.

EXPERIMENTAL

Figure 1b depicts the block cell used to support sample plates accurately and reproducibly. The cell consists of upper and lower Plexiglas halves containing sample plate channels (76 × 26 × 12.5) mm which accommodate standard glass microscope slides with room for a 254-μm-thick sheet of Silicone Rubber gasket which serves to secure the plates in the channels and prevent leakage at the plate–cell interface. Cell halves (127 × 51 × 16) mm are separated by a 100-μm-thick Teflon gasket which serves two functions: microspacing between sample plates to yield a 220:1 aspect ratio and cell leak prevention. Six verticle pressure clamps (Destaco 201) hold the cell together. Silver, silver chloride electrodes (2, 10) are inserted into chambers (32 × 16 × 18) mm on both ends of the cell via 7/15 $\mathbb{S}$ glass joints. Streaming electrolyte flows through the cell–plate system via 10/18 $\mathbb{S}$ joints afixed to the lower cell half ends.

Figure 2 illustrates the combined streaming system used for the comparative study of capillaries and sample microscope slides. The following system components were borosilicate glass: electrolyte reservoirs (A), interfacing manifolds (B, E), dip tubes (D), electrode chambers (C), and 7/15, 19/22, and 14/20 $\mathbb{S}$ joints. Electrolyte bulk conductance, K_B, and pH were monitored via a precalibrated platinum electrode conductivity dip cell-ac impedance bridge (General Radio 1650-B) and a glass electrode (Corning 12), respectively. Small thermal fluctuations were noted and corrections in η and ϵ were incorporated into Eq. [11] since ψ_ζ is invariant in the range 20–37°C if temperature correction for η, ϵ, and K_B are included (2). A system of valves (V1, V2) regulator (V3) and Teflon stopcocks (TSC) connected the electrolyte driving pressure source of compressed N_2 (99.999% pure) and filter of anhydrous $CaSO_4$/granular carbon (F') to the electrolyte reservoirs. Electrolyte driving pressure could be directed to either reservoir and consequently

flow could pass through either the capillary or plate system. Driving pressure was monitored (T) with an accuracy of 0.05 cm Hg. The system was electrically isolated within a grounded Faraday cage (FC). Streaming potentials were measured using a high input impedance electrometer (Keithley 616) and shielded coaxial cable.

All borosilicate components were cleaned in dichromate-sulfuric acid, rinsed in filtered, distilled water and ethanol, and degreased in a Freon TF ethanol nitro-methane azeotrope vapor. Streaming electrolyte was 0.01 M KCl buffered to a pH of 7.4 via $2 \times 10^{-4} M$ KH_2PO_4, $8 \times 10^{-4} M$ Na_2HPO_4, and doubly distilled conductivity water.

Streaming potentials, E_{str}, at steady flow were measured at a number of driving pressures, P, in both flow directions. This cyclic data acquisition of typically 0.1 sec^{-1} frequency minimized electrode asymmetry polarization potentials, E_a, at postflow to several microvolts. It also served to minimize differences in electrolyte levels in both reservoirs. Electrodes exhibiting asymmetry potentials exceeding 0.02 mV were replaced. Following a series of measurements, E_a, pH, K_B, and temperature were recorded. Streaming measurements constituting a run were repeated three times to confirm electrokinetic stability and reproducibility.
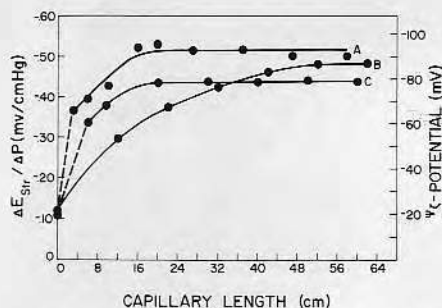

FIG. 3. The variation in $\Delta E_{str}/\Delta P$ and ψ_ζ as a function of length for three borosilicate glass capillaries of different internal diameter; A (160 ± 5 μm), B (1284 ± 34 μm), and C (595 ± 15 μm).
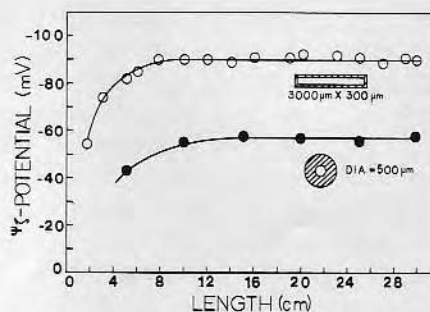

FIG. 4. The variation in ψ_ζ as a function of length for a borosilicate glass Microslide (○) and a Kimble Standard Flint capillary (●).

Streaming data for both flow directions were fitted to a least-squares linear relationship between E_{str} and P via a Hewlett-Packard 9820A programmable calculator (see Fig. 5). All data had a coefficient of determination, $r^2 > 0.99$. The maximum errors in the $\Delta E_{str}/\Delta P$ ratio and calculated ψ_ζ were typically ±0.05 mV (cm Hg)$^{-1}$ and ±1.0 mV, respectively. The standard deviation as a measure of the total technique and sample error was obtained from measurements on at least three capillaries or plate systems and was typically ±2 mV.

RESULTS AND DISCUSSION

Figure 3 illustrates electrokinetic results (10) for three borosilicate glass (Corning 7740) capillaries of internal diameters 160 ± 5 μm (A), 1284 ± 34 μm (B), and 595 ± 15 μm (C). In all cases, flow rates and $\Delta E_{str}/\Delta P$ were determined and a small section was removed from each capillary until it was consumed. The same procedural analysis was followed when the lumen of the flow conduit was a rectangular cross section (300 × 3000 μm), borosilicate Microslide (Vitro Dynamics), as shown in Fig. 4. In each case, the $\Delta E_{str}/\Delta P$ ratio attains a constant value at critical lengths, L_c, of 18, 52, 20, and 8 cm for A, B, C, and the Microslide. Figure 4 also illustrates results for a soft glass capillary of Kimble Standard Flint. Again, there is a critical length defining the end of a constant ψ_ζ value.

These results appear to be at odds with classical electrokinetic theory and research (11, 12) which showed ψ_ζ to be independent of flow path geometry. Both Helmholtz and Smoluchowski were well aware of the hydrodynamic stipulations embodied in Poiseuille flow (12, 13); however, in recent decades some investigators particularly in biomedical research have relied upon laminar flow as the only essential flow criterion to be met (14, 15).

The derivation of Eq. [11] assumed the existence of an equilibrium, parabolic velocity profile throughout the flow field, and a uniform dP/dL. Such conditions are impossible to meet completely since equilibrium flow requires a finite distance, L_e,

to develop. The classical solution is to minimize L_e with respect to L, i.e., a long capillary or a microporous plug of particles.

Figure 5 illustrates the effect both undeveloped and turbulent flow have on $\Delta E_{str}/\Delta P$. The maximum standard deviation of ± 0.02 mV for E_{str} is sufficient to confirm that $\Delta E_{str}/\Delta P$ is linear up to a critical driving pressure, P_c, of 9 cm Hg. At pressures exceeding P_c there is a significant departure from the linear projection based on data below P_c. On the basis of flow rates and calculated Reynolds members, L_e is less than 10% of L below P_c even though turbulent flow does not develop until pressures of 12 cm Hg are attained. A similar flow analysis on the data of Figs. 3 and 4
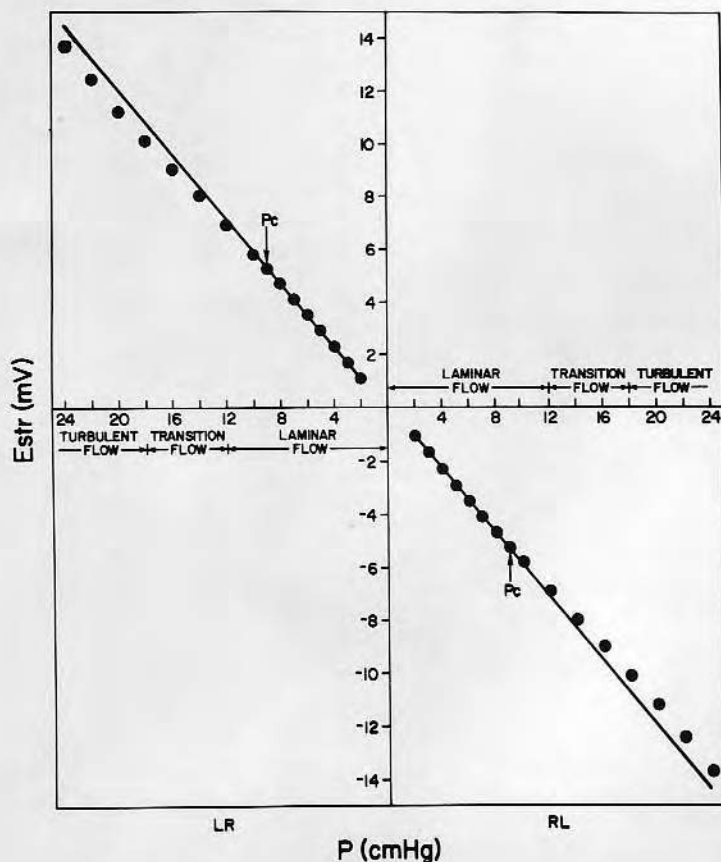

FIG. 5. The variation in measured streaming potential as a function of driving pressure in both flow directions for a borosilicate capillary 60 cm long and 1100 μm internal diameter.
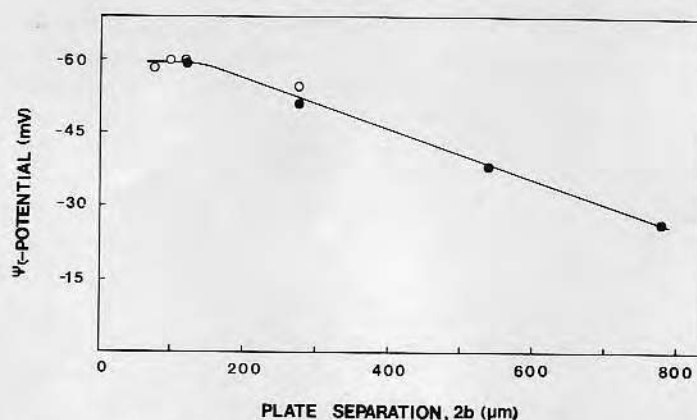
FIG. 6. The variation in ψ_ζ for a flat plate microscope slide system as a function of plate separation, $2b$, accomplished with both Teflon (O) and Silastic (●) gaskets.

indicated that flow was laminar in all cases and that the $\Delta E_{str}/\Delta P$ ratio only began to fall when L_e exceeded $10 \pm 1\%$ of L.

The onset of turbulent flow seemed to cause no abrupt variation in the $\Delta E_{str}/\Delta P$ values of Fig. 5. This is probably due to the existence of a laminar sublayer at least 30 μm thick adjacent to the conduit wall. Since κ^{-1} is at most 30 Å the region responsible for the electrokinetic phenomena is contained entirely within a laminar flow region where Poiseuille flow prevails (16). Consequently, the anomalous behavior seems to result from pressure drops associated with entrance loss effects in conduits with substantial flow development lengths. Streaming studies conducted on plugs of particles or fibers would also be expected to display such phenomena if packing was insufficient to reduce L_e to a minute amount of L or in this case plug thickness.

Figure 6 illustrates the effect of entrance region flow on ψ_ζ in a different way, i.e., parallel plate separation, $2b$, is varied using Teflon and Silastic Rubber gaskets while flow length remains constant. Here again, variations in ψ_ζ occur as $2b$ decreases until a plateau is reached. Flow was laminar and calculations based on Eq. [12] again confirmed that when L_e exceeded 10% of L ψ_ζ began decreasing. The gasket material

did not significantly affect ψ_ζ since it comprised only 0.5% of the total sample area exposed to flow.

The establishment of a diffusion boundary layer as discussed by Levich (17) may be postulated as one possible explanation for the variation of ψ_ζ. A solute may diffuse either toward or away from the interior wall if the bulk electrolyte is not at equilibrium with the surface, i.e., adsorption of potential determining ions or limited dissolution of the surface. Such a phenomena would create a time variation in E_{str} at constant P until the equilibrium establishment of the diffusion boundary layer occurred. Such variations in E_{str} were never observed during the course of this research.

Good agreement in plateau ψ_ζ occurred for borosilicate glass conduits regardless of geometry as long as Poiseuille flow predominated, i.e., hand drawn capillary A, commercial capillaries 20 cm long and 600 μm i.d., and Microslides all had a ψ_ζ in the range -93 ± 3 mV (see Figs. 3 and 4). A confirmation of the parallel plate design was attempted by a comparative streaming study utilizing soft glass capillaries of Kimble Standard Flint 20 cm long and 500 μm i.d. and soft glass plate systems based on Gold Seal microscope slides. The ψ_ζ for capillaries and plates differed by a -8 mV, i.e.,

TABLE I

The Approximate Bulk Chemical Composition in Percentage of Kimble Standard Flint Capillaries, Gold Seal Microscope Slides, and Borosilicate Microslides and Capillaries Utilized in This Research[a]

Com-ponent	Standard flint capillary	Soft glass microscope slide	Borosilicate glass
SiO_2	68	70	81
Na_2O	15	15	4
K_2O	1	Trace	Trace
CaO	5	1–2	Trace
MgO	4	1–2	Trace
Al_2O_3	3	1–2	2
Fe_2O_3	—	1–2	Trace
SO_3	—	Trace	—
BaO	2	—	—
B_2O_3	2	—	13
TiO_2	—	Trace	—
As_2O_5	—	Trace	—

[a] Trace signifies presence at less than 1%.

-75.9 ± 0.7 mV versus -68.3 ± 0.3 mV, respectively. An absolute methanol rinse under ultrasonic conditions at 24°C caused no significant change in ψ_ζ for either the capillaries or plate systems. Exposure to an aqueous solution of 20% (v/v) sulfuric acid for 12 days at 25°C did reduce ψ_ζ for both capillaries and plates, but to differing degrees, i.e., a 24% reduction in ψ_ζ for capillaries to -57.9 ± 0.8 mV and 6% reduction to -64.5 ± 1 mV for plates. This suggests that the surfaces of the two systems

were chemically different since they responded differently to acid exposure.

The overall bulk chemical compositions of the two soft glass systems are similar although not identical (see Table I). It is conceivable that subtle bulk differences may be reflected as much larger perturbations in composition at the electrokinetic surface. Energy dispersive analysis of X-rays (EDAX) in conjunction with scanning electron microscopy (SEM) was utilized to investigate possible chemical differences in the flat plate slides as well as the fracture face and interior and exterior capillary surfaces (see Table II). There was no evidence of iron, sulfur, barium, or arsenic and no significant compositional difference between the capillary lumen and fracture face which represented bulk chemical composition. There were significant differences in quantitative EDAX analyses between the capillary lumen and flat plate surfaces. Titanium is consistently present in the capillary lumen but absent on the slide surface (see Fig. 7). There also seemed to be significant differences in the aluminum, sodium calcium, and silicon composition perhaps resulting from differences in production and processing treatments, e.g., cooling rates, environments, washing, polishing, etc.

EDAX analyses are only an approximation to realistic "surface" composition

TABLE II

Composition (Atomic Percent) of "Surfaces" Analyzed via EDAX[a]

Element	Gold seal microscope slide	Standard flint capillary lumen	Standard flint capillary fracture face	Standard flint capillary exterior
Cr	15.7 ± 0.1	14.8 ± 1.4	14.7 ± 0.6	11.8 ± 0.5
Si	53.5 ± 0.4	50.2 ± 0.5	50.9 ± 0.9	54.3 ± 0.7
Ca	5.2 ± 0.2	3.8 ± 0.2	4.1 ± 0.3	4.7 ± 0.3
Na	17.4 ± 0.1	20.2 ± 1.3	19.6 ± 0.3	18.7 ± 0.9
Mg	4.5 ± 0.4	4.9 ± 0.6	4.8 ± 0.1	4.7 ± 0.2
K	0.2 ± 0.0	0.4 ± 0.1	0.4 ± 0.1	0.5 ± 0.1
Al	3.4 ± 0.5	5.2 ± 0.4	5.0 ± 0.4	4.9 ± 0.5
Ti	0.0 ± 0.0	0.5 ± 0.1	0.5 ± 0.1	0.6 ± 0.1

[a] Data presentation [average $\pm \sigma$] based on analysis of three distinct sites.
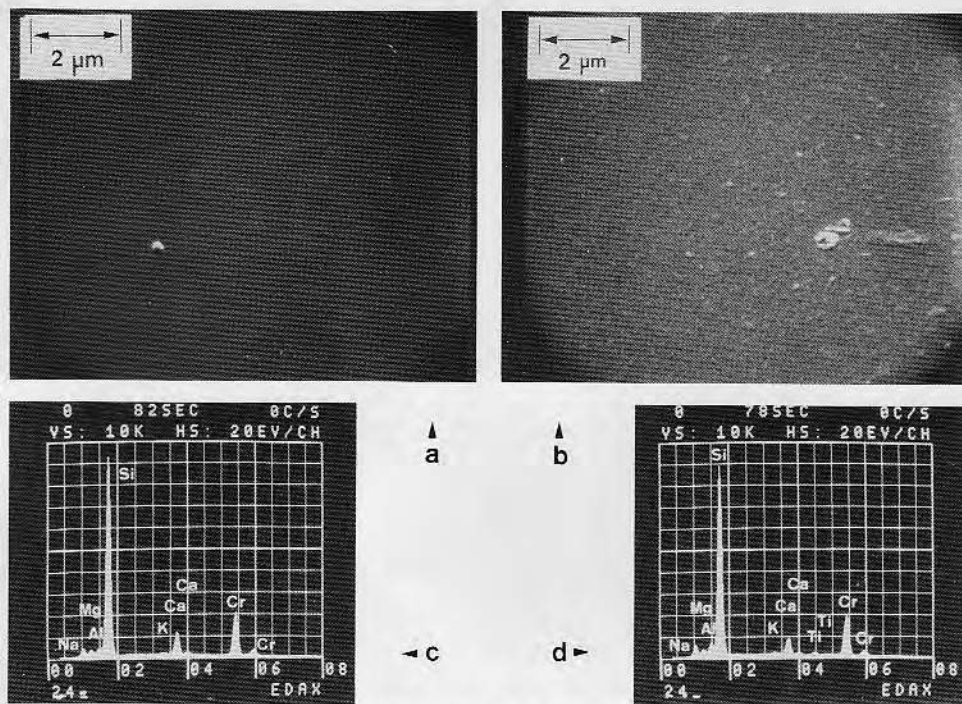
FIG. 7. Scanning electron micrograph (a) and EDAX spectra (c) of Gold Seal Microscope sample plate. Scanning electron micrograph (b) and EDAX spectra (d) of Kimble standard flint capillary.

since EDAX X-rays may originate several micrometers below the real surface and the technique is insensitive to elements with atomic numbers less than 11. Consequently, an organic surface film affecting electrokinetic results would be undetectable. More realistic surface compositional information could be attained via XPS where sampling depth is less than 50 Å (18). Unfortunately, an X-ray beam cannot be focused onto the small capillary lumens of this study.

Differences in sample roughness are currently the largest single unknown in the interpretation of electrokinetic results (19). Most real surfaces are rough at least on the level manifesting electrokinetic phenomena, i.e., several tens of Angstroms. An SEM analysis of the capillary and plate systems indicated that differences in surface roughness did exist (see Fig. 7). The scale of this roughness is on the order of 0.1 μm for the capillary lumen while the microscope

slide surface roughness was below the resolution of the SEM no doubt due to its highly polished nature. The charge neutralizing chromium coating would be expected to mask any roughness on the hundred Angstrom scale and TEM would seem to offer the only possibility of analysis at this level.

CONCLUSIONS

Accurate streaming potentials can be measured on flat plate systems if the hydrodynamic conditions of steady, incompressible, laminar, and established flow are met. The requirement of established flow is rarely addressed in the literature but it seems to be of great importance. Our findings suggest that combinations of conduit and fluid flow properties producing significant entrance losses and flow establishment lengths exceeding about 10% of the flow field under investigation will result in anomalously low streaming potentials and

thus erroneous zeta-potentials. The phenomena of turbulent flow does not appreciably alter ψ_ζ probably due to the presence of a laminar sublayer adjacent to the wall which contains the electrical double layer.

Comparative electrokinetic studies conducted on soft, soda lime glass in the form of both plates and capillaries indicated a 10% difference in ψ_ζ. This discrepancy could not be attributed to the hydrodynamic factors previously mentioned, but rather is probably a reflection of true differences in the electrokinetic surfaces under comparison. Such differences may reflect the effect of slightly different bulk chemical compositions between the capillaries and plates. The manufacturing and processing conditions were probably not identical for the glass comprising the two systems and it is likely that any of several proprietary surface treatments may be responsible for the observed discrepancies. Scanning electron microscopy and EDAX analysis both suggest that differences in surface roughness and near surface chemical composition may be responsible for the discrepancy in the zeta-potentials.

ACKNOWLEDGMENTS

REFERENCES

1. Sawyer, P. N., *J. Electrochem. Soc.* **125**, 419 c (1978).
2. Van Wagenen, R. A., Ph.D. Dissertation, University of Utah (1976).
3. DePalma, V. A., Ph.D. Dissertation, University of New York at Buffalo (1976).
4. Davies, J. T., and Rideal, E. K., "Interfacial Phenomena," 2nd ed., p. 118. Academic Press, New York, 1963.
5. Eskinazi, S., "Principles of Fluid Mechanics," 2nd ed., p. 378. Allyn and Bacon, Boston, 1968.
6. Rutgers, A. J., and DeSmet, M., *Trans. Faraday Soc.* **43**, 102 (1947).
7. Dukhin, S. S., *in* "Surface and Colloid Science" (E. Matijević, ed.), Vol. 7, p. 193. John Wiley, New York, 1974.
8. Ball, B., and Fuerstenau, D. W., *Miner. Sci. Eng.* **5**, 267 (1973).
9. Knudsen, J. G., and Katz, D. L., "Fluid Dynamics and Heat Transfer," p. 240. McGraw–Hill, New York, 1958.
10. Van Wagenen, R. A., Andrade, J. D., and Hibbs, J. B., Jr., *J. Electrochem. Soc.* **123**, 1438 (1976).
11. White, H. L., Urban, F., and Krick, E. T., *J. Phys. Chem.* **36**, 120 (1932).
12. Bocquet, P. E., Trans. *Michigan Univ. Eng. Res. Inst. Eng. Res. Bull.* **33**, 1 (1951).
13. Bocquet, P. E., Ph.D. Dissertation, University of Michigan (1952).
14. Edmark, K. W., Davis, J., and Milligan, H. L., *Thromb. Diath. Haemorrh.* **24**, 287 (1970).
15. Srinivasan, S., and Sawyer, P. N., *J. Colloid Interface Sci.* **32**, 456 (1970).
16. Rutgers, A. J., DeSmet, M., and DeMyer, G., *Trans. Faraday Soc.* **53**, 393 (1957).
17. Levich, V. G., "Physicochemical Hydrodynamics," 2nd ed., pp. 112–116. Prentice–Hall, Englewood Cliffs, 1962.
18. Holm, R., and Storp, S., *in* "Molecular Spectroscopy" (A. R. West, Ed.), p. 482. Heyden and Son, Philadelphia, 1977.
19. Bikerman, J. J., "Physical Surfaces," p. 420. Academic Press, New York, 1970.
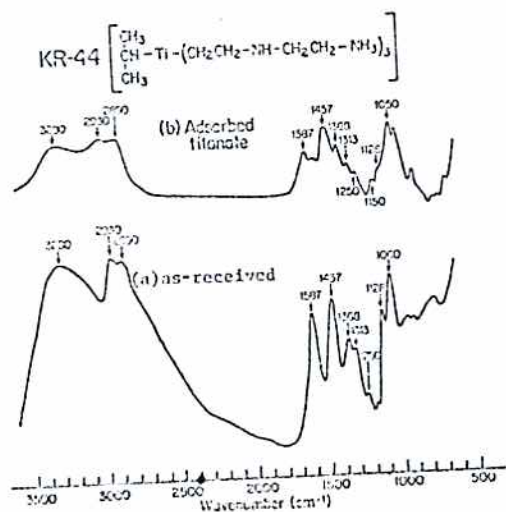
Total Internal Reflection Fluorescence Studies of Albumin
Adsorption onto Quartz

by

R. A. Von Wagenen, B. J. Odaniuk and J.D. Andrade
Department of Bioengineering
College of Engineering, University of Utah
Salt Lake City, Utah 84112

Introduction

The adsorption of both natural and synthetic macromolecules on organic surfaces has been studied for many years by a variety of interfacial techniques. Such studies have applicability in the fields of protein adsorption at the blood-biomaterials interface, protein separation and purification on chromatographic supports, protein or polymer-membrane interactions, etc.

The optimum interfacial technique should produce quantitative information concerning the in situ adsorption of macromolecules in a real time context under a variety of interfacial conditions. All adsorption techniques to date are approximations to this optimum with varying degrees of success. For instance, solution depletion techniques yield accurate indications of average surface adsorption but are often not applicable to low surface area materials of biomedical relevance. The adsorption of radio-tagged macromolecules is highly quantitative on flat surfaces but the presence of the foreign label may alter physical properties with a subsequent alteration in the adsorption behavior. Infrared techniques suffer from the disadvantage of a strong water signal overshadowing the amide band.

The above methods entail substantial substrate manipulations such as rinsing and relatively long analysis times which make desorption studies as well as real time adsorption measurements difficult. In principle, dynamic, automated ellipsometry can provide real time, in situ data on adsorption at the liquid-solid interface with time resolution of one second. However, the accuracy of the ellipsometrically determined film thickness and optical properties are questionable due to the minimal difference in the refractive indices between the film, substrate, adsorbing macromolecules and liquid media.

Total Internal Reflection Fluorescence (TIRF) and its associated spectroscopy (TIRFS) promise to simplify the quantitative analysis of macromolecular adsorption at solid-liquid interfaces. The essential feature of TIRF is interfacial fluorescence induced by evanescent wave excitation in the liquid phase. The evanescent wave originates at the point of total internal reflection within the solid phase; the essential criteria being that the incident angle θ, exceed the critical angle θ_c, where $\theta_c = \sin^{-1}[u_2/n_1]$. Refer to Figure 1. TIRF is a true interfacial technique in that the effective penetration depth of the evanescent wave does not exceed 1500 Å at $\lambda = 438$ nm.

Harrick and Loeb [1] pioneered the applicability of TIRF in a study demonstrating the adsorption of bovine albumin on quartz. This principle was later applied to the study of the binding of antibody to an antigen-protein conjugated film on a quartz substrate [2,3]. More recently, TIRF has been utilized to quantitate the adsorption of bovine γ-globulin onto silicone rubber surfaces; one major finding being the strong evidence for the existence of both tightly and loosely bound layers of adsorbed γ-globulin under static and laminar flow conditions [4]. Walton and Maenpa have utilized fluorescence spectroscopy to study the adsorption behavior of bovine serum albumin onto colloidal particles of silica and copolypeptide substrates [5].
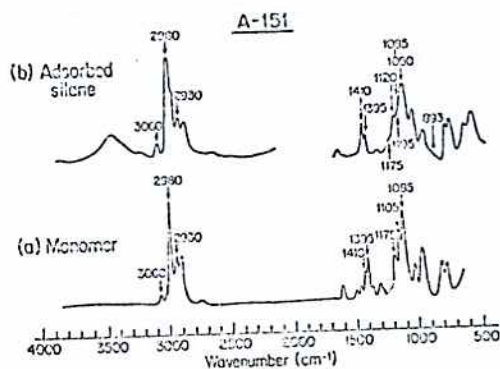

Figure 2. IR spectra of monomeric vinyl-silane (a) and adsorbed silane on sapphire (b).

Figure 3. IR spectra of as-received organic titanate (KR-44) (a) and adsorbed titanate on sapphire (b).

Experimental

The adsorption of bovine serum albumin (BSA) Fraction V on the hydrophilic surface of a fused quartz dovetail prism was studied. The light source utilized to excite interfacial fluorescence was the 488 nm line of an argon-ion laser (Spectra Physics #164). The laser beam was directed into a light tight housing via a series of front silvered mirrors and iris diaphragms and then through a quartz beam splitter which directed approximately eight percent of the light to a following photomultiplier tube (PMT) (RCA 7528). The remainder of the beam traveled through another iris diaphragm to minimize scattering before it entered the fused quartz prism (2cm x 3cm x 2.9cm) normal to the 70° face. See Figure 1.

A Teflon block with a 2mm deep milled flow channel was interfaced to the quartz prism via a 2 mm thick Silastic gasket and clamp system. Entrance and exit ports in the flow cell allowed phosphate buffered normal saline, 0.145 M NaCl (PBS) or BSA in PBS to be introduced and exposed to the quartz-electrolyte interface. The laser beam incident upon the solid-liquid interface at an incidence angle θ of 70° was totally reflected out of the prism normal to the second 70° prism face and was extinguished in a beam trap. Total internal reflection occurred since the critical angle, θ_c, for the quartz-aqueous electrolyte interface was $\sin^{-1}[1.33/1.46]$ or 65°. The penetration depth, dp, of the evanescent wave required for the electric field amplitude in the PBS to fall to e^{-1} of its surface value is a function of the incident light wavelength in the denser medium, the angle of incidence, θ, and the refractive index ratio (n_2/n_1) [6].

The BSA molecule was rendered fluorescent by the covalent attachment of between 1 and 2 residues of fluorescein isothiocyanate (FITC) to the ε-amino groups of lysine and/or the terminal α-amino groups of the BSA. The FITC absorbs maximally at 490 nm and emits the maximum fluorescence intensity at approximately 520 nm. The FITC labeling was accomplished by mixing equal volumes of the following two solutions at 4°C with stirring for 12 hours: 10% (w/v) BSA in normal saline and 10% (w/v) FITC in carbonate buffer (pH 9.6). The labeled protein is then separated from unreacted FITC via centrifugation through a Sephadex G-25 column. The yield was approximately 60 percent of FITC-BSA with 12 μg FITC per milligram of BSA.

A portion of the interfacial fluorescence emitted from the BSA-FITC conjugate passes through the prism, enters the aperture of an emission monochromater (Kobin Yvon H-10) and is amplified by the emission PMT (RCA 7528). Both signal PMT outputs were preamplified, fed to signal intensity discriminators (Citec 9302) and then into a photon counting system (Citec 9315). Digital data was transformed to analog signals (Citec 9325) and outputed to a strip chart recorder (Pharmacia). The following PMT system was used to correct for laser intensity fluctuations with time, i.e., a predetermined number of counts in the following channel had to be accumulated before the emission PMT would step data acquisition. The time resolution for each emission PMT output was adjusted to approximately one second.

For reproducibility, the quartz surface was cleaned in a standard way prior to each adsorption experiment. Cleaning of protein films was accomplished by soaking for 10 minutes in Microclean detergent, thorough rinsing in distilled water, 4 rinses in filtered, distilled water, 2 rinses in filtered absolute ethanol and vapor degreasing in a Freon ethanol azeotrope vapor for 5 minutes. Care was taken to keep the prism wet, thus minimizing the attachment of particles which scatter light causing higher background signals. The final cleaning step was a radio frequency induced oxygen gas plasma at a pressure of 200 μm Hg and power of 30 watts for 2 minutes (Tegal, Plasmod).

After preparation, the quartz prism was clamped to the flow cell and emission monochromater-PMT unit and aligned for proper position in the laser beam. The cell was primed with deaerated, filtered PBS and the light tight

being secured in place. The emission monochromater was set to 520 nm with 1 mm slits to maximize the fluorescent signal. Photon counting was timed and after the background count rate had stabilized the BSA-FITC at the desired concentration was introduced into the flow cell. The result was an immediate increase in count rate representing the fluorescent signal from the interfacial region excited by the evanescent wave. As protein adsorption occurred, the fluorescent signal intensity increased. At equilibrium, adsorption for any particular protein concentration resulted in a time invariant output. See Figure 2. The preadsorption background counts were numerically subtracted yielding the true adsorption signal. Bulk protein was then rinsed from the flow cell with PBS and BSA-FITC desorption behavior recorded. After equilibrium was obtained, counts above background were noted. At this point, the emission monochromater was automatically scanned with the narrowest slits (4 nm band pass) from 500 to 550 nm to obtain the fluorescence emission spectrum of the adsorbed BSA-FITC molecules. This spectrum was then compared to an emission spectrum of bulk solution BSA-FITC obtained in the conventional way on an Aminco Bowman spectrophotofluorometer.

Adsorption isotherms were obtained at 25°C by incrementally increasing the protein concentration from 0.2 mg% to 100 mg%. The adsorption, rinsing and flushing sequence described above was repeated at each protein concentration. This also provided desorption kinetics and spectral data at each concentration.

Results and Discussion

Figure 2 illustrates emission fluorescence intensity variations during BSA-FITC adsorption on hydrophilic quartz. Interfacial fluorescence emission spectra were taken before protein adsorption, after maximum adsorption had occurred (a) and after a PBS rinse to remove all protein not tightly bound to the surface (b). Accurate numerical comparisons of fluorescence intensity from experiment to experiment as well as actual surface protein concentrations in μg/cm² await further calibration studies. However, a number of interesting features are evident from this preliminary study.

First, 10 mg% BSA-FITC adsorption onto hydrophilic quartz reaches equilibrium within 20 to 30 minutes (Figure 2). Desorption of the BSA-FITC conjugate following a PBS rinse is not even complete after two hours. It appears that some small proportion of the adsorbed protein remains tightly bound to the quartz surface, ie., less than 5 percent. If complete desorption ever occurs it must require tens of hours. The spectrum of Figure 2 (b) confirms the presence of adsorbed BSA-FITC following an extensive PBS rinse and 2 hour desorption. The intensity of the λ_{max} at approximately 515 nm is extremely low and could only be obtained by using maximum laser power and optimum emission PMT counting times. Even then, it was almost obscured by stray light photons originating from the 488 nm laser. The spectra taken before protein adsorption (not shown) illustrate there is no fluorescent signal and after equilibrium adsorption there is a pronounced spectra originating from interfacial BSA-FITC, some of which is adsorbed but much of which is probably originating in the interfacial region excited by the evanescent wave. The λ_{max} of the emission is 518-550 nm in all cases. This suggests that there is not much if any wavelength shift in the FITC emission properties following adsorption on hydrophilic quartz. The adsorption experiment depicted in Figure 2 was representative of the results obtained 5 times on both argon-ion and He-Cd lasers in different laboratories. Re-exposing the quartz surface to a second quantity of BSA-FITC produces essentially the same result as in Figure 2.

Figure 3 illustrates and adsorption isotherm for BSA-FITC on hydrophilic fused quartz. Data were obtained at bulk protein concentrations of 0.2 to 100 mg%. This agrees well with the data of Morrissey et al [7] showing an equilibrium plateau of 100-120 mg% for BSA on silica[7].

Conclusions

Interfacial total internal reflection fluorescence promises to advance our understanding of protein adsorption at a variety of interfaces. The advantages of TIRF are in situ, real time measurement, accuracy and time resolution of one second or less. The ability to obtain interfacial fluorescence emission spectra is another plus for this technique. Current effort is being directed toward developing an independent way of quantitating exactly how much protein is adsorbed at the surface. Such information could then be used to calibrate future TIRF signal data for more comparative studies on both hydrophilic and hydrophobic polymer films.

Acknowledgement

We thank Dr. Joel Harris and Mr. Norm Dovichi of the University of Utah Department of Chemistry for their loan of a He-Cd laser to initiate preliminary TIRF trials and for discussions and assistance with the technique.

References

1. N.J. Harrick and G.I. Loeb, Analytical Chem. 45 687 (1973).
2. M.N. Kronick and W.A. Little, J. Immunological Methods 8 235 (1975).
3. M.N. Kronick and W.A. Little, United States Patent 3939350 (1974).
4. R.W. Watkins and C.R. Robertson, J. Biomed. Mater. Res. 11 915 (1977).
5. N.J. Harrick, Internal Reflection Spectroscopy (Wiley & Sons, Inter-science, N.Y.) 1967 p.13.
6. A.G. Walton and F.C. Maenpa, J. Colloid Sci. in press.
7. D.W. Morrissey, L.E. Smith, C.A. Fenstermaker, R.R. Stromberg and W.H. Grant, National Bureau of Standards Special Publication 415 p.83 (1975).

Figure Captions

Figure 1. Schematic diagram of TIRF assembly indicating the light source (A), excitation and emission monochromators (B&C), following and emission photomultiplier tubes (D&E), quartz dovetail prism (F), flow cell (G), beam step (H), preamplifiers (I), light tight housing (J), iris diaphrams (K), beam splitter (L), and silver mirrors (M). Photon signals are processed in amplifier discriminators (N), counted and displayed in a photon counter (P), converted to analog signal and graphically recorded (R). The insert depicts conditions at the BSA-FITC aqueous electrolyte (n =1.33)-quartz (n =1.47) interface.

Figure 2. The adsorption of 10 mg% BSA-FITC conjugate on to hydrophilic quartz as a function of time. Point A represents the replacement of priming PBS with the protein solution. Point B represents a 120 ml flush with PBS to remove bulk protein. Inserts a and b illustrate spectral scans of FITC emission for the case of maximum equilibrium protein adsorption and following bulk protein removal via the PBS rinse.

Figure 3. An adsorption isotherm for BSA-FITC on hydrophilic quartz derived via the TIRF technique at 25°C. The equilibrium number of photon counts, above background signal after a 120 ml PBS rinse, Ns, is plotted versus the bulk protein concentration, Co.
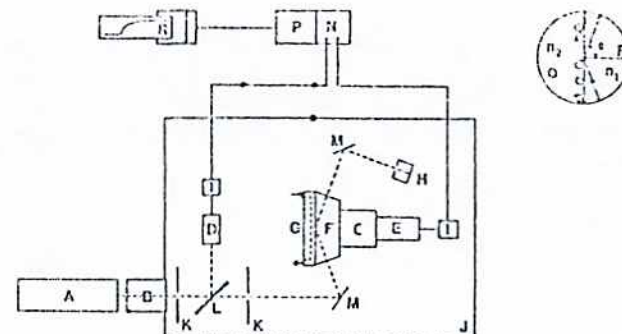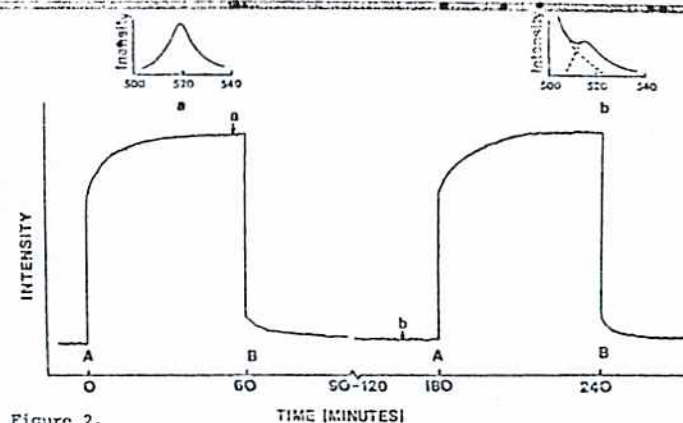
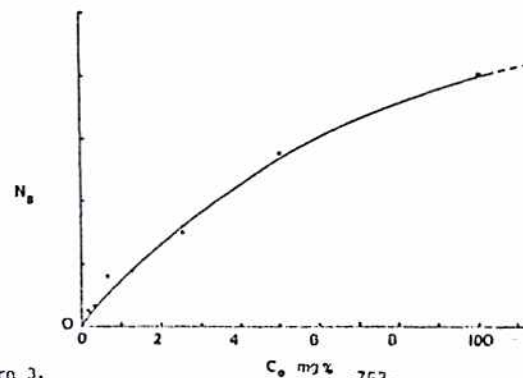

Figure 1.

Figure 2.

Figure 3.

Streaming Potential Investigations: Polymer Thin Films

R. A. VAN WAGENEN, D. L. COLEMAN, R. N. KING, P. TRIOLO, L. BROSTROM,
L. M. SMITH, D. E. GREGONIS, AND J. D. ANDRADE

Department of Bioengineering, College of Engineering, University of Utah, Salt Lake City, Utah 84112

Streaming potential evaluations were carried out on a wide variety of biopolymer and synthetic polymer thin films supported on glass microscope slides. The film-forming and streaming evaluation techniques are sufficiently accurate to provide reproducible results between different investigators. Films evaluated to date include various silanes, albumins, agarose, and synthetic polymers based on hydroxyethyl methacryle (HEMA), n-butyl methacrylate (n-BMA), and methylacrmethylate (MMA). The effect of negative and positive charge incorporation upon the streaming potential and thus the ζ potential was studied via incorporation of methacrylic acid (MAA) and both HCl and CH_3Cl salts of dimethylaminoethyl methacrylate (DMAEMA) into the neutral polymer chains of HEMA, n-BMA, and MMA via copolymerization. Thin films of polystyrene, polydimethyl siloxane, polyvinyl chloride, and avcothane were also evaluated successfully.

INTRODUCTION

A number of surface properties have been postulated as having a significant influence on protein adsorption, cell adhesion, and prosthetic material biocompatibility, e.g., interfacial free energy (1), surface hydrophilic:hydrophobic ratio (2), water structure (3), and surface charge (4). A parallel-plate streaming potential system has been developed (5) which allows reproducible determination of streaming potential, E_{str}, and thus ζ potential, ψ_ζ, of any material formable into a flat plate configuration. Such an approach makes it possible to characterize a wide variety of surfaces by a number of analytical techniques and to correlate those results with protein adsorption, cell adhesion, and *in vitro* biocompatibility. We here report on the electrokinetic characterization of neutral and charged synthetic and biopolymer thin films supported on glass substrates.

MATERIALS AND METHODS

Support substrates for all films were standard microscope slides (25.4×76.2 × 1 mm) having a typical soft glass composition: 70–74% SiO_2, 14–15% Na_2O, 2–6% CaO, 1–4% MgO, Al_2O_3, Fe_2O_3, and less than 1% K_2O, SO_3, As_2O_5, B_2O_3, and TiO_2. Both Gold Seal (Clay Adams No. 3010) and Bev-1-edge (No. DSO, Propper Mfg. Co.) glass slides were utilized and unless specified otherwise were cleaned prior to film deposition. Cleaning of all glassware and slides occurred under class 10,000 clean room and class 100 laminar flow hood conditions and consisted of a sequential rinse in warm tap water containing 2% (v/v) Micro (International Products Corp.) cleaner followed by a thorough rinse in running tap water, 5 min exposure to 80°C chromic acid, four sequential rinses in filtered (DFA 4001 ARP, 0.22-μm filter, Pall Trinity Micro Corp.) distilled water, two rinses in filtered (DFA 3001 BNP, 1- to 2-μm filter, Pall) absolute ethanol, and vapor degreasing in a Freon TES–ethanol azeotrope vapor for 5 min.

Surface silanization was essential in some instances for adequate polymer film adhesion to the clean hydrophilic glass surface. The vapor-phase silanization technique was that of Haller (6) and utilized

155

either 5% (v/v) γ-aminopropyltriethoxysilane in anhydrous p-xylene to yield aminopropyl silanized (APS) glass or 5% (v/v) n-pentyl-triethoxysilane and 1.5% (v/v) anhydrous 2,6-lutidine in anhydrous p-xylene to yield n-pentyl silanized (n-PS) glass. Clean glass substrates were vapor silanized for 16–18 hr in a glass refluxing apparatus. Vinyl silanized glass was prepared by dip coating from a 1% (v/v) solution of vinyltrichlorosilane in anhydrous 2,2,4-trimethylpentane followed by rinses in 2,2,4-trimethylpentane, ethanol, and distilled water. These slides were oven dried at 60°C for 12 hr.

Unless specified otherwise polymer films were spun cast onto glass slides using a rotating disk spinner (Headway Research Inc.) and a vacuum chuck. Polymer solutions were dispersed onto and totally covered the slide surface in 2-ml aliquots. Solution deposition and spin cycle (4000 rpm, 15–20 sec) were repeated thrice to remove excess solution and produce a uniform film approximately 800–1000 Å thick. Spun cast polymer film thicknesses were initially determined using ellipsometric and gravimetric techniques. Once film-forming conditions were developed, uniformity and approximate thicknesses were derived from the distribution and eventual disappearance of interference colors. Thicknesses were not determined for silane and adsorbed protein films. Films were cured at $60 \pm 10°C$ under dry N_2 for 3 hr, extracted in either filtered, doubly distilled water or streaming electrolyte, and analyzed as pairs.

All polymer solutions were 1% (w/v) in analytical grade solvents. Solutions were filtered (Millipore PTFE, 1 μm) and stored in particulate-free, cleaned glass bottles under either nitrogen or argon. Synthetic polymer solutions were: polyvinyl chloride (PVC) secondary standard (Aldrich, Lot 01, $M_n = 85,500$) in tetrahydrofuran, polystyrene (PS) secondary standard (Scientific Polymer Products, Lot 03, $M_n = 84,600$) in toluene, unfilled polydimethyl siloxane (PDMS) (Avco Medical Products, SR-RTV-

80-68M-01L, $M_n = 23,000$) in chloroform, and Avcothane 51 (Avco Medical Products) in tetrahydrofuran:dioxane (2:1).

A synthetic series of methacrylate ester copolymers possessing both variable hydrophilic:hydrophobic ratios and charge moieties were prepared and characterized as detailed elsewhere (7). Variations in the philic:phobic ratio were accomplished by random copolymerization of hydroxyethyl methacrylate (HEMA) and methyl methacrylate (MMA). Charge was incorporated into the neutral polymer systems via copolymerization of HEMA or n-butyl methacrylate (n-BMA) with methacrylic acid (MAA) or two quaternary ammonium salts of dimethylaminoethyl methacrylate (DMAEMA) monomers (HCl or CH_3Cl). The monomer DMAEMA quaternized with either hydrogen chloride or methyl chloride was provided by Alcolac (marketed as Sipomer Q-6 monomer). We abbreviate these monomers as DMAEMA–HCl and DMAEMA–CH_3Cl which would be synonymous with the terminology methacryloxyethyltrimethylammonium chloride.

Biopolymer solutions were deposited in both spun cast and adsorption modes. Solutions were: SeaKem agarose (FMC Corp. Lot No. 62349) in doubly distilled water spun cast at 60°C and Fraction V serum albumin–glutaraldehyde solutions in streaming electrolyte as follows: rabbit (Sigma, No. 53C-0890), bovine (Miles, No. 288), human (Sigma, No. 84C-0152-1), ovine (Sigma, No. 102C-1540), and goat (Sigma, No. 92C-1820). Albumins were spun cast thrice from 5% (w/v) solutions also containing 20 μl/ml of 50% (v/v) aqueous glutaraldehyde (Polysciences). Films were allowed to crosslink at 23°C, 40% relative humidity overnight and then hydrated 4 hr in streaming buffer. Fraction V bovine serum albumin, BSA, (Miles, No. 81-003-3) as 1 mg/ml in acetate buffer (pH 4.8, 0.025 g ions liter^{-1}) was adsorbed onto clean slides for 30 min at 24°C, rinsed in acetate buffer for 60 sec, crosslinked with 0.25% (v/v)

TABLE I

Average ζ Potential and $\Delta E_{str}/\Delta P$ Ratio for Glass Substrates and Silane Films Evaluated on n Samples

Sample description	$\Delta E_{str}/\Delta P \pm 1\sigma$ (n) (mV/cm Hg)	$\psi_\zeta \pm 1\sigma$ (n) (mV)	Investigator comment key^a
Gold Seal	-0.419 ± 0.002 (3)	-65.2 ± 0.3 (3)	RVW (a, c, f, j)
Gold Seal	-0.417 ± 0.010 (2)	-66.1 ± 1.4 (2)	LB (a, c, f, j)
Gold Seal	-0.410 ± 0.003 (3)	-63.1 ± 0.9 (3)	PT (a, c, f, j)
Gold Seal	-0.408 (1)	-62.7 (1)	DLC (a, c, g, j)
Clean Gold Seal	-0.397 ± 0.013 (3)	-63.2 ± 0.6 (3)	RVW (a, c, f, j)
Clean Gold Seal	-0.426 ± 0.007 (3)	-65.2 ± 1.1 (3)	RNK (a, c, g, j)
Clean Gold Seal	-0.344 ± 0.013 (3)	-53.2 ± 2.0 (3)	PT (a, c, i, j)
Bev-1-edge	-0.337 ± 0.010 (3)	-51.9 ± 1.5 (3)	PT (b, c, g, j)
Bev-1-edge	-0.357 (1)	-53.2 (1)	LB (b, c, f, j)
Bev-1-edge	-0.334 (1)	-49.6 (1)	DLC (b, c, g, j)
Clean Bev-1-edge	-0.357 ± 0.007 (3)	-53.6 ± 1.2 (3)	DLC (b, c, g, j)
VS	-0.275 ± 0.012 (4)	-43.6 ± 1.9 (4)	RVW (a, c, f, j)
n-PS	-0.324 ± 0.014 (3)	-50.8 ± 1.8 (3)	LB (a, e, g, j)
n-PS	-0.368 (1)	-56.7 (1)	PT (b, e, f, k)
n-PS	-0.368 (1)	-56.7 (1)	PT (a, e, f, k)
APS	-0.204 ± 0.017 (4)	-32.0 ± 3.0 (4)	RVW (a, d, f, j)
APS	-0.249 ± 0.011 (3)	-39.9 ± 1.9 (3)	LB (a, d, g, j)

^{a} Abbreviations: (a) Gold Seal or (b) Bev-1-edge, (c) no silane, (d) APS or (e) n-PS, (f) no extraction, (g) extraction overnight in streaming electrolyte, (h) 24 hr or (i) 35 hr extraction in doubly distilled water and less than (j) or more than (k) 5% total variation in three or more $\Delta E_{str}/\Delta P$ ratios per sample.

buffered glutaraldehyde for 20 min, and rinsed again in acetate buffer for 60 sec. This was repeated five additional times on some slides to yield six albumin "layers" or successive treatments. Adsorbed films resulting from both one and six treatments were exposed to fresh BSA (1 mg/ml) to quench residual unreacted glutaraldehyde and stored overnight in streaming electrolyte.

For all cases where multiple investigators analyzed polymer films, substrate cleaning, silanization, and spin casting were identical. Differences in glass substrates and pre-streaming extraction conditions are specified in the last column of Tables I–III.

Streaming potential measurements were conducted on glass substrates and thin polymer films supported on these substrates in a parallel-plate streaming cell having a plate separation of 120 μm. All design and measurement techniques, as well as all necessary hydrodynamic requirements, have been detailed elsewhere (5, 8). Measurement of streaming potentials, E_{str}, at various

flow driving pressures, P, produced a locus of points which were linear and of slope $\Delta E_{str}/\Delta P$. This ratio is utilized in Eq. [1]

$$\psi_\zeta = 8.4922 \times 10^8 \frac{\Delta E_{str}}{\Delta P} \frac{K_B \eta}{\epsilon} \quad [1]$$

to determine the ζ potential, ψ_ζ (in mV). Bulk values for the electrolyte viscosity ($\eta = 0.010$ P) and dielectric constant ($\epsilon = 80.14$) were utilized at the streaming temperature, 20°C. Specific conductance of bulk electrolyte, K_B, was calculated on the basis of a measured ac resistance ($R_{ac} = 180$ ohm) in a precalibrated, platinized-platinum conductivity cell ($C = 0.262$ cm^{-1}), where K_B was C/R_{ac}. Streaming electrolyte was 0.01 M KCl, 8×10^{-4} M Na$_2$HPO$_4$, 2×10^{-4} M KH$_2$PO$_4$, pH 7.4. Values of ψ_ζ are an average of at least three sets of plates unless indicated otherwise.

RESULTS AND DISCUSSION

The average $\Delta E_{str}/\Delta P$ ratios and calculated ζ potentials, ψ_ζ, are tabulated in

TABLE II

Average ζ Potential and $\Delta E_{str}/\Delta P$ Ratio for Biopolymer Films Evaluated on n Samples

Sample description	$\Delta E_{str}/\Delta P \pm 1\sigma$ (n) (mV/cm Hg)	$\psi_\zeta \pm 1\sigma$ (n) (mV)	Investigator comment key[a]
Agarose	-0.120 ± 0.012 (3)	-18.0 ± 1.9 (3)	LB (a, d, g, j)
Human albumin	-0.367 ± 0.007 (3)	-58.3 ± 1.0 (3)	LB (a, d, g, j)
Bovine albumin	-0.360 ± 0.006 (2)	-57.6 ± 0.7 (2)	LB (a, d, g, j)
Ovine albumin	-0.360 (1)	-56.7 (1)	LB (a, d, g, j)
Rabbit albumin	-0.360 ± 0.018 (3)	-57.2 ± 2.6 (3)	LB (a, d, g, j)
Goat albumin	-0.327 (1)	-51.5 (1)	LB (a, d, g, j)
1× adsorbed and crosslinked BSA	-0.277 ± 0.008 (3)	-44.1 ± 1.3 (3)	RVW (a, c, f, j)
6× adsorbed and crosslinked BSA	-0.280 ± 0.002 (3)	-45.6 ± 0.3 (3)	RVW (a, c, f, j)

[a] See note for Table I.

Tables I–III for glass and silane substrates, biopolymer and synthetic polymer films, respectively. In each case, the final column identifies the investigator—substrate: Gold Seal (a) or Bev-1-edge (b), silane linkage: none (c), APS (d), or n-PS (e), extraction conditions: none (f), overnight in streaming electrolyte (g), 24 hr (h), or 35 hr (i) in doubly distilled water, and degree of electrokinetic data stability during the 15 min required for analysis, i.e., less than (j) or more than (k) 5% total variation in three or more $\Delta E_{str}/\Delta P$ ratios per sample. Values for both $\Delta E_{str}/\Delta P$ and ψ_ζ are given in the event that any assumptions leading to the derivation of Eq. [1] are found to be erroneous in the future.

Electrokinetic reproducibility for most substrates and films prepared and evaluated by different investigators was generally good with ranges in ψ_ζ of 0 mV (HEMA, 97% MMA–3% MAA), 2 mV (PDMS, PVC, MMA, 97%–HEMA–3% MAA), 3 mV (Gold Seal), 4 mV (Bev-1-edge), 5 mV (97% HEMA–3% DMAEMA–CH$_3$Cl) and 6–7 mV for n-PS and APS, respectively. Both PS and 97% MMA–3% DMAEMA–CH$_3$Cl exhibited substantial variability (17–19 mV) which seemed to result from differences arising during sample preparation and extraction. Several films, notably some

n-PS, PDMS, PVC, MMA, and PS exhibited significant variations in $\Delta E_{str}/\Delta P$ with time. In these instances, $\Delta E_{str}/\Delta P$ and thus ψ_ζ became more negative. This often seemed to be attributable to inadequate film extraction or preequilibration prior to streaming analysis. Polystyrene was the most difficult film to analyze exhibiting the largest electrokinetic time variability (8 mV in 15 min), the largest degree of sample heterogeneity, and in some instances partial film detachment.

Spun cast serum albumin films were electrokinetically stable and essentially identical (-57.5 ± 1 mV) for a variety of vertebrate species with the exception of goat albumin (-51.5 mV). See Table II. Adsorbed and subsequently crosslinked BSA showed no electrokinetic difference between the first adsorption–crosslinking sequence and the sixth (-45 ± 1 mV). The 12.5-mV difference in ψ_ζ between spun cast and adsorbed BSA films may be due to different sources of Fraction V, methods of glutaraldehyde crosslinking, or film depositing. Spun cast agarose films were also evaluated and this material seemed to have the lowest ψ_ζ of all the "neutral" materials.

The electrokinetic potential of all "neutral" hydrophobic and hydrophilic polymers was

TABLE III

Average ζ Potential and $\Delta E_{str}/\Delta P$ Ratio for Synthetic Polymer Films Evaluated on n Samples

Sample description	$\Delta E_{str}/\Delta P \pm 1\sigma$ (n) (mV/cm Hg)	$\psi_\zeta \pm 1\sigma$ (n) (mV)	Investigator comment key[a]	
PDMS	-0.320 ± 0.008 (2)	-49.0 ± 0.7 (2)	RVW/LS	(a, c, g, k)
PDMS	-0.328 ± 0.024 (4)	-49.6 ± 3.3 (4)	DLC	(b, c, g, j)
PDMS	-0.272 ± 0.021 (3)	-41.6 ± 3.1 (3)	PT	(b, e, f, k)
PDMS	-0.330 ± 0.014 (3)	-51.0 ± 2.2 (3)	PT	(b, e, i, k)
PDMS	-0.333 ± 0.013 (3)	-51.2 ± 2.6 (3)	PT	(b, e, h, k)
PVC	-0.265 ± 0.010 (3)	-40.2 ± 2.3 (3)	PT	(b, e, f, k)
PVC	-0.285 ± 0.005 (3)	-42.4 ± 1.3 (3)	PT	(b, e, h, k)
PVC	-0.272 ± 0.015 (3)	-39.6 ± 2.1 (3)	PT	(b, e, i, k)
PS	-0.235 ± 0.028 (2)	-38.6 ± 4.0 (2)	RVW/LS	(a, e, g, k)
PS	-0.314 ± 0.006 (3)	-45.6 ± 1.6 (3)	PT	(b, e, f, k)
PS	-0.287 ± 0.011 (3)	-42.7 ± 2.2 (3)	PT	(b, e, h, k)
PS	-0.308 ± 0.014 (3)	-47.4 ± 1.9 (3)	PT	(b, e, i, k)
PS	-0.372 ± 0.012 (3)	-57.7 ± 1.6 (3)	PT	(b, e, i, k)
Avcothane	-0.256 ± 0.021 (3)	-38.6 ± 3.1 (3)	DLC	(b, c, g, j)
HEMA	-0.154 ± 0.009 (3)	-24.1 ± 1.3 (3)	DLC	(a, c, g, j)
HEMA	-0.157 ± 0.012 (3)	-24.0 ± 1.8 (3)	RNK	(a, c, g, j)
MMA	-0.214 ± 0.014 (3)	-33.9 ± 2.2 (3)	RVW/LS	(a, e, g, k)
MMA	-0.202 ± 0.019 (3)	-31.5 ± 3.1 (3)	DLC	(a, e, g, j)
50% HEMA–50% MMA	-0.190 ± 0.012 (3)	-28.7 ± 1.8 (3)	DLC	(b, c, g, j)
99% HEMA–1% MAA	-0.160 ± 0.022 (3)	-24.8 ± 3.4 (3)	RNK	(a, d, g, j)
97% HEMA–3% MAA	-0.165 ± 0.007 (3)	-25.7 ± 1.1 (3)	RNK	(a, d, g, j)
97% HEMA–3% MAA	-0.184 ± 0.044 (8)	-28.3 ± 6.6 (8)	DLC	(a, d, g, j)
75% HEMA–25% MAA	-0.248 ± 0.008 (3)	-38.4 ± 1.2 (3)	RNK	(a, d, g, j)
50% HEMA–50% MAA	-0.286 ± 0.008 (3)	-44.0 ± 1.2 (3)	RNK	(a, d, g, j)
25% HEMA–75% MAA	-0.305 ± 0.011 (3)	-46.7 ± 1.8 (3)	RNK	(a, d, g, j)
99% HEMA–1% DMAEMA–HCl	-0.096 ± 0.016 (3)	-14.8 ± 2.4 (3)	RNK	(a, c, g, j)
99% HEMA–1% DMAEMA–CH$_3$Cl	-0.079 ± 0.017 (3)	-13.3 ± 1.4 (3)	RNK	(a, c, g, j)
97% HEMA–3% DMAEMA–HCl	-0.086 ± 0.013 (3)	-13.2 ± 2.0 (3)	RNK	(a, c, g, j)
97% HEMA–3% DMAEMA–CH$_3$Cl	-0.039 ± 0.019 (3)	-6.0 ± 3.0 (3)	RNK	(a, c, g, j)
97% HEMA–3% DMAEMA–CH$_3$Cl	-0.006 ± 0.040 (3)	-0.9 ± 5.5 (3)	DLC	(a, c, g, j)
95% HEMA–5% DMAEMA–HCl	-0.042 ± 0.020 (3)	-5.1 ± 0.9 (3)	RNK	(a, c, g, j)
95% HEMA–5% DMAEMA–CH$_3$Cl	0.00 ± 0.014 (3)	0.0 ± 2.4 (3)	RNK	(a, c, g, j)
90% HEMA–10% DMAEMA–CH$_3$Cl	$+0.024 \pm 0.003$ (3)	$+3.7 \pm 0.5$ (3)	RNK	(a, c, g, j)
85% HEMA–15% DMAEMA–HCl	-0.009 ± 0.006 (3)	-1.2 ± 1.1 (3)	RNK	(a, c, g, j)
85% HEMA–15% DMAEMA–CH$_3$Cl	$+0.064 \pm 0.004$ (3)	$+9.9 \pm 0.6$ (3)	RNK	(a, c, g, j)
65% HEMA–35% DMAEMA–HCl	$+0.020 \pm 0.008$ (3)	$+3.1 \pm 1.2$ (3)	RNK	(a, c, g, j)
97% MMA–3% MAA	-0.315 ± 0.021 (3)	-49.2 ± 3.1 (3)	DLC	(a, d, g, j)
97% MMA–3% MAA	-0.303 ± 0.009 (3)	-48.7 ± 1.5 (3)	RVW/LS	(a, d, g, j)
97% MMA–3% DMAEMA–HCl	-0.157 ± 0.013 (3)	-25.1 ± 1.5 (3)	RVW/LS	(a, e, g, j)
97% MMA–3% DMAEMA–CH$_3$Cl	$+0.121 \pm 0.010$ (3)	$+19.1 \pm 1.4$ (3)	DLC	(a, c, g, j)
97% MMA–3% DMAEMA–CH$_3$Cl	$+0.010 \pm 0.028$ (3)	$+1.6 \pm 4.5$ (3)	RVW/LS	(a, e, g, j)
n-BMA	-0.285 ± 0.004 (4)	-41.6 ± 2.1 (4)	DLC	(b, e, g, j)
97% n-BMA–3% MAA	-0.421 ± 0.005 (3)	-63.3 ± 0.65 (3)	DLC	(b, d, g, j)
97% n-BMA–3% DMAEMA–CH$_3$Cl	-0.158 ± 0.028 (4)	-23.9 ± 4.0 (4)	LB	(a, c, g, j)
90% n-BMA–10% DMAEMA–CH$_3$Cl	-0.079 ± 0.003 (2)	-12.8 ± 0.4 (2)	LB	(a, c, g, j)

[a] See note for Table I.

net negative as shown in Table III, i.e., PDMS $(-51 \pm 1\,mV)$, PVC $(-41 \pm 1\,mV)$, PS $(-44 \pm 4\,mV)$, n-BMA $(-42\,mV)$, avcothane $(-39\,mV)$, HEMA $(-24 \pm 0\,mV)$, and MMA $(-33 \pm 1\,mV)$. Equimolar mixtures of HEMA–MMA copolymer had

an intermediate ψ_ζ of -29 ± 2 mV. Incorporation of negatively charged MAA residues into HEMA, MMA, and n-BMA resulted in copolymers which exhibited increasingly negative values of ψ_ζ with increasing amount of bulk charge. Similarly, copolymers having positive residues (DMAEMA–HCl and DMAEMA–CH₃Cl) incorporated into neutral HEMA, MMA, and n-BMA always had a ψ_ζ which was less negative than that of the neutral base polymer. At sufficiently high percentages of charge incorporation, ψ_ζ became net positive. The CH₃Cl salt of DMAEMA seemed to be more effective in manifesting the positive charge than the HCl salt at equivalent concentrations. This may arise from differences in local microenvironment and subsequent influences on pK_a's of the two species. These studies suggest that incorporation of charged residues into the polymer network has a predictable effect on the electrokinetic surface charge and thus ψ_ζ.

The origin and distribution of charge and resultant potential field at the insulator–electrolyte interface is not completely understood for glass or polymers. The net negative charge on soft glass may arise from the ionization of surface silanol groups having a pK_a of 7.1–7.2 (9, 10) or the adsorption of potential-determining ions (11) or a combination of both (12). Soft glass preexposed to an aqueous environment possesses an extensively hydrated, leached surface of porous, amorphous silica characterized by at least three kinds of silanol species (9). Differences between ψ_ζ for Gold Seal (-64 mV) and Bev-1-edge (-52 mV) slides are significant and may arise from processing variations, e.g., forming, polishing, cleaning, hydration, etc., leading to differences in silanol content, ion profiles, surface porosity, and roughness. The degree of surface roughness and subsequent effect on shear plane position is probably the single largest unknown remaining in electrokinetic research (13). One model (14) arising

from electrokinetic titration studies envisions the glass surface as possessing hydroxyl adsorption sites distributed throughout an open, porous hydrated surface with proportionately fewer sites at the surface in the vicinity of the electrokinetic shear plane. Consequently, titratable charge greatly exceeds the electrokinetic charge responsible for ψ_ζ and the electrokinetic potential approaches a plateau value at increasing pH since ion-binding sites at the shear plane are occupied at low pH first.

The origin of charge at the polymer–electrolyte interface is even less clear. Our preliminary electrokinetic studies (15) showed that many neutral polysaccharide and synthetic polymers acquire a net negative surface potential in contact with aqueous electrolyte. While incorporation of either positive or negative moieties as copolymer residues was reflected at the electrokinetic surface as a decrease or increase in net negative potential, respectively, the amount of measured charge greatly exceeded that attributable to charge incorporated as ionizable groups. Those results agree with this study in that small amounts of charge added to hydrophilic methacrylates, such as HEMA, were found to increase streaming potential values, but the incorporation of additional larger amounts had a less prominent effect on ψ_ζ as evidenced by a plateau for both positive and negative charge addition on a graph of ψ_ζ versus mole percent added charge. ζ Potential as a function of net charge incorporated as HEMA–DMAEMA–HCl, HEMA–DMAEMA–CH₃Cl, or HEMA–MAA copolymer exhibited an obvious symmetry around 0 mole percent charge for the positive and negative copolymers (15, 16).

All synthetic, neutral polymers as well as agarose had a net negative ζ potential. Other researchers have found similar results for a variety of synthetic polymer (4, 17–19) and natural polymer surfaces (20–23) many of which have biomedical applications. The most widely quoted explanation for net

negative electrokinetic charge on non-ionizable polymers is the specific adsorption of potential-determining ions such as OH^- and Cl^- from solution (17, 18, 24). In principle, the smaller, more polarizable, and less hydrated anions in an aqueous electrolyte have a greater tendency to partition at an interface particularly if the polymer surface is hydrophobic. Hydrated proteins and neutral polysaccharide surfaces adsorb ions less readily than hydrophobic polymers. However, albumin molecules seem to be an exception adsorbing anions (24) to hydrophobic sites (25) on the molecule surface. The orientation and structure of water at interfaces of differing hydrophilicity have been postulated as playing a role in specific anion adsorption and subsequent interfacial charging (17).

Polystyrene lattices with no titratable surface charge have been shown to possess substantial electrophoretic mobilities which were explained by the adsorption of chloride and hydrogen anions (26). However, Fowkes and Hielscher (27) provided an alternative explanation which evoked electron injection from cationic water states into anionic states of polystyrene thin films as the mechanism for providing negative electrokinetic potentials. Their data obtained with a depletion mode P-channel FET indicated that both PS and chlorinated polyethylene reached equilibrium surface charge densities of about 1×10^{12} electrons cm^{-2} within 20 sec. Many of our "neutral" polymer films have ψ_ζ in the -40 mV range which corresponds to a diffuse double-layer charge component of about 3×10^{12} charges cm^{-2}. It is also interesting to note the existence of time-dependent electrokinetic drift in some of our polymer thin film results. This is attributed to physical changes in the film during streaming. Most films were pre-equilibrated in streaming electrolyte prior to analysis; however, those films exhibiting the largest time variability (PS) were equilibrated in doubly distilled water. This variability then may reflect the process of interfacial charging and ion diffusion potentials accompanying exposure to electrolyte rather than actual film detachment. Also, additional research associated with this study has shown a strong correlation between bulk water content and both ψ_ζ and the component of the interfacial free energy for unchanged hydrophilic and hydrophobic polymers (16, 28). Modeling and experimental studies are currently underway to more fully elucidate the origin of interfacial charge and its relationship to water structure, surface hydropholicity, and protein adsorption.

REFERENCES

1. Andrade, J. D., *Med. Instrum.* 7, 110 (1973).
2. Ratner, B. D., *J. Polym. Sci. Symp.* 66, 53 (1979).
3. Andrade, J. D., Lee, H. B., Jhon, M. S., Kim, S. W., and Hibbs, J. B., Jr., *Trans. Amer. Soc. Artif. Intern. Organs* 19, 1 (1973).
4. Sawyer, P. N., *J. Electrochem. Soc.* 125, 419C (1978).
5. Van Wagenen, R. A., and Andrade, J. D., *J. Colloid Interface Sci.* 76, 305 (1980).
6. Haller, I., *J. Amer. Chem. Soc.* 100, 8050 (1979).
7. Gregonis, D. E., Chen, C. M., and Andrade, J. D., *Amer. Chem. Soc. Symp. Ser.* 31, 88 (1976).
8. Van Wagenen, R. A., Ph.D. dissertation, University of Utah, 1976.
9. Hair, M. L., and Hertl, W. J., *J. Phys. Chem.* 74, 91 (1970).
10. Marshall, K., Ridgewell, G. L., Rochester, C. H., and Simpson, J., *Chem. Ind. London* 19, 775 (1974).
11. Kruyt, H. R., "Colloid Science," Vol. 1. Elsevier, New York, 1952.
12. Tadros, Th.F., and Lyklema, J., *J. Electroanal. Chem. Interfacial Electrochem.* 17, 267 (1968).
13. Bikerman, J. J., "Physical Surfaces," p. 420. Academic Press, New York, 1970.
14. Lyklema, J., *J. Electroanal. Chem. Interfacial Electrochem.* 18, 341 (1968).
15. Ma, S. M., Gregonis, D. E., Van Wagenen, R., and Andrade, J. D., *Amer. Chem. Soc. Symp. Ser.* 31, 241 (1976).
16. King, R. N., Ph.D. dissertation, University of Utah, 1980.

17. Eagland, D., and Allen, A. P., "Surface Hydration and ζ Potential, International Conference on Surfaces and Colloids, Puerto Rico, June 1976."

18. Benes, P., and Paulenova, M., *Kolloid Z. Z. Polym.* **251,** 766 (1973).

19. Stone-Masui, J., and Watillon, A., *J. Colloid Interface Sci.* **52,** 479 (1975).

20. Parreira, H. C., and Schulman, J. H., *Amer. Chem. Soc. Advan. Chem. Ser.* **33,** 160 (1961).

21. Fromageot, H. P. M., Groves, J. N., Sears, A. R., and Brown, J. F., Jr., *J. Biomed. Mater. Res.* **10,** 455 (1976).

22. Brown, J. F., Jr., Bergeron, J. A., Fromageot, H. P. M., Groves, J. N., Slusarczuk, G. M. J., and Dodds, W. J., "Studies of Elastin as a Biomaterial," NIH Report N01-HV-4-2981-1, 1977.

23. Brooks, D. E., *J. Colloid Interface Sci.* **43,** 670 (1973).

24. Shaw, D. J., "Electrophoresis," pp. 4, 43. Academic Press, New York/London, 1969.

25. Hofstee, B. H. J., and Otillio, N. F., *J. Chromatogr.* **161,** 153 (1978).

26. Ma, C. M., Micale, F. J., El-Aasser, S., and Vanderhoff, J. W., *Amer. Chem. Soc. Prepr.* **43,** 358 (1980).

27. Fowkes, F. M., and Hielscher, F. H., *Amer. Chem. Soc. Prepr.* **42,** 169 (1980).

28. Coleman, D. L., Ph.D. dissertation, University of Utah, 1980.

24. MacRitchie, F. *J. Colloid Interface Sci.* **1972**, *38*, 484.
25. Morrissey, B. W.; Stromberg, R. R. *J. Colloid Interface Sci.* **1974**, *46*, 152.
26. Brash, J. L.; Davidson, V. *J. Thromb. Res.* **1976**, *9*, 249.
27. Tarasevich, Yu.I.; Smirnova, V. A.; Monakhova, L. I. *Colloid J. USSR* **1978**, *40*, 1029.
28. Hofstee, B. H. J.; Otillio, N. F. *J. Chromatogr.* **1978**, *161*, 153.
29. Burnstein, E. A.; Vedenkina, N. S.; Ivkova, M. N. *Photochem. Photobiol.* **1973**, *18*, 263.
30. Spector, A. A.; John, M. K. *Arch. Biochem. Biophys.* **1968**, *127*, 65.
31. Guilbault, G. G. "Practical Fluorescence"; Dekker: New York, 1973, p. 497.

23

Probing Protein Adsorption: Total Internal Reflection Intrinsic Fluorescence

R. A. VAN WAGENEN, S. ROCKHOLD, and J. D. ANDRADE

University of Utah, Department of Bioengineering, College of Engineering, Salt Lake City, UT 84112

Interfacial intrinsic fluorescence induced by evanescent wave total internal reflection was developed to study protein adsorption at solid–aqueous buffer solution interfaces. The technique has a number of advantages over conventional methodologies for the study of adsorption including (1) continuous, real-time sampling with 0.1-s resolution; (2) in situ sensing; (3) application to biomedically relevant, flat, low surface area samples; (4) quantitation of the amount adsorbed calculated on the basis of an internal standard; and (5) ability to obtain fluorescence emission spectra of intrinsic tryptophan moieties that are sensitive to local microenvironmental changes produced during the protein adsorption process. These advantages are illustrated for bovine serum albumin and γ-globulins adsorbed on hydrophilic quartz.

An understanding of protein adsorption behavior is applicable in numerous fields including blood–synthetic materials interfaces, macromolecular-membrane interactions, receptor interactions, enzyme engineering, adhesion, and protein separation on chromatographic supports. Many methods have evolved to study interfacial adsorption, but no single independent method seems adequate. The ideal technique should produce quantitative, real-time, in situ data concerning the amount, activity, and conformation of proteins adsorbed on well-characterized surfaces. All adsorption techniques are approximations to this optimum.

Protein solution depletion via adsorption on finely divided substrates is quantitative, but applicability to low surface area materials of biomedical relevance is often minimal. Adsorption of radiolabeled macromolecules is

quantitative on low surface area substrates; however, the presence of an extrinsic label may alter protein physical properties and subsequent adsorption behavior. Automated ellipsometry can, in principle, provide in situ, real-time information on film thickness and refractive index, but the minute differences in substrate, film, and buffer refractive indices often preclude this approach. Multiple internal reflection infrared spectroscopy is complicated by strong water signals that obscure protein amide bands and, while Fourier transform analysis seems promising, the interpretation remains difficult and the equipment is expensive.

Interfacial protein fluorescence induced by internal reflection evanescent wave excitation offers a number of advantages over conventional adsorption techniques. The total internal reflection fluorescence (TIRF) concept was originally patented by Hirschfeld (1) and applied to protein adsorption by Harrick and Loeb (2). Since then TIRF has been utilized in a limited number of investigations to study the adsorption of extrinsic fluor-labeled plasma proteins on quartz (3, 4), hapten-protein conjugates (5), and poly-dimethylsiloxane films (6). Our preliminary development of TIRF also employed covalently bound fluorescein isothiocyanate (FITC) as an extrinsic fluor (7, 8); however, research has indicated that FITC labeling of albumin is labile and also alters the proteins chromatographic and electrophoretic properties (9). Extrinsic labels per se are not objectionable as long as the presence of the label can be shown not to alter the biochemical and physicochemical properties of the molecule being studied. However, the attractiveness of intrinsic TIRF is that the difficulties in labeling and confirming the inertness of the label are completely obviated. We report here the successful development of intrinsic, interfacial protein fluorescence based on tryptophan excitation. The advantages offered by intrinsic TIRF are illustrated with data for albumin and γ-globulin adsorption on quartz.

Principles of Internal Reflection Fluorescence

When light of wavelength λ, traveling in a medium of refractive index n_1, encounters a second medium of refractive index n_2 ($n_2 < n_1$), it undergoes total internal reflection if the angle of incidence, θ, exceeds the critical angle θ_c, where $\theta_c = \sin^{-1}(n_2/n_1)$. The rectangular coordinate system of Figure 1 illustrates this phenomenon. The electric field vectors may be resolved into components parallel, $E_\parallel$, and perpendicular, $E_\perp$, to an optical plane delineated by the incident and reflected beams. The superposition of incident and reflected radiation establishes a standing wave normal to the reflecting interface as illustrated in Figure 1. The electric field amplitude has a nonzero value E at the surface, which then decays exponentially into the less dense medium. The perpendicular polarization-mode electric field amplitude at
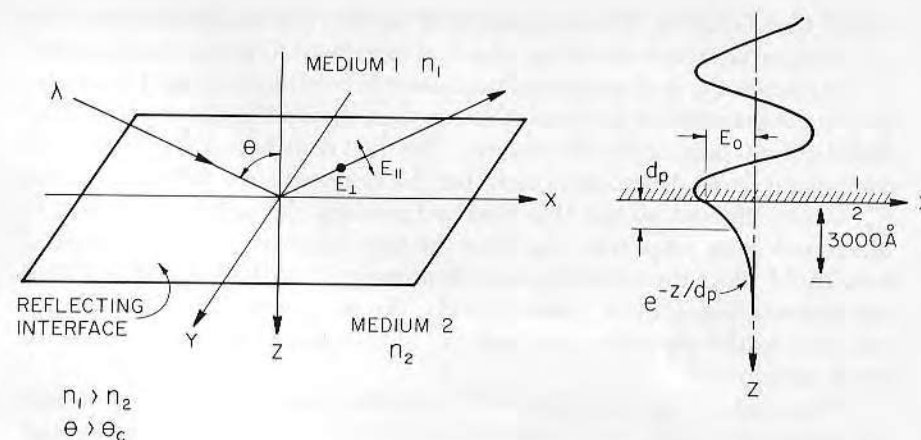
Figure 1. Left: Schematic of the coordinate system at a totally reflecting interface separating two media of refractive index n_1 and n_2. Right: Standing wave pattern and exponential decay of the electric field vector into the less dense medium, 2.

the interface (10), $E_\perp{}^\circ$, can be represented as

$$E_\perp{}^\circ = E_y{}^\circ = \frac{2\cos\theta}{[1-(n_{21})^2]^{1/2}} \tag{1}$$

where $n_{21} = (n_2/n_1)$.

An electromagnetic disturbance termed the evanescent wave penetrates the rarer medium to a finite depth. It has a wavelength λ and is continuous with the sinusoidal field of the standing wave, but the electric field amplitude E decreases exponentially with distance from the surface z as

$$E = E^\circ \exp[-z/d_p] \tag{2}$$

The effective wave penetration depth d_p is the distance z, where the electric field amplitude E has decayed to e^{-1} of its surface value E°, as given by Equation 3.

$$d_p = \frac{\lambda}{2\pi n_1 [\sin^2\theta - (n_{21})^2]^{1/2}} \tag{3}$$

The value of d_p decreases at shorter wavelengths, greater index mismatching ($n_1 \gg n_2$), and incident angles approaching the critical angle ($\theta \to \theta_c$).

Interfacial fluorescence provides an excellent means of studying protein adsorption. The maximum energy available for excitation is localized within a few hundred angstroms of the surface where most of the protein is concen-

trated. Consequently, the vast majority of the fluorescence signal arises from adsorbed protein molecules. An adsorbed interfacial film of refractive index n_3 complicates the analysis of interfacial electric field distribution. Generally, the film is assumed to be much thinner than d_p and the film electric field distribution is assumed to be uniform. The field distribution for the parallel component depends strongly on n_3, but the perpendicular field component $E_\perp$, is not affected by the thin film and remains defined by Equation 1. Macromolecular properties may alter the film refractive index n_3, which in turn could affect the available excitation energy distribution and resulting flourescence signal levels. Consequently, the perpendicular component $E_\perp$ was used in this research. (*See* Refs. *8, 10, 11,* and *12* for more details on TIRF principles.)

The study of macromolecular adsorption on thin polymer films should also be feasible. Adsorption isotherms can be obtained on any nonfluorescing polymer that can be deposited in thin-film form on quartz. The only limitation is that the film be nonabsorbing at the excitation wavelength and exhibit minimal fluorescence. Thin films of depth d can be studied if $[2\pi d/\lambda] < 0.1$ and if the film attenuation index κ is less than 0.1 (*10*). Thin films on quartz substrates can then be characterized by other surface analytical techniques.

Molecular interaction with radiation is proportional to the radiation intensity, and thus to the square of the electric field vector, $E_\perp^2$. Equations 1–3 were used to generate Figure 2 which illustrates the variation of $E_\perp^2$ with z for both intrinsic and extrinsic TIRF at the quartz–aqueous electrolyte interface. Intrinsic fluorescence is more localized in the interfacial region ($d_p = 1040$ Å) than is extrinsic fluorescence using FITC ($d_p = 2235$ Å).

Experimental

Figure 3 illustrates the experimental configuration. The light source (A) was a 200-W mercury–xenon high-pressure lamp, and the monochromator (B) selected the fluorescence excitation wavelength. A 10-cm focal length quartz lens (L) reduced the beam diameter and, in conjunction with a front-surface, silvered mirror (M), redirected the light through a UV-polarizing filter (Oriel 2732) (0) oriented to pass the perpendicular component of radiation. Light entered one face of the quartz dove tail prism (Q), and illuminated approximately 1/cm² of the central prism face contacting the aqueous buffer in the flow cell (F). The prism was UV-grade quartz (Markson Science Inc.)—3-cm wide, 9-cm long, and 2.9-cm thick with face angles of 70° to the base. The flow cell base was a 3-cm wide, 9-cm long, and 1.3-cm thick block of marine-grade aluminum alloy (5086-Hll) anodized flat black after machining rectangular slit-flow ports at the surface of each end. Aluminum was chosen because of its ease of machining, passivity to cleaning solvents, and good thermal conductivity. The anodized film endowed the cell base with excellent inertness to aqueous saline solutions. The flow cell base and prism were separated by a Silastic rubber medical-grade polydimethylsiloxane gasket 0.05 cm thick. The effective cell flow field was 7.9 × 2.1 × 0.05 cm. Flow rates during sample injection and flush ranged from 1.5 to 2.0 mL/s. Flow at the sampling area was laminar (Reynolds numbers 140–190) and well established (flow development length 0.12 cm). Flow cell surface area and
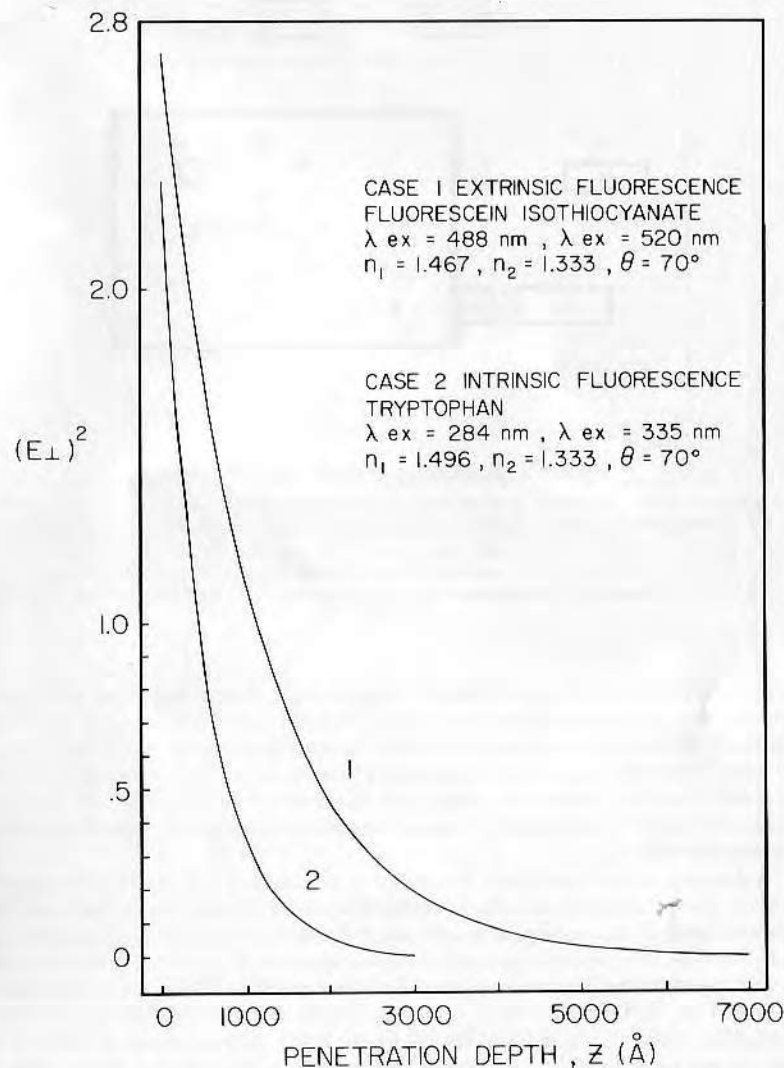

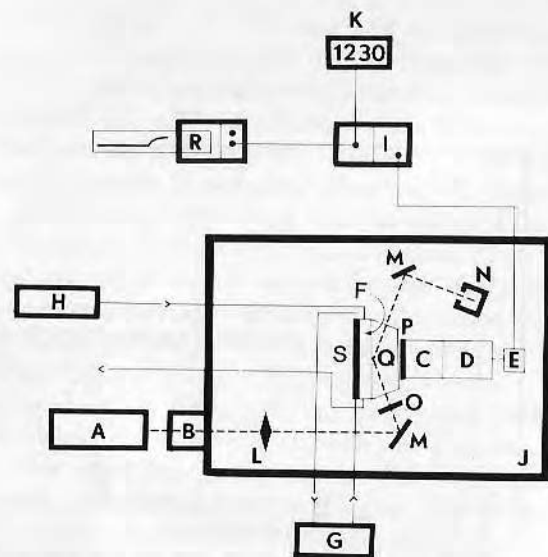Figure 2. Exponential decay in $(E_\perp)^2$ with distance z from the reflecting interface.

Figure 3. Schematic of experimental system.

Light source (A), excitation and emission monochromators (B and C, respectively), PMT (D), preamplifier (E), flow cell (F), constant temperature recirculator (G), syringe pump (H), photon counter (I), light tight enclosure (J), digital disc storage (K), quartz lens (L), mirrors (M), beam stop (N), excitation and emission polarizing filters (O and P, respectively), trapezoidal quartz prism (Q), chart recorder (R), and copper heat exchanger base plate (S).

volume were 34.1 cm^2 and 0.83 cm^3, respectively. The amount of bulk solution depletion due to protein adsorption on the cell walls was not measured, but order of magnitude calculations suggest that it could be significant for C_B less than 0.1 mg/mL. However, this result depends on how much protein is assumed to adsorb to the flow cell walls. Flow cell base temperature and all solutions entering the cell were maintained at 37° ± 1°C by an attached copper base plate (S) thermally linked to a constant-temperature bath (G).

A fraction of the interfacial fluorescence penetrated the prism and entered an emission monochromator (C). Both monochromators (B) and (C) (Jobin Yvon, H-10) were used with 16-nm bandpass resolution, the only exception being for spectra scans where the emission monochromator bandpass was 4 nm for optimal resolution. Fluorescence quantitation was accomplished by using an RCA 8850 photomultiplier tube (D) linked to an Ortec photon counting system with the following components: preamplifier 9301 (E), amplifier-discriminator 9302, photon counter 9315 (I), sampling control module 9320, and digital data storage using a 5¼-in. floppy disk on an Apple II Plus Computer (K). Digital signals were converted to analog (Ortec 9325) and displayed on a Pharmacia 481 strip chart recorder (P). Well-defined flow parameters were maintained by a Sage Instruments 341 syringe pump (H). An acrylic, light tight housing (J) and beam stop (N) helped keep extraneous light signals at low levels.

All solutions were made with analytical-grade reagents and low-conductivity (6 megohm) water purified by a combination of reverse osmosis, ion exchange, activated-carbon adsorption, and microfiltration. Phosphate-buffered saline (PBS) (0.145M NaCl, $2 \times 10^{-4}M$ KH$_2$PO$_4$, $8 \times 10^{-4}M$ Na$_2$HPO$_4$) had a pH of 7.3 and

osmolarity of 310 mosmol. All solutions were deaerated initially, but because this procedure had no effect on fluorescence intensity, deaerating was not a routine procedure.

Proteins were obtained from Miles Laboratories as bovine serum albumin (BSA) monomer standard Fraction V (81-028-1-P338) and bovine γ-globulins Fraction II (82-041-2-1086). L-Tryptophan (Matheson Coleman & Bell), 0.3 mg/mL in PBS, was used as an intrinsic fluorescence experimental reproducibility standard.

The quartz prism surface was cleaned prior to each experiment in the following sequence: (1) 5 min soak in 2% (v/v) Microclean, (2) 15-min soak in dichromate-sulfuric acid (25/mL Manostat Chromerge chromic acid in 4.1 kg of concentrated sulfuric acid), (3) thorough rinse in low-conductivity, filtered water, (4) rinse in filtered, absolute ethanol, (5) 5-min vapor degreasing in Freon TES-ethanol azeotrope vapor, (6) 2-min radiofrequency (RF) glow discharge at 30 W tuned RF power (Tegal, Plasmod), 200 μm mercury pressure oxygen plasma, and (7) 10-min purge in ultra-pure (99.999%) oxygen. All surface cleaning and assembly were carried out under Class 10,000 clean room conditions to minimize particulates and enhance experimental reproducibility.

Figure 4 illustrates schematically the time course of a TIRF experiment. The PBS background is due to scatter in the primed flow cell and stray light passed by the wide monochromator slits. The fluorescence signal intensity is expressed as counts per unit time above the PBS background. Injection of a tryptophan standard was used as an internal reference point for comparing the reproducibility of each experiment. With high recording speeds (10 cm/s), short count times (0.1 s), and rapid solution injection (1.5–2.0 mL/s), the speed with which the tryptophan bulk signal reached its equilibrium count level was determined. This procedure typically required 1–2 s after the first hint of signal increase. Similarly, the time required to remove all of the tryptophan from the cell at 2.0 mL/s was about 2 s. The cell priming volume, including flow ports, was 1.5 cm^3. No indication that tryptophan adsorbed irreversibly was observed, since count rates before and after the standard were identical.

Protein was introduced under the same sampling and flow conditions. At bulk concentrations greater than 0.5 mg/mL, a small signal step of 1–2 s, N_B, was immediately evident on the recorder at high speed and short sampling times (see Figure 5). The adsorption signal then rapidly developed on top of N_B. With the exception of injecting and flushing out protein solutions, all adsorption and desorption occurred under nonflow conditions. After reaching equilibrium signal level for any particular bulk protein concentration, the bulk protein was removed via a 50-mL flush of PBS at 2 mL/s. A rapid incremental signal drop N_B occurred due to removal of the bulk solution contribution followed by a slower decrease in signal as the protein molecules desorbed from the surface (see Figure 4). Protein adsorption dynamics could then be monitored. Alternatively, additional protein at a greater bulk concentration could be added in a stepwise manner to determine the adsorption isotherm. Solutions of higher bulk protein concentration were added when the equilibrium plateau signal had remained stable for 10–15 min. Since the time required to reach the plateau was generally about 20 min, the total elapsed time between different concentrations was typically 40 min. This entire step isotherm was determined on a single surface rather than the more classical and lengthy approach of obtaining one datum point at a particular C_B on a single fresh surface. Emission spectra of adsorbed protein were taken following the PBS flush. In this way only the spectra of adsorbed protein were determined. These spectra were then compared to bulk solution spectra of non-adsorbed protein obtained with the same equipment, but with the TIRF prism and cell replaced by a conventional transmission fluorescence bulk cell. Tryptophan amino acid emission spectra were recorded both in a conventional spectrofluorometer bulk cell and with the standard in the TIRF flow cell.
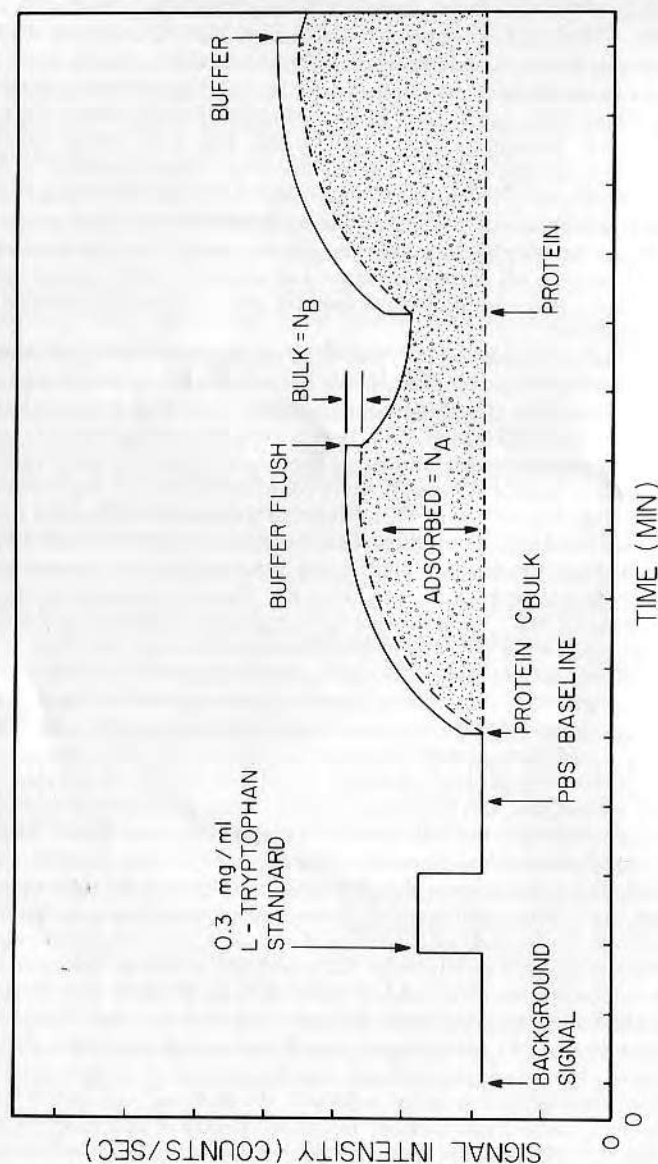
Figure 4. Schematic of TIRF data during a typical experiment. A tryptophan standard initiates each experiment. The stippled area represents adsorbed protein producing N_A counts per unit time.
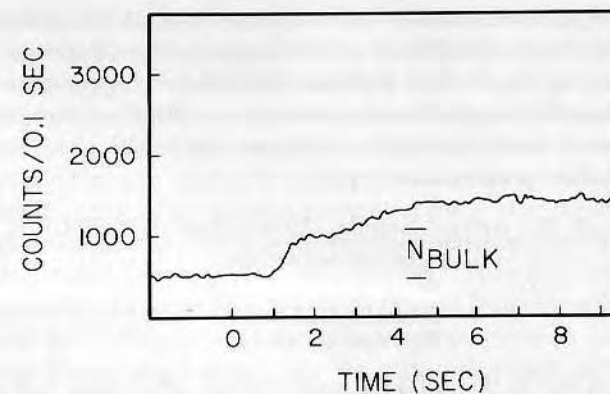
Figure 5. Fluorescence data for γ-globulin on quartz. The bulk signal N_B arises during the first 1–2 s of flow.

Results and Discussion

Interfacial fluorescence signals did not yield direct information on the amount of adsorbed protein. This lack of quantitation appears to be the major weakness of the method. Calibration studies have been attempted (6), but the ideal solution would be a second, independent quantitative technique such as FTIR or use of unaltered radiolabeled protein. An independent calibration method is now being developed.

Our approach was to use the fluorescence background signal N_B emanating from evanescent wave–excited protein in the bulk solution as an internal calibration signal. Consider the 3000-Å decay depth of $E_\perp^2$ for the intrinsic fluorescence case of Figure 2. The evanescent wave penetration depth was divided into 30 lamellae, each 100 Å thick and 1/cm². Adsorption was defined as those molecules occupying the first lamella adjacent to the surface. Molecules in Lamellae 2–30 were considered to have bulk properties and to constitute the bulk signal. The total fluorescence signal was proportional to the area under Curve 2 of Figure 2, but it was unequally weighted to the first few lamellae, where most of the energy was available to excite the majority of the molecules. The area of each lamella was integrated and expressed as field intensity units squared (FIU²). The first lamella had 2.11 FIU² while the sum of Lamellae 2–30 was 9.9 FIU². At a bulk protein concentration C_B of 1.0 mg/mL, each bulk lamella contained 1×10^{-9} g of protein. Protein in the bulk lamellae ($29 \times 0.001\ \mu g/cm^2$) was excited by 9.90 FIU² and produced N_B counts, while adsorbed protein Γ ($\mu g/cm^2$) was excited by 2.11 FIU² and produced N_A counts. Bulk signal N_B was resolved from adsorbed protein signal N_A during the first 1–2 s of protein injection and flush (See Figures 4 and 5). N_B was accurately determined for $C_B \geq 0.5$ mg/mL. Consequently, for the quantitation of N_B at lower bulk concentrations, a

linear plot of N_B as a function of $(0.5 \leq C_B \leq 4.0)$ mg/mL was extrapolated to a C_B of 0 mg/mL between $(0.0 \leq C_B < 0.5)$ mg/mL. The equality of Equation 4 results assuming that in both bulk and adsorbed states, a certain quantity of protein excited by a given amount of energy (FIU^2) produced an equal amount of fluorescence signal per unit time, that is, the quantum yields of bulk and adsorbed protein were equal.

$$\frac{(C_B)\ (0.001\ \mu g/cm^2\ \text{lamella})\ (29\ \text{lamellae})\ (9.90\ \text{FIU}^2)}{N_B\ \text{counts/unit time}} =$$

$$\frac{(\Gamma)\ (2.11\ \text{FIU}^2)}{N_A\ \text{counts/unit time}} \tag{4}$$

The correction for bulk protein concentrations other than 1.0 mg/mL is represented by C_B. Surface concentrations Γ ($\mu g/cm^2$) were calculated on the basis of Equation 4 and presented as a function of time or bulk concentration C_B for adsorption–desorption dynamics or adsorption isotherms, respectively.

This research and its associated quantitation rests on several assumptions. First, lamp power output was assumed to be invariant with times comparable to the course of an experiment. This assumption was reasonable since source intensity monitoring via background counts N for 6–8 h showed no significant drift if the lamp and photon counting system were equilibrated for 1 h prior to an experiment. Count rates N were typically 500 counts and the counting statistics error rarely exceeded $\sqrt{N}$ by more than several (0.1/s) percent. Second, the excited bulk concentration and thus N_B are time invariant. This assumption is probably correct if C_B is not reduced by adsorption within the flow cell and if no photobleaching occurs. Also, our fast sampling data indicated that for both tryptophan standard and protein solution, a bulk signal component could be resolved during the first 1–2 s following sample injection. The protein adsorption signal intensity then builds on top of this. Assuming that C_B is established more slowly by diffusional processes alone, some interfacial time-variant distribution function would have to be incorporated into Equation 4. Such a function would initially lower the interfacial concentration and reduce Γ. Third, quantum yields of adsorbed- and bulk-fluorescing species are identical. This is probably the most questionable assumption, particularly if conformational changes occur following adsorption. Quantum yield determinations of adsorbed species are planned in the future. Fourth, light scattered from both adsorbed molecules and bulk molecules within the evanescent zone does not generate significant bulk protein solution fluorescence. This assumption would have the effect of reducing N_A, increasing N_B, and consequently lowering Γ. Fifth, the adsorbed film is 100 Å thick, that is, it is the first lamella. Assuming that the adsorbed film and thus the first lamella was 50 or 150 Å thick, the calculated value of Γ would be altered by less than ±5%. Sixth, N_B could not be determined

accurately below a C_B of 0.5 mg/mL. Consequently, a plot of N_B as a function of $(0.5 \leq C_B \leq 4.0)$ mg/mL was linearly extrapolated to zero in the range $(0 \leq C_B < 0.5)$ mg/mL to yield values of N_B.

Finally, we assume no occurence of interfacial photochemistry. This was generally true for the light intensities and times utilized in our research as illustrated in Case 1 of Figure 6 for adsorbed bovine γ-globulin. Following protein introduction, the surface concentration Γ rose to an equilibrium value, and remained time invariant even when additional protein of the same bulk concentration was injected into the cell. However, when the light source intensity was increased beyond a critical level by either increasing lamp power or replacement with a fresh mercury–xenon lamp bulb, the equilibrium fluorescence signal was not attained. Signal intensity peaked quickly and then decayed continuously. This phenomenon is referred to as Case II behavior and is illustrated in Figure 6.

This behavior is not surprising in that many investigators have detected photoeffects under conventional spectrofluorometric conditions. Studies conducted on the UV-irradiation of lysozyme (*13*) and L-glutamate dehydrogenase (*14*) revealed a concomitant loss in enzyme activity and fluorescence emission with irradiation time. The primary photoeffects were destruc-
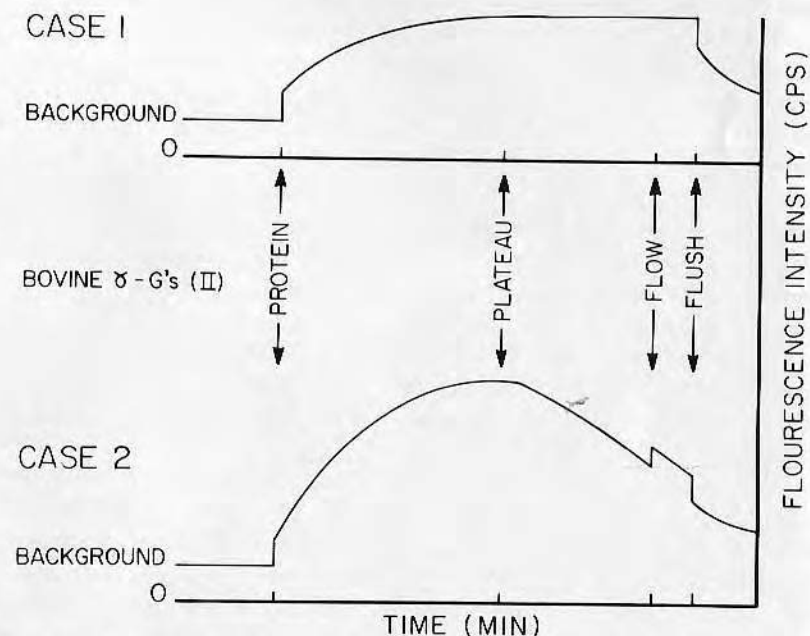

Figure 6. Schematic of typical TIRF data with no photoeffects (Case 1) and with photoeffects causing a time variable signal (Case 2) for bovine γ-globulin adsorbed on hydrophilic quartz.

tion of tryptophan residues and the appearance of SH groups (13) as disulfide bonds were disrupted. Enzymatic inactivation may have resulted from tertiary structure loss due to scission of the four disulfide bonds cross-linking the single polypeptide chain of lysozyme.

The destruction of aromatic and sulfur-containing amino acid residues and resulting loss of helical structure following 68 mW UV-irradiation also have been reported for albumin (15). However, in our research, signal instabilities postulated to result from photochemical effects were always associated with γ-globulin, but not albumin adsorption. Also, our calculated maximum UV light power was typically much less, that is, several megawatts at most. On the basis of tryptophan content alone, 25 residues in γ-globulin and two in BSA, the likelihood of photochemical susceptibility in γ-globulins is great. Both proteins have at least 16 disulfide bridges that maintain structural integrity, but both molecules appear to have substantial chain flexibility. At wavelengths of 270–290 nm or greater, aromatic residues and disulfide bonds of proteins adsorb well, and because tryptophan has the lowest triplet state energy of all the amino acids, light adsorption by other residues results in excited states that may migrate to specific tryptophan moieties via a nonradiative transfer mechanism. One primary oxidation reaction of photoexcited tryptophan is electron transfer to an acceptor molecule and C2–C3 bond cleavage of the indole ring yielding N-formylkynurenine (16).

The adsorption isotherm for bovine γ-globulin on hydrophilic quartz is illustrated in Figure 7. The equilibrium plateau concentration of 3.60 μg/cm² is substantially higher than most other γ-globulin adsorption data on silica and glass substrates, that is, several tenths of a microgram per square centimeter (17, 18). This result probably occurs because TIRF is an in situ technique yielding values of Γ obtained immediately after removal of the bulk signal. This is in contrast to most adsorption methods employing an extensive prequantitation buffer rinse that may cause desorption of a loosely bound, rapidly desorbing layer(s) (6), the presence of which would not be generally discernible.

Quantitation of Γ was made on the basis of bulk background counts N_B determined by a discrete step change in fluorescence intensity occurring either as protein was initially introduced or during the first few seconds of the buffer flush. Alternatively, N_B, and thus Γ, could be determined later during the flush sequence, for example, at 50 mL total flush volume rather than at 4 mL. This would be a closer approximation to sample washing conditions described for the more conventional approaches. The result would be a higher value of N_B, a lower value of N_A, and a value of Γ more than 50 percent lower than our data. In situ fluorescence appears to give larger values of Γ because conventional methods require longer rinse times which in turn remove substantial amounts of loosely adherent molecules.

Preliminary data determined for reproducibility studies at a C_B of 1.0 mg/mL on clean, hydrophilic quartz gave an equilibrium plateau adsorbed
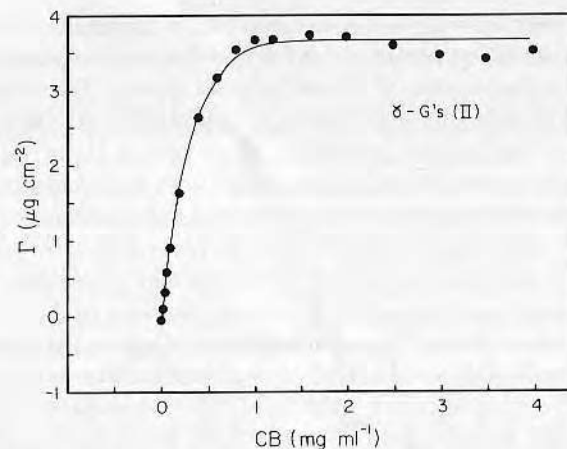
Figure 7. Adsorption isotherm for bovine γ-globulin on hydrophilic quartz at 37°C.

value of 1.69 ± 0.16 μg/cm² (n = 4). Not surprisingly, step isotherm and discrete adsorption isotherm maxima were substantially different. The conformational state of an adsorbed protein may be a function of surface residence time, solution activity, and number of adsorbed neighbors. Because adsorption is only partially reversible, C_B cannot be increased or decreased to obtain a particular value of Γ, that is, hysteresis effects do occur. Such hysteresis behavior has been well documented in adsorption experiments on well-defined chromatographic substrates (19). The application of TIRF to both desorption and adsorption dynamics as well as both approaches to isotherm determination should make the study of hysteresis effects more productive in the future.

A significant decrease occurred in adsorbed protein signal as reflected in Γ at bulk concentrations exceeding 2 mg/mL. This decrease was also evident in our earlier extrinsic TIRF adsorption studies with γ-globulin-FITC and fibrinogen-FITC (8), and also has been observed by others studying γ-globulin adsorption (3). The actual cause is as yet unresolved. However, this significant drop in fluorescence and thus in apparent Γ may be due to fluorescence quenching at high surface concentrations or protein conformational changes and subsequent lowering of quantum yield that may occur with increased surface packing density. Morrissey et al. (18, 20) have shown that γ-globulin does undergo substrate-induced conformational changes during adsorption on silica, and the degree of conformational alteration appeared to depend on surface concentration.

Since our isotherms are derived in a bulk concentration step-increase fashion, higher bulk concentrations (> 2 mg/mL) were not evaluated for several hours after protein first contacted the quartz surface. This delay may

provide sufficient time for γ-globulin molecules to change conformationally in such a manner tha quantum yields fall and the corresponding fluorescence signal drops or desorption of altered protein occurs. Transmission circular dichroism (CD) studies have shown major conformational changes during the adsorption and subsequent activation of Hageman factor on quartz (21). Recently, conformational changes associated with the adsorption of albumin, γ-globulin, and fibrinogen on to copolypeptide and silicone substrates were reported (22). Three stages characterized by reversible adsorption, irreversible adsorption, and slow structural alteration and desorption of denatured protein molecules were reported. However, the time course of these events was many hours to several days. Morrissey et al. saw no significant effect of time on the conformation of adsorbed γ-globulin (21).

Alternatively, an ordered, stable array of macromolecules may evolve at the surface with increasing time and/or bulk concentration. Since the excitation light is plane-polarized, the decay in emission signal may be a reflection of preferential orientation of γ-globulin molecules with time or enhanced surface packing densities. Fluorescence emission polarization studies should tell us more about this in the future.

Figure 8 illustrates the adsorption isotherm for BSA on hydrophilic quartz. The value of Γ is now on the order of 0.1 μg/cm^2, and the amount adsorbed is directly proportional to bulk concentration C_B with no hint of plateau saturation below 5.0 mg/mL. These surface concentrations are comparable to data reported by others (23–27) for BSA adsorption on silica and glasses. At a C_B of 1 mg/mL, reported values range from 0.02–0.2 μg/cm^2, depending on pH, temperature, ionic strength, and substrate. Our value of 0.08 μg/cm^2 at the same C_B is intermediate in this range. These results parallel our qualitative findings for BSA-FITC adsorption on quartz (8). Albumin adsorption continues to occur at concentrations exceeding those required for monolayer coverage. This result is at odds with most research, which indicates an equilibrium coverage of several tenths of a microgram per square centimeter at a C_B greater than several milligrams per milliliter. However, the means of obtaining these isotherms are not directly comparable with our TIRF data, where reversible desorption is more accurately based on rapidly removing only the bulk signal prior to reversible desorption of "peripheral protein." The continual buildup of BSA with increasing C_B may result from hydrophobic bonding between molecules comprising different layers. The surface of the BSA molecule may have hydrophobic patches (28), which may in turn facilitate multilayer binding at increasing concentrations via hydrophobic bonding.

Interfacial protein fluorescence is an in situ method that can provide real time data with a resolution of 0.1 s. This technique is a major advantage in that the protein adsorption–desorption dynamics may be determined without resorting to sample manipulation prior to analysis. Figure 9 illustrates adsorption–desorption dynamics for both BSA and γ-globulin at bulk equimolar concentrations of 6.67 μM/L. The γ-globulin required 40 min to reach
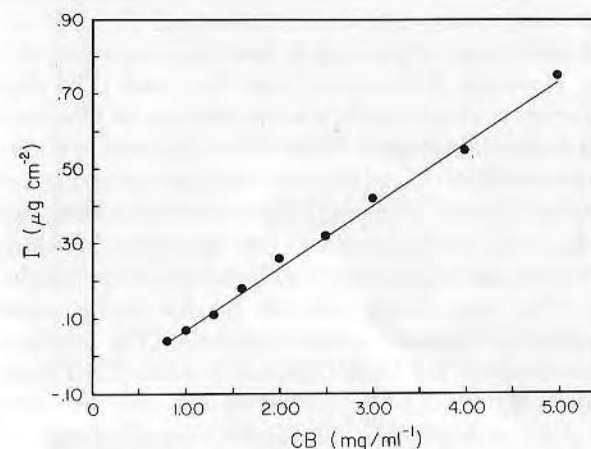
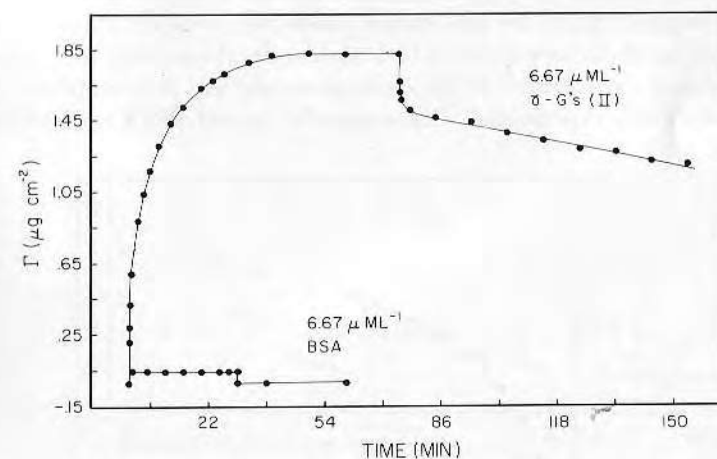*Figure 8. Adsorption isotherm for BSA on hydrophilic quartz at 37°C.*

Figure 9. Adsorption–desorption dynamics for equimolar concentrations of BSA and γ-globulin on hydrophilic quartz at 37°C.

an equilibrium of 1.80 $\mu g/cm^2$, while the BSA adsorbed to an equilibrium value of 0.06 $\mu g/cm^2$ in approximately 8 s, as illustrated in Figure 10. The initial desorption dynamics were extremely rapid for both proteins (see Figure 11). During the first 3 s, BSA desorbed at a rate of 24 $ng/cm^2/s$, and within 6 s, most of the protein had desorbed. However, a small amount of BSA always seemed to remain irreversibly adsorbed (7), that is, about 0.01 $\mu g/cm^2$. Such rapid rates might simply have been the result of bulk solution fluorescence. However, if this were true, the same TIRF behavior would occur on all surfaces, which clearly was not the case, as illustrated already for γ-globulin on hydrophilic quartz. Virtually no data exist in the literature with which we may compare this adsorptive behavior occurring in the first few seconds of surface contact. Dynamic ellipsometry is too slow, and radiolabled protein experiments are inappropriate due to required washing steps.

The initial desorption rate for γ-globulin was linear for the first 30 s at 6.7 $ng/cm^2/s$. This rapid desorption may be due to the presence of a reversibly adsorbed peripheral layer of γ-globulin. The existence of this adsorbed γ-globulin layer has been reported in other TIRF research as well (3, 6). A transition time of several minutes separates two essentially linear regions of γ-globulin desorption. The second linear desorption phase has a rate of 0.067 ng/cm/s over a 60-min period, that is, a factor one hundred times slower than the initial desorption rate. After more than 1 h of desorption, a substantial amount of γ-globulin remains "irreversibly" adsorbed on the quartz surface. Based on the second phase rate, at least 13 days would be required for all of the γ-globulin to desorb under these conditions. However, over periods exceeding 2 h, the desorption rate was not completely linear, but was weakly exponential. Consequently, irreversibly adsorbed layers of
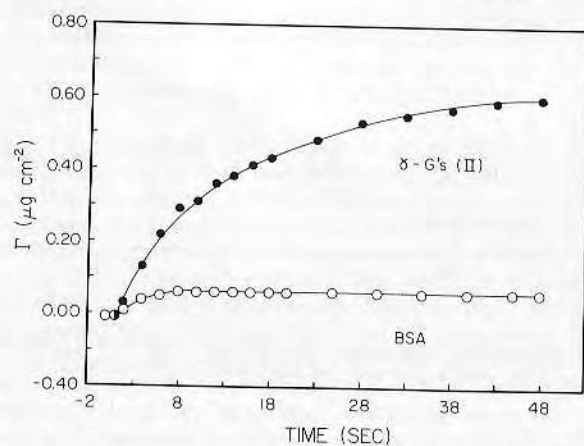

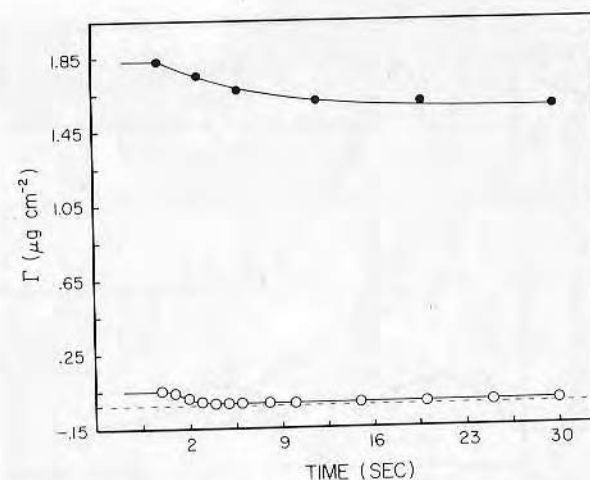*Figure 11. Desorption dynamics for 6.67 μM/L BSA (○) and γ-globulin (●) on hydrophilic quartz at 37°C.*

BSA and γ-globulin appear to exist on hydrophilic quartz, and the surface molar ratio of BSA: γ-globulin is 0.02 picomol/cm²: 8.0 $picomol/cm^2$ after 1 h of desorption. Since desorption was performed statically, such proteins might contribute to an excess in bulk solution, and "irreversible" protein then would not be in equilibrium with a true zero bulk concentration, but this does not seem to be a significant effect. Preliminary experiments indicate that if additional rinsing occurs during the desorption phase, that is, reestablishing zero for C_B, the desorption rate does not change appreciably.

Perhaps the single greatest advantage of TIRF is its ability to determine an adsorbed protein emission spectrum, which is illustrated in Figure 12 for bulk tryptophan and adsorbed γ-globulin and BSA. In all three cases, the emission spectra are broad (300–460 nm), and several have shoulders at wavelengths exceeding 350 nm, which is understandable for both proteins, particularly γ-globulin. The heterogeneity of the proteins as well as the local microenvironment of particular tryptophan moieties contribute to a wide range of fluorescence emissions. Cellulose acetate electrophoresis indicated that BSA and bovine γ-globulin were 99% pure. However, bovine serum Fraction II γ-globulins comprise a variety of different immunoglobulin types, and each of these may be further subdivided into variations in the F_{ab} section. The local tryptophan microenvironment probably contributes the most diversity to the emission spectra. At least three distinct spectral classes of tryptophan exist, one buried deep in nonpolar regions of the protein and two at the surface, one completely and one only partially exposed to the aqueous environment (29). Such spectral classification for the 26 tryptophans in γ-globulin and the two tryptophans in BSA can be employed to elucidate the
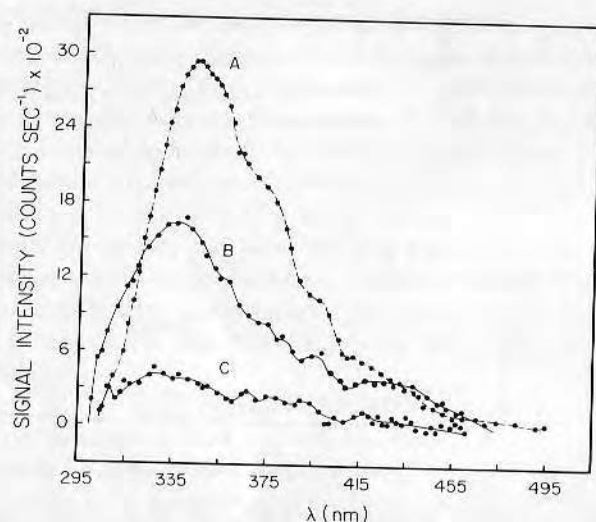

Figure 10. Adsorption dynamics for 6.67 μM/L BSA (0) and γ-globulin (●) on hydrophilic quartz at 37°C.

Figure 12. Fluroescence emission spectra for evanescent wave excited "interfacial" L-tryptophan (A), adsorbed bovine γ-globulin (B), and adsorbed BSA (C).

emission spectra of both proteins between 300–360 nm. The amount and kind of fatty acid complexed to BSA molecules affect the λ_{MAX} and intensity of their emission spectrum (30). Note the tyrosine emission peak λ_{MAX} at 305 nm for BSA. Albumin is one of the few proteins that exhibit tyrosine fluorescence primarily because of its low quantum yield and the existence of several quenching mechanisms (31).

The shoulders at wavelengths exceeding 360 nm are difficult to explain, particularly for the tryptophan case. Tryptophan molecules were possibly concentrated at the quartz-buffer interface in some kind of weak, but sufficiently close association to create resonance fluorescence phenomena exhibiting several peaks between 360–460 nm. Similar peaks exist for both BSA and γ-globulin, and since the background spectra were subtracted to leave the corrected spectra of Figure 12, envisioning how an instrumental artifact could cause the phenomena is difficult. Bulk fluorescence spectra taken in a conventional Aminco Bowman spectrofluorometer showed no such shoulder behavior for L-tryptophan, BSA, or γ-globulin; however, the spectral resolution was not as good as that in the TIRF system. Bulk fluorescence emission spectra obtained with a conventional 1-cm quartz cell and the same TIRF optical and electrical equipment produced data comparable to those obtained in the spectrofluorometer. Consequently, the shoulders appear to be independent of the instrumentation, and the strong possibility exists that conformational changes are reflected in altered fluorescence emission spectra that accompany the adsorption of BSA and γ-globulin on quartz.

In summary, TIRF offers a number of advantages over conventional techniques for studying macromolecular adsorption. First, it is an in situ method yielding real time data with resolutions of 0.1 s. Second, the geometry of the prism flow cell system makes possible the study of factors affecting protein adsorption, that is, interfacial shear stress, temperature, buffer properties, etc. Third, fluorescence emission spectra of adsorbed macromolecules are, in principle, capable of providing information on macromolecular conformational changes accompanying adsorption. This fact is particularly true for the intrinsic fluorescence emission of tryptophan residues that are extremely sensitive to local microenvironments within and upon the protein surface. Finally, by selectively labeling one type of protein, studying competitive protein adsorption with all of the previously mentioned advantages should be possible. This theory is, of course, predicated upon the use of a fluor that does not alter the physicochemical and biochemical properties of the macromolecule to which it is attached.

Acknowledgments

Literature Cited

1. Hirschfeld, T. U.S. Patent 3, 604, 937, 1971.
2. Harrick, N. J.; Loeb, G. I. *Anal. Chem.* 1973, 45, 687.
3. Beissinger, R. L.; Leonard, E. F. *ASAIO J.* 1980, 3, 160.
4. Burghardt, T. P.; Axelrod, D. *Biophys. J.*, in press.
5. Kronick, M. N.; Little, W. A. *J. Immunol. Methods* 1975, 8, 235.
6. Watkins, R. W.; Robertson, C. R. *J. Biomed. Mater. Res.* 1977, 11, 915.
7. Van Wagenen, R. A.; Zdasiuk, B. J.; Andrade, J. D. *Am. Chem. Soc., Div. Org. Coat. Plast. Chem., Prepr.* (Houston, Mar., 1980) 42, 749.
8. Zdasiuk, B. J., Masters Thesis, Univ. of Utah, 1980.
9. Crandall, R. E.; Janatova, J.; Andrade, J. D. *Prep. Biochem.* 1981, 11, 111.
10. Harrick, N. J. "Internal Reflection Spectroscopy"; Interscience: New York, 1967; pp. 25–55.
11. Watkins, R. W., Ph.D. Dissertation, Stanford Univ., 1976.
12. Kronick, M. N., Ph.D., Dissertation, Stanford Univ., 1974.
13. Churchich, J. E. *Biochim. Biophys. Acta* 1966, 126, 606.
14. Chen, R. F. *Biochem. Biophys. Res. Commun.* 1964, 17, 141.
15. Colson, C.; Frederico, E. *Bull. Cl. Sci. Acad. R. Belg. Ser. 5* 1970, 56.
16. Coyle, J. *Chem. Br.* 1980, 16 Ser. 5, 460.
17. Bresler, S. E.; Kolikov, V. M.; Katushkina, N. V.; Ponomareva, R. B.; Zhdanov, S. P.; Koromal'di, E. V. *Colloid J. USSR, Engl. Trans.* 1974, 36, 682.
18. Morrissey, B. W.; Fenstermaker, C. A. *Trans. Am. Soc. Artif. Intern. Organs* 1976, 22, 278.
19. Jennissen, H. P.; Botzet, G. *Int. J. Biol. Macromol.* 1979, 1, 171.
20. Morrissey, B. W. *Ann. N. Y. Acad. Sci.* 1977, 283, 50.
21. McMillin, C. R.; Walton, A. G. *J. Colloid Interface Sci.* 1974, 48, 345.
22. Soderquist, M. E.; Walton, A. G. *J. Colloid Interface Sci.* 1980, 75, 386.
23. Bull, H. B. *Biochim. Biophys. Acta* 1956, 19, 464.

TOTAL INTERNAL REFLECTION INTRINSIC FLUORESCENCE

(TIRIF) STUDIES OF IgG ADSORPTION

by

R.A. Van Wagenen, J.D. Andrade*, and T. Dunn**
Department of Bioengineering
University of Utah
Salt Lake City, Utah 84112

**Becton Dickinson Research Center
Research Triangle Park, North Carolina 27709

*To Whom Correspondence and reprint requests should be directed.

INTRODUCTION

The interaction of immunoglobulins (IgG) with solid surfaces is important in the development of heterogeneous or solid phase immunoassays, in the blood compatibility of medical devices and blood contacting materials, and may be related to surface-induced complement activation.

Adsorption of proteins at solid–liquid interfaces is generally studied by one of two methods: 1) the classical approach uses high surface area adsorbents and measures bulk solution depletion as protein adsorbs; this solute depletion technique is very effective but is limited to high surface area materials; and 2) radiolabelling the protein, generally with I^{125} although other isotopes may also be used, and directly measuring the surface concentration of adsorbed proteins. This method has the disadvantage that the protein must be labelled and that, in some cases, the label may influence the adsorption process itself. Also, quantitation is generally only done following removal of the aqueous bulk phase, thus prohibiting in situ real time studies.

Spectroscopic methods may also be used, such as total internal reflection infrared spectroscopy, which can be done in situ to obtain direct kinetic information on protein adsorption without the use of any label [1]. A related spectroscopic technique, also using total internal reflection optics, relies upon the intrinsic UV fluorescence arising from tryptophan moieties in the protein. When excited at 290 nm, many proteins fluoresce maximally in the 320–350 nm range, depending on the micro-environment of the tryptophan groups present. This intrinsic fluorescence, which has a relatively low quantum yield, of about 0.10, is sufficient to permit the sensitive detection of protein in the vicinity of the interface [2]. The technique, called total internal reflection intrinsic fluorescence (TIRIF) spectroscopy, has been used to study the adsorption of albumin [2], insulin [3], IgG [2], and fibronectin [4] on previous occasions. Other groups have utilized the same approach but

-1-

with an extrinsic fluorescein [5] or rhodamine [6] label, which has the advantage of greatly increased sensitivity and simplified optics and instrumentation, but the disadvantage of a ponderous label which may alter protein physicochemical properties. The TIRF experiment can be performed with a conventional laboratory fluorometer [7] or with homebuilt relatively inexpensive instrumentation [2]. The reflection of a beam of light at the interface between a high index solid surface and a low index aqueous phase, given the proper conditions, results in total internal reflection. This well known phenomenon can be used to probe interfacial processes because the incident and reflected beams can be treated as an interfacially localized standing wave which decays exponentially into the low refractive index or aqueous phase. See Figures 1 and 2. The exponential decay at an excitation wavelength of 290 nm occurs within about 1000 angstroms of the interface. This means that one can study an interfacial process in the presence of bulk solution without the bulk solution signal overwhelming the interfacial signal, as would be the case with transmission optics. In fact, roughly 20% of the bulk signal comes from within 100 angstroms of the solid surface if one assumes a uniform solution concentration all the way to the interface [2].

Adsorption concentrates the solution species at the interface. Due to this concentration effect, the interfacial signal can be, and generally is, much greater than the signal from the bulk solution. Thus, the TIRF technique is particularly sensitive to interfacial processes and is an ideal method to study protein interactions with solid surfaces [2-7]. The high refractive index optical element used, in our case amorphous silica, can be coated with thin films of transparent polymer without compromising total internal reflection conditions [8]. The polymer thin films certainly influence the electric field intensity at the interface, but this can be rigorously modelled

in a straightforward manner [8]. Thus, it is possible to study protein

adsorption on polymer surfaces by the TIRIF technique.

The fluorescence signal can be converted to surface concentration by

direct calibration or via theoretical consideration of the exponentially

decaying electric field [9]. Both methods of quantitation, however, must

assume that the quantum yields of the protein in the adsorbed state and in the

bulk solution are identical. Although this is not generally a good assumption

for proteins containing only a few tryptophans, it is probably a fairly good

assumption for IgG, where many tryptophans are uniformly distributed

throughout the molecule. Thus it is unlikely that a majority of them could

have their micro-environments significantly changed as a result of the

adsorption process. This is encouraging because it permits quantitation but

it is a disadvantage, in the case of IgG, because local macromolecular micro-

environmental changes may not be readily detectable by this method.

One of the advantages of the TIRIF technique is that the intrinsic

fluorescence emission spectrum of tryptophan may shift and its quantum yield

may change in response to local micro-environmental perturbations as the

macromolecule changes conformation. This has been observed, for example, in a

study of the adsorption of human plasma fibronectin on hydrophilic and

hydrophobic surfaces [4] by studying the fluorescence emission spectrum via

the TIRIF spectroscopy technique.

MATERIALS AND METHODS

The TIRIF technique, the apparatus, and the methods for quantitation

have all been described [2,9]. For this preliminary study a lyophilized Cohn

Fraction II human gamma globulin (Miles 64145) was used. This fraction

represented a heterogeneous population of gamma globulin molecules, each which

may adsorb slightly differently. Preliminary work is now being done with

-3-

affinity purified immunoglobulins and monoclonal antibodies. These results will be reported later.

Materials

The hydrophilic "quartz" surface was clean, amorphous silica which was negatively charged under the pH and ionic strength conditions used: pH 7.4 phosphate buffered saline (PBS), 0.145 M NaCl. The surface was cleaned in chromic acid, followed by water and ethanol rinsing, Freon degreasing and air drying in a low particle count clean room environment. The surface was completely wetting with no water contact angle hysteresis observed. This surface is referred to as hydrophilic or clean quartz. The quartz surface was rendered hydrophobic by a vapor phase silanization [10] using n-pentyl silane, resulting in a relatively hydrophobic hydrocarbon-type surface. The polystyrene surface consisted of a ~~Becton Dickinson Falcon Plastic polystyrene~~ (Monsanto 77-300) resin, dissolved in spectral grade toluene and deposited onto clean quartz plates (1 x 30 x 90 mm) by a solution dip casting procedure. Polystyrene thicknesses in the range of 500-2000 angstroms could be attained by controlling the solution concentration and dipping conditions. All surfaces were characterized by advancing and receding water contact angles and by X-ray photoelectron spectroscopy for quality control and surface characterization purposes.

RESULTS

Figure 3 illustrates a typical TIRF protein adsorption experiment with fluorescence intensity plotted as a function of time. Fluorescence was generated by exciting at 285 nm and observing at 335 nm. At the far left a series of control and calibration data are taken. The cell is prefilled with phosphate buffered saline (PBS) and fully equilibrated with that medium prior to any data acquisition. There is a background count rate which is

approximately 2400 counts per second. See A in Figure 3. The excitation

light is shuttered off so that the photomultiplier tube dark count can be

observed, which is of the order of 100 counts per second (B).

Tryptophan solutions, 0.02, 0.05, and 0.10 mg/ml, were used for

calibration purposes. See C,D,E, respectively, in Figure 3. The fact that

the signal comes back down to base line following a PBS flush to remove each

standard means that the tryptophan is not irreversibly adsorbed to the quartz

surface. At time zero a 1 mg/ml human IgG solution is introduced at a flow

rate of 13 ml/min, corresponding to a shear rate, γ, of 210 sec^{-1}, for about

60 seconds. Then the flow rate was reduced to 1 ml/min ($\gamma = 16$ sec^{-1}). This

protocol results in rapid displacement of the buffer by the protein solution

via convective flow. In the boundary layer at the interface the buffer and

protein solution are exchanged by diffusion processes which are kinetically

much slower. Within the first 10 to 30 seconds after injection, protein

arrives at the interface and begins to adsorb. This is observed as a rapidly

increasing signal which tends to plateau at about four minutes reaching a near

constant level (F).

After ten minutes PBS buffer is pumped through the cell at 13 ml/min

for 60 seconds to displace the protein solution. The bulk solution

component of the signal, of course, disappears; thus a rapid drop in signal is

observed (G). The remaining decay in the signal (H) is due to two processes.

The first is the diffusion of protein solution from the boundary layer into

the bulk; the second is the actual desorption of adsorbed protein from the

surface. These will be discussed in more detail later. Thus, both the

adsorption and desorption kinetics can be observed directly.

The time scale in Figure 3 is compressed in order to show the whole

experiment. The time resolution of the technique is of the order of one

second and fairly rapid kinetics can, therefore, be followed. The fairly high background observed, 2400 counts per second, is in part due to the fact that this is a polystyrene film. The polymer molecules in the film, of course, scatter light which contributes a higher scatter background than if one were using an uncoated quartz plate. In addition, polystyrene is intrinsically fluorescent in the ultraviolet due to the phenomenon of exciton fluorescence, due in part to overlap of the aromatic groups. The exciton fluorescence has a maximum fluorescence emission of about 320 nm, right in the range at which tryptophan emits [12].

Diffusion into and out of the boundary layer cannot be modeled using a tryptophan standard because it has, of course, a much higher diffusion rate than does the protein. One can, however, use a nonadsorbing fluorescein- or tryptophan-labeled dextran of the molecular weight which produces a diffusion coefficient approximating that of the IgG molecule. Figure 4 shows a typical experiment where fluorescence intensity is given as a function of $(time)^{1/2}$ for a 64,000 Dalton fluorescein-labeled dextran. The diffusion coefficient of 64,000 molecular weight Dextran is approximately identical to that of 150,000 Dalton IgG ($D \simeq 4 \times 10^{-7}$ cm^2 sec^{-1}). The data is presented at high time resolution. The feature one observes at about six seconds has been well described and is due to scattered light generated at the interface and in the polymer film. Some of this scattered light passes into the bulk solution and excites fluorescence. The total internal reflection process previously described assumes an optically perfect interface. In reality there are some imperfections present; the quartz prism itself can scatter light and any polymer film on the surface will scatter light. In addition, in our particular set-up, a quartz sample plate supporting the polymer film is optically coupled to the prism using glycerol as a refractive index matching

fluid; thus, the interface is not perfect and also scatters light. The scattered light which penetrates into the bulk solution phase produces bulk solution fluorescence. Although this is a fairly minor component for correctly assembled cells, it must be considered in rigorous quantitation. In the first six seconds, one is observing the protein solution flowing into and through the cell. This has been modeled by Lok and Robertson in some detail [5].

The remaining 25 seconds required to reach a plateau concentration is attributed to diffusion of the FITC-labelled dextran into the 3000 angstrom thick region where fluorescence can be excited by the exponentially decaying evanescent wave. This tells us that under these flow conditions (210 sec^{-1}) the interface is fully equilibrated with protein within 30 seconds of injection. The desorption sequence is then initiated via buffer flush at 210 sec^{-1}. Although the kinetics are slightly different due to the different boundary conditions, roughly 30 seconds after desorption the protein solution has been removed and the proteins have successfully diffused from the boundary layer into the bulk. This means that the first 30 seconds of the process are not due to the kinetics of adsorption or desorption but are due to the fluid mechanics and diffusion process involved. The fact that the data is relatively linear between roughly seven and 16 seconds suggests a diffusion-controlled, $(time)^{1/2}$, process. We chose a high injection and flush shear rate (210 sec^{-1}) in order to minimize the time required for diffusion to get protein to and from the surface so adsorption could be clearly discerned. The lower shear rate domain (16 sec^{-1}) was used to (1) prevent bulk protein depletion and (2) to carry away desorbed proteins during PBS flush.

Figure 5 shows the early phase of adsorption and desorption for a typical IgG adsorption experiment; this is comparable to an expanded version

of Figure 3. One can clearly see the seven second inflection due to the bulk solution component. Diffusion into the boundary layer and adsorption are mixed and difficult to separate until one looks at the desorption profile. The first component of desorption is bulk flow, i.e., removal of the bulk protein solution, followed by diffusion from the boundary layer to the bulk solution. This diffusion process equilibrates within 50 seconds. The remainder of the curve is best studied with reference to Figure 6a which plots the entire desorption profile over 60 minutes.

The desorption curve can be broken up very nicely into four components. Component 1 is believed to be due to flush and removal of the bulk protein solution; component 2 is due to diffusion from the boundary layer into the bulk; components 3 and 4 are due to true desorption of the IgG from the surface. Component 3 might be considered a loosely bound component and component 4 a more tightly bound slower desorbing component. The latter two desorption components are observed on hydrophobic polystyrene but are not observed on hydrophilic quartz. See Figure 6b. A two stage desorption profile also seems to occur on the n-pentyl silane treated quartz surface which is also very hydrophobic. See Figure 6c.

Figure 7 shows step isotherms for IgG adsorption onto hydrophilic quartz and onto a 500 angstrom thick polystyrene film on quartz. Each kinetic experiment was allowed to run until an obvious plateau had been reached at a given bulk concentration, C_B. The bulk protein was then flushed out with PBS buffer which made it possible to discern any bulk signal component present. Then a second protein solution of higher bulk concentration was added to the same cell and adsorption was allowed to proceed to equilibrium. This sequence continued to the highest bulk concentration evaluated. The result is a sequential or step isotherm. The background subtracted data are plotted as

post flush bound protein fluorescence intensity vs. bulk protein concentration. Bulk protein concentrations as low as 0.01 mg/ml were readily detected. We have calculated that at a bulk protein concentration of .002 mg/ml, it would be possible to detect a minimum of 0.002 µg cm^{-2} of adsorbed protein on the polystyrene surface. The results are somewhat better for the adsorption of IgG onto clean quartz due to the lower background scatter signal.

The role of polymer film thickness on the overall results was of considerable interest. Different polystyrene film thicknesses were produced by dipping quartz plates in four different polystyrene solutions: 1,2,3, and 5 wt. % polystyrene in toluene. Fluorescence emission spectra were obtained both before and after protein exposure to the surfaces. Adsorption experiments were conducted at two bulk protein concentrations, 0.05 and 1.0 mg/ml. It was very easy to detect IgG adsorption onto polystyrene thin films at bulk concentrations as low as 0.05 mg/ml. The one, two, and three percent solutions give film thicknesses of roughly 500, 1000, and 1500 angstroms, respectively, as determined gravimetrically. In progressing to five percent solutions, the films became considerably thicker with a resultant higher background scatter signal and a loss of protein detectability. Also, as polystyrene film thickness increased, the exciton fluorescence emission peak at about 323 nm also increased significantly, contributing an even higher background to the signal. This would probably not be the case with other polymer systems which do not have this fluorescence mechanism. Optimum results were obtained for the 500 Å thick film. The fluorescence due to adsorbed protein was the predominant signal with such films. With thicker films the film fluorescence was larger than the adsorbed protein fluorescence.

Conclusions

Intrinsic UV TIRF has been used to study the adsorption of IgG on clean hydrophilic quartz, n-pentyl silanized hydrophobic quartz, and polystyrene-coated quartz.

On clean, hydrophilic quartz, the detectability limits were 0.001 mg/ml bulk solution concentration and 0.002 $\mu g/cm^2$ adsorbed protein concentration. The two numbers are coupled because the greater the bulk solution concentration, the greater the signal due to the bulk and the higher adsorbed protein concentration becomes. The detectability limits on polystyrene-coated surfaces are slightly higher owing to the higher background resulting from increased scattering observed in the presence of the polystyrene film. In the case of polystyrene, a 500 angstrom thick film seems optimum. Thicker films cause increased bulk scattering which compromise the detectability limits. This is in large part due to the fact that polystyrene has an intrinsic UV fluorescence due to exciton mechanisms. This effect is not present with most other polymer systems. Future studies will indicate whether or not one can go to much thicker films with other polymers without any adverse background scattering effects.

Adsorption and desorption kinetics were readily observed for IgG adsorption on hydrophilic and polystyrene-coated quartz. The fluid mechanics components of the signal can be readily evaluated and essentially removed from the rest of the signal. The diffusion components of the signal can also be readily evaluated and removed. The desorption kinetics of IgG from hydrophobic surfaces, such as polystyrene and n-pentyl silane, show two processes or different rates, perhaps relating to a loosely bound and more tightly bound protein population. On hydrophilic quartz only one desorption rate is evident.

Much more data analysis is necessary before definitive conclusions can be drawn with respect to the adsorption mechanisms on these surfaces. Also a multiplicity of experiments under different buffer and related conditions must be performed. Nevertheless, we have demonstrated the practical usefulness of intrinsic TIRF for the study of protein adsorption on practical polymer surfaces.

ACKNOWLEDGEMENTS

REFERENCES

1. Winters, S., Gendreau, R.M., Leininger, R.I., and Jakobsen, R.J., _Appl. Spect._ 36, 404 (1982).

2. Van Wagenen, R.A., Rockhold, S., and Andrade, J.D., in "Biomaterials: Interfacial Phenomena and Applications," (S.L. Cooper and N.A. Peppas, Eds), pp. 351-370, Adv. Chemical Series #199, American Chemical Society, 1982.

3. Iwamoto, G.K., Van Wagenen, R.A., and Andrade, J.D., _J. Colloid Interface Sci._ 86, 581 (1982).

4. Iwamoto, G.K., Winterton, L.C., Stoker, R.S., Van Wagenen, R.A., Andrade, J.D., and Mosher, D., submitted for publication (1983).

5. Lok, B., Cheng, Y., and Robertson, C.R., _J. Colloid Interface Sci._ 91, 87, 104 (1983).

6. Burghardt, T.P. and Axelrod, D., _Biophys. J._ 33, 455 (1981).

7. Beissinger, R.L. and Leonard, E.F., _ASAIO J._ 3, 160 (1980).

8. K. Knutson and M. Reichert, "Total Internal Reflection Spectroscopy," Plenum Press, in press.

9. Rockhold, S.A., Quinn, R.D., Van Wagenen, R.A., Andrade, J.D., and Reichert, M., _J. Electroanal. Chem. and Interfacial Electrochem._ in press (1983).

10. Haller, I., _J. Amer. Chem. Soc._ 100, 8050 (1978).

11. Smith, L., Doyle, C., Gregonis, D.E., and Andrade, J.D., _J. Appl. Polymer Sci._ 26, 1269 (1982).

12. Torkelson, J.M., Lipsky, S., Tirrell, M., and Tirrell, D.A., _Macromolecules_ 16, 326 (1983).

FIGURE CAPTIONS

Figure 1. Coordinate system at the interface between two media of different refractive indices n_1 and n_2. The incident radiation is reflected at an angle θ where θ exceeds the critical angle, θ_c. See References 2, 8, and 9.

Figure 2. The standing and evanescent interfacial electromagnetic waves at a totally reflecting interface.

Figure 3. ⌐Results for A typical TIRF protein adsorption experiment. See text for TIRIF details.

Figure 4. Inflow and outflow kinetics for a nonadsorbing fluorescein-labelled dextran of 64,000 Daltons.

Figure 5. The first 40-50 seconds in the adsorption and desorption of IgG on polystyrene. (See text for details).

Figure 6. Desorption profiles for IgG from (a) polystyrene, (b) hydrophilic quartz, and (c) n-pentyl silanized quartz (see text for details).

Figure 7. Step isotherms for IgG adsorption onto hydrophilic quartz (●) and hydrophobic polystyrene (O). (See text for details).
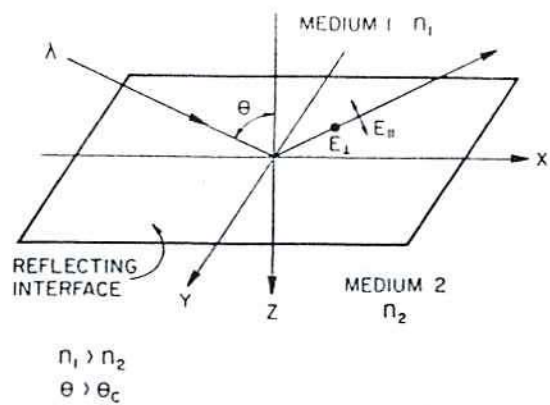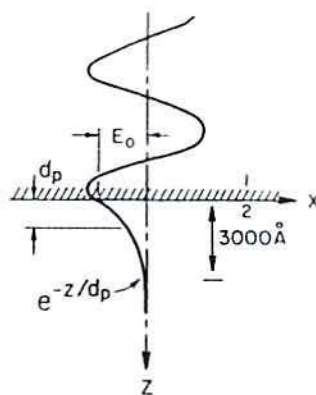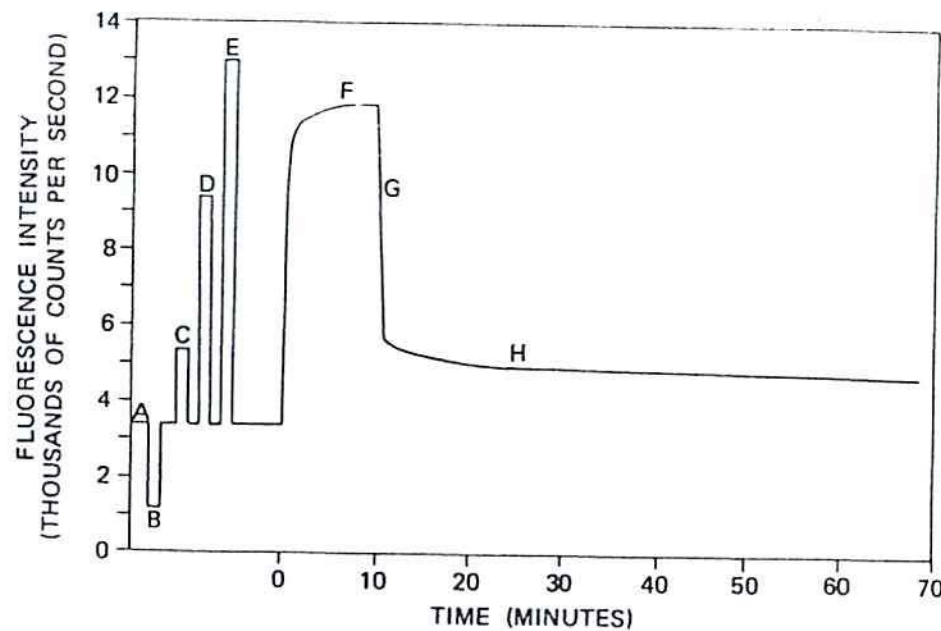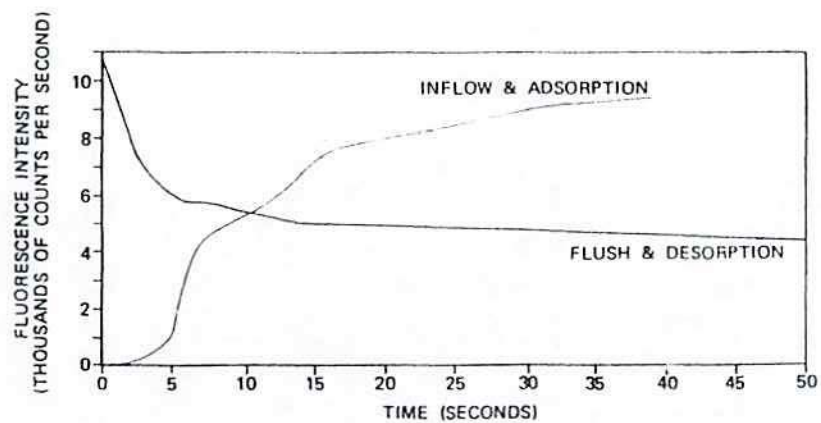
Fig. 1

MEDIUM 1 n_1

λ

θ

$E_\perp$ $E_{\parallel}$

X

REFLECTING INTERFACE

Y

Z

MEDIUM 2 n_2

$n_1 > n_2$

$\theta > \theta_c$

Fig. 2

E_o

d_p

$\frac{1}{2}$

3000 Å

e^{-z/d_p}

X

Z

Fig. 3

FLUORESCENCE INTENSITY (THOUSANDS OF COUNTS PER SECOND)

TIME (MINUTES)

A B C D E F G H

Fig. 5

FLUORESCENCE INTENSITY (THOUSANDS OF COUNTS PER SECOND)

INFLOW & ADSORPTION

FLUSH & DESORPTION

TIME (SECONDS)

Fig. 4

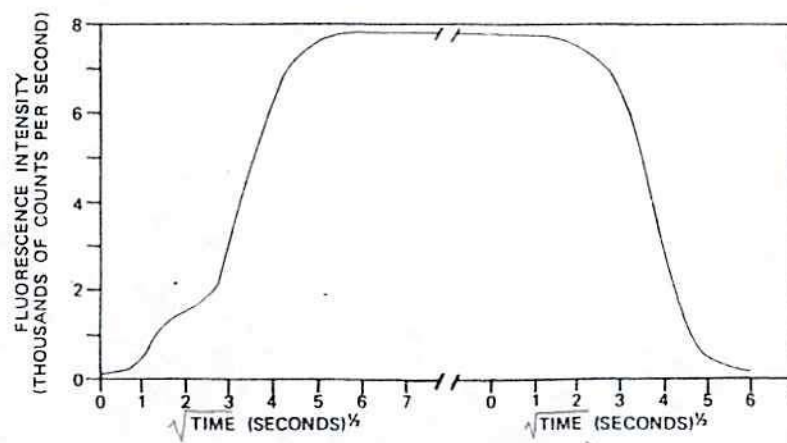FLUORESCENCE INTENSITY (THOUSANDS OF COUNTS PER SECOND)

$\sqrt{\text{TIME (SECONDS)}}$ ½

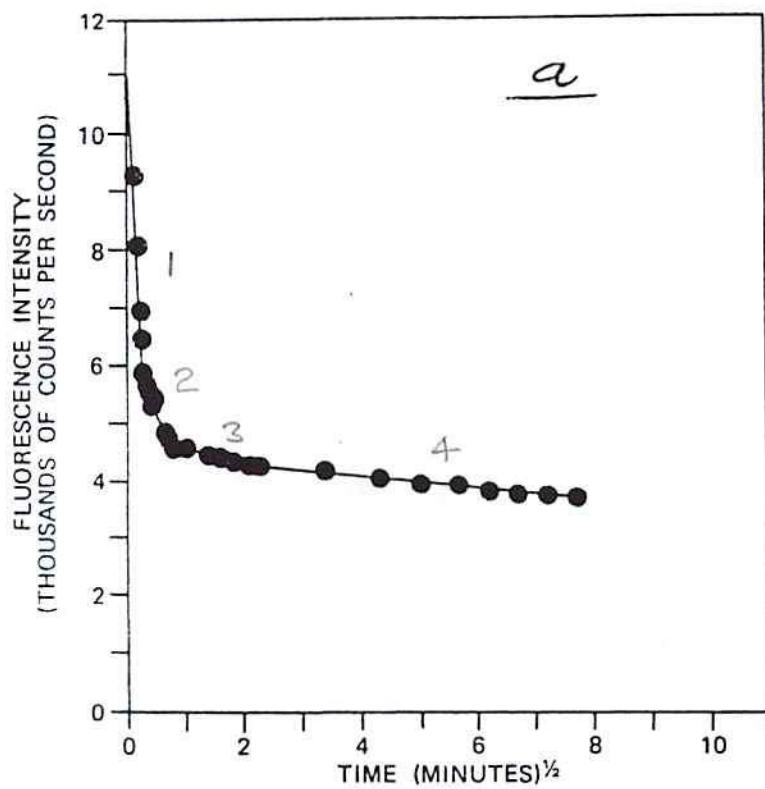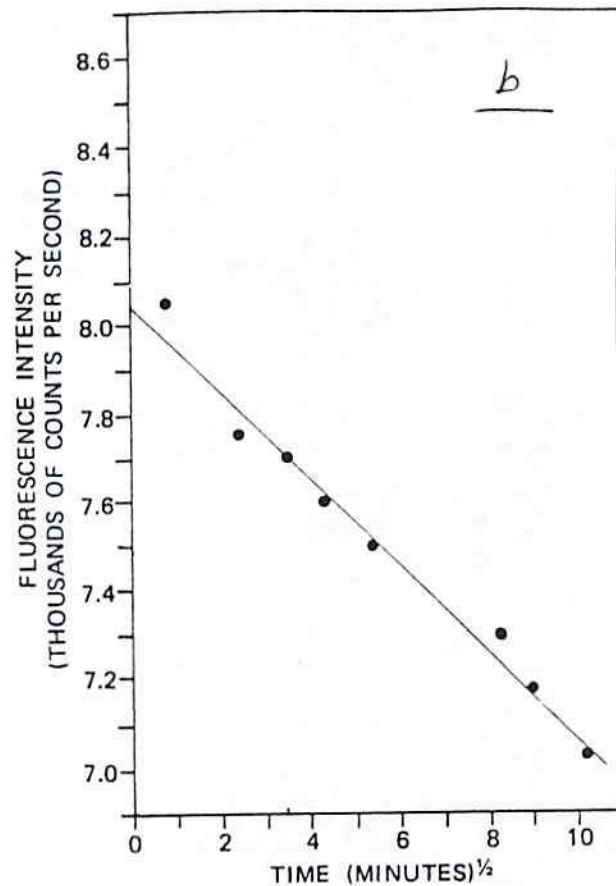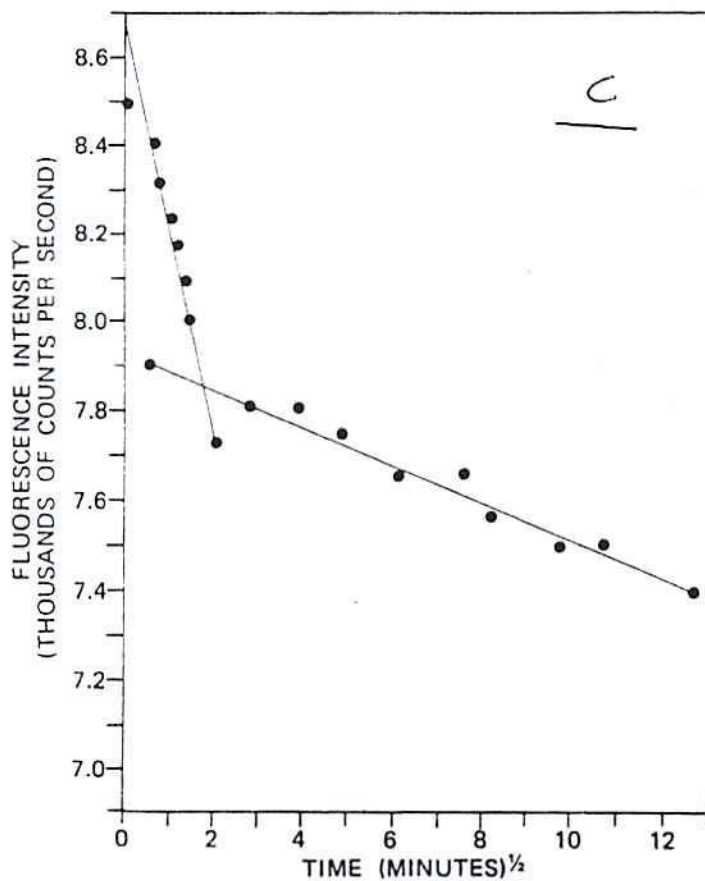$\sqrt{\text{TIME (SECONDS)}}$ ½
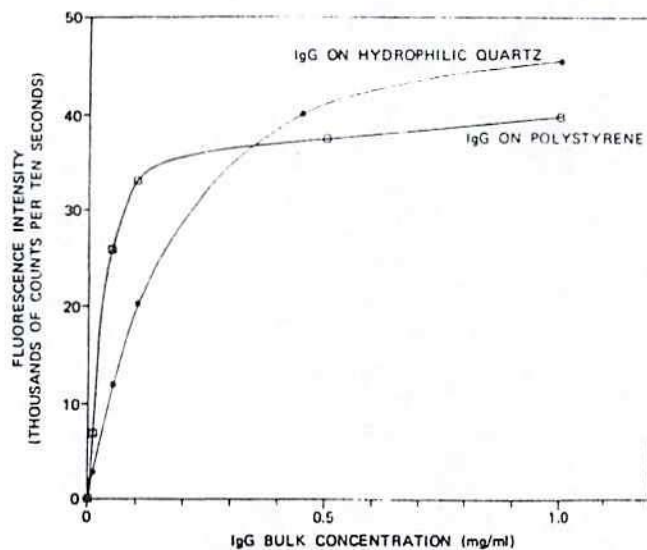
Fig. 6a

Fig. - 6b

Fig. 6c

Fig. 7

Evaluation and selection of activated carbon for hemoperfusion

JOHN M. WALKER, ENNIO DENTI, RICK VAN WAGENEN and JOSEPH D. ANDRADE

*Institute for Biomedical Engineering, University of Utah, Salt Lake City, Utah, and
Sorin—Societa Ricerche Biomediche p. A., Saluggia, Italy*

Activated carbon has been used for a long time in medicine, mainly as an oral antidote in cases of acute poisoning. In the last decade investigations have started in the use of activated carbon to remove toxins in uremia, hepatic failure and acute poisoning. The treatment involves either perfusing the patient's blood through a column containing coated activated carbon or oral ingestion of the adsorbent. Another area of importance is dialysate regeneration, in which adsorbents are used to reduce the volume of dialysate required for hemodialysis.

Different criteria are required for selecting the carbon to be used in each application. Activated carbon used for hemoperfusion must be clean, generate very low numbers of particulates and be non-thrombogenic. To enhance blood compatibility the carbon is coated with a biocompatible material. The size and geometry of the particles are important in hemoperfusion to minimize hemolysis and platelet drop and to ensure satisfactory hemodynamics.

Properties of activated carbon

Smisek and Cerny [1] have reviewed activated carbon, its preparation and its properties. Activated carbon is a highly porous material prepared by carbonizing and activating organic substances mainly of biological origin, such as wood, petroleum, coal, peat and shells. The high porosity and high surface area is the reason for the carbon's large adsorptive capacity. The product of simple carbonization is an inactive material with a specific surface area of the order of several square meters per gram. A sorbent with a highly developed porosity and a correspondingly large surface area is obtained by reaction with an activating agent. Activated carbon is prepared either by physical activation (reaction with steam or CO_2) or by chemical activation (reaction with zinc chlo-

ride). The resulting pores can be classified into micropores (radius < 20 Å), transitional pores (radius, 20 Å to 500 Å) and macropores (radius, 500 Å or greater). Each of these pore types has its own function; the micropores determine the adsorptive capacity, whereas the transitional and macropores enable diffusion to the micropores to occur.

Activated carbons can be divided into two distinct classes according to their physical shape, which is related to the method of manufacture. The first is granular carbon, produced by breaking and sieving activated carbon into a narrow range of particle sizes. In this case, the particle shape is irregular and the macropore structure is a function of the original raw material because during carbonization the volatiles are removed as the macropore structure is formed. The second is extruded granular carbon, produced by extruding previously carbonized powdered material with a binder, carbonizing and activating with steam. In this case any large macropores present in the original carbonized material have been destroyed by grinding. Very spherical activated carbon beads can also be produced by carbonizing and activating synthetic polymer beads [46, 47].

Kinetically the solute molecule must first diffuse externally through the liquid medium to the carbon particle. Internal diffusion then occurs through the macropores into the micropores where actual solute adsorption takes place. The overall rate-limiting step is diffusion within the macropore structure of the carbon [2, 3].

The amount of solute adsorbed at a given temperature and concentration of the bulk phase depends on the nature of the adsorbent and on the components of the solution. As a general rule, nonpolar solutes are better adsorbed from aqueous solution than polar ones. A further factor influencing adsorption from solutions is the steric arrangement and chemical constitution of the molecule.

Adsorption generally increases with increasing molecular weight in a homologous series, but other factors must be taken into account. Adsorption is greater for molecules with straight chains than with branched chains. The particle size of the carbon can affect the rate of adsorption—the smaller the particle the quicker it attains adsorption equilibrium. Other parameters that affect adsorption are temperature, pH and the presence of other constituents.

The activated carbons commercially available in the United States include Darco, Columbia, Witco, Fisher, Nuchar, Barneby-Cheyney, Norit and Pittsburgh. The main producer of carbon in Europe is the Dutch Company Norit; France has Acticarbon; West Germány has Lurgi and Degussa; Italy has Montecatini and Great Britain has Sutcliffe and Speakman Company and Norit-Clydesdale Co., Ltd. A number of activated carbons are made in Japan, by such companies as Takeda Chemical Industries, Mitsubishi International Corporation and Nimura Chemical Industries. Nearly every country has its own carbon.

Activated carbon in medicine

The use of activated carbon in medicine to treat disturbances in the digestive system and to remove poisons has been known since the time of Hippocrates. The first systematic studies of carbon as an antidote were made in 1846. Holt and Holz [4] stated that the most effective antidote for poisons is orally administered activated carbon.

Carbon hemoperfusion began with the report by Yatzidis in 1964 [5, 6] in which he reported that creatinine, uric acid, indican, phenolic compounds, guanidine bases and barbiturates are readily removed by activated carbon. Urea, phosphate and sulfate were poorly removed. Dunea and Kolff [7] reported that platelets were reduced by 50% and Hagstam, Larsson and Thysell [8, 9] found carbon particles in the lungs, spleen, liver and kidneys in their studies of activated carbon hemoperfusion. To minimize blood damage and fine particle generation during carbon hemoperfusion, various investigators have used coatings of polyhydroxyethyl methacrylate (PHEMA) [10–13], cellulose nitrate [14, 15], cellulose acetate [16, 17], cellulose triacetate [18], methacrylate copolymer [19], acrylic polymer [20] and combinations with albumin either adsorbed or crosslinked [21]. Table 1 lists the variety of coatings used for activated carbons. Hemoperfusion has also been used very successfully in the treatment of drug overdoses. It effectively removes paracetamol, paraquat [22, 23], barbiturates, methyprylon, glutethimide, methaqualone and salicylates [24, 25, 27]. Other investigators have evaluated the use of carbon to treat hepatic failure, but conclusive results are not yet available [28, 29].

Greenbaum and Gordon [30] developed REDY, a recirculating dialysate system which uses a combination of activated carbon, urease, zirconium phosphate and zirconium oxide and uses six liters of dialysate. Problems with the nonspecificity of zirconium phosphate require the infusion of magnesium, potassium and calcium ions. The dialysate side of the wearable artificial kidney being developed at the University of Utah [31] uses 250 g of activated carbon.

Activated carbon may also remove the so-called middle molecular weight toxins. Chang et al [45] have documented the efficiency of this in removing compounds of 1000 to 1500 mol wt in serum of patients with chronic renal failure. The carbon hemoperfusion column could be used in conjunction with a hemodialyzer to assist in the removal of creatinine, uric acid and middle molecular weight toxins or in series with an ultrafilter to remove water.

Activated carbon has also been used successfully to remove certain uremic toxins from the gastrointestinal tract, mainly uric acid and creatinine [32, 33].

There are a number of problems with activated carbons. Uncoated carbon is quite traumatic to the formed elements in blood. This is an example of a material that first appeared very promising (high adsorption capacity) but had to be extensively modified (washing and encapsulating) before it was suitable for medical use. The generation of small particulates may lead to microembolic problems. These microparticles or fines are probably generated during activation and shipping of the carbon, and for most industrial applications they are not a problem. However, for a specialty application such as hemoperfusion the fines are a major disadvantage. If not removed from the surface of the carbon before use, it is likely that these microparticles would be carried into the patient's body by his own blood during hemoperfusion. Several investigators have shown that microemboli are a serious problem if the carbon is not adequately washed before use and as a result have questioned the safety of hemoperfusion [8, 17, 34, 35]. Activated carbons before being used medically should be properly evaluated.

Evaluation of activated carbon

A series of tests should be employed to evaluate activated carbons. Table 2 presents these evaluation tests. If an investigator wishes to use an activated carbon that is easily available, the minimum tests that should be performed are microparticle generation, adsorption capacity and ion elution. A simple

Table 1. Coating of activated carbon for medical applications [26][a]

Coating	Investigator	Year[b]	Institution	City
Albumin, adsorbed	Coleman and Andrade	1974	Univ. of Utah	Salt Lake City, Utah
	Herbert et al[c]	1964	Mt. Sinai Hosp.	New York
Albumin, adsorbed on cellulose nitrate	Chang	1969	McGill Univ.	Montreal
Albumin, crosslinked	Andrade et al	1971	Univ. of Utah	Salt Lake City
	Coleman and Andrade	1974	Univ. of Utah	Salt Lake City
Cellulose acetate	Yatzidis	1966	Univ. of Athens	Athens
	Rosenbaum et al	1968	Temple Univ. Med School	Philadelphia
Cellulose triacetate, deacetylated	Denti et al	1973	SORIN	Saluggia, Italy
Cellulose nitrate (collodion)	Chang	1968	McGill Univ.	Montreal
	Rietema and Van Zutphen	1972	Tech Hoge School	Eindhoven
Dextran, adsorbed	Herbert et al[c]	1965	Mt. Sinai Hosp.	New York
Haemoglobin, adsorbed	Lau et al[c]	1965	Mt. Sinai Hosp.	New York
Heparin complexed cellulose nitrate	Chang	1967	McGill	Montreal
Hydroxyethyl cellulose	Davis et al	1974	So. Research Inst.	Birmingham, Alabama
Methacrylate copolymer	Gilchrist et al	1974	Strathclyde Univ.	Glasgow
Nylon	Chang	1966	McGill Univ.	Montreal
Polyhydroxyethyl methacrylate	Andrade et al	1971	Univ. of Utah	Salt Lake City
	Willson et al	1973	King's College Hospital	London
Unidentified acrylic polymer	Fennimore et al	1974	Smith & Nephew Research Ltd.	Harlow, Essex

[a] Refer to [26] for list of references.
[b] Year of first report or, for unpublished work, year of our first knowledge of the work.
[c] For clinical assay applications.

method should be used to ensure that the carbon is properly washed and coated and, if it is used for *in vivo* purposes, to ensure that the carbon column is sterile, nontoxic and pyrogen-free. The ensuing discussion will be concerned with evaluating some of the different types of activated carbons.

Activated carbons as sent by the manufacturer should be subjected to an initial cleanliness test to determine the amount of microparticles present on the surface. The test could simply consist of washing the carbon, filtering out the released fines on a filter and weighing the filter [34].

An important factor associated with the fine carbon particle problem is removal of these potential emboli before the carbon is used in an *in vivo* experiment. Different investigators use different washing techniques [15, 34, 36, 37]. In each case water is used to wash off the microparticles. The effectiveness of the washing technique could be determined either by examining the carbon surface before and after wash-

ing by scanning electron microscopy or by filtering and weighing the microparticles in the final wash solution.

If a fluidized bed is selected, continuous carbon particle collisions occur, resulting in particle fragmentation and the creation of particles small enough to escape the restraining screens and be carried into the blood stream as emboli. In a nonfluidized bed, particle agitation is almost nil and the pressure drop over the column is much lower. The nonfluidized bed has been selected by nearly every investigator studying hemoperfusion. Two main types of attrition testing have been developed. One is use of compressed

Table 2. Summary of tests to evaluate carbon

1. Cleanliness	6. Microparticle generation
2. Washability	7. Ion elution
3. Attrition resistance	8. Blood compatibility
4. Surface morphology	9. Sterility, toxicity,
5. Adsorption capacity	pyrogenicity

air to agitate the particles in a column and the other is use of a rod or ball mill. In each case the fine particles or the granules remaining are weighed to determine the weight change [34].

The surface area of the activated carbon is the deciding factor in the adsorption capacity. Carbons vary in available surface area with the type of activation and its duration. Simple *in vitro* screening tests for measuring the carbon's adsorption capacity for creatinine or other solutes are available. More complicated tests, such as benzene adsorption, are available to measure surface area.

Scanning electron microscopy can yield significant information with regard to the shape of the carbon particle, its macropore structure and the number of microparticles present on the surface. If the pore size distribution is required, mercury porosimetry is used.

It is important to quantitate the number of microparticles being generated during hemoperfusion. Some of the techniques available are nephelometry, coulter counting and filtering. In nephelometry a vertical beam of light is passed through the test solution, and the degree of light scattering is a function of the number of particulates present. The scattered light can be detected by a photoelectric device. Coulter counting counts particulates by measuring changes in resistance caused by the particulates displacing an equal volume of electrolyte. The filtering method uses a 0.2μ or 0.8μ Millipore or Nuclepore filter, through which the test solution is filtered. The amount of microparticles is found by weighing the filter or counting the fines [38]. The number of particulates being produced should be less than that recommended for i.v. fluids [43].

Variable levels of heavy metals are present in the raw carbon, and high levels of copper contamination have been noted [39]. Proper ion elution techniques must be used, which generally consist of acid washing followed by water washing. This necessitates the use of water that is free of heavy metal ions.

To improve blood compatibility and to decrease the number of microparticles being generated by attrition, activated carbon has been encapsulated with a variety of coatings. Unfortunately, the coating often decreases the carbon's adsorption rate and may decrease the capacity. Various investigators have used different techniques of coating from spray coating to pan coating. Different solvents have been used, depending on the polymer. Albumin can be adsorbed or crosslinked to the surface.

Proper tests must be made to ensure that the activated carbon and the hemoperfusion column are sterile, nonpyrogenic and nontoxic.

This paper has not discussed column design, material of construction, flow parameters or pressure drops. Dunlop and Langley [44] concluded that diffusion through the boundary layer is the rate-limiting step in the adsorption onto activated carbon. They also suggested that a long, small-diameter column may be the optimal design for mass transfer. However, a very long column may not be optimal for blood compatibility.

Results and discussion

Commercially available granular and pelletized activated carbons vary widely in terms of initial microparticle content. The studies by Van Wagenen et al [34] on U.S.A. carbons showed that Witco 517 and 256, Columbia carbons JXC, LCK and MBV, Barneby-Cheyney FP and pelletized Norit RBI were the cleanest carbons in the as-received state.

Various carbons differ in terms of efficiency of water washing. Some carbons can be effectively cleaned, depending on the washing process being used. Van Wagenen et al [34] reported that the Witco carbons 517, 256 and 337 as well as the Columbia carbons JXC, MBV and LCK were all effectively cleaned by water washing. Water washing a strong carbon cleans it by washing off the microparticles. Collisions between carbon granules are not sufficient to produce more microparticles. On the other hand, washing a weaker carbon under the same conditions may be sufficient to produce a sizable number of microparticles from collisions. A point of diminishing returns is reached and the carbon does not get any cleaner, since as many microparticles are being created as are being washed away. Various investigators have used different washing techniques, and these are well documented [15, 34, 36, 37].

Witco carbons 517, 125 and 337 and Columbia LCK were found to be more resistant to attrition than Norit, Darco and Pittsburgh SGL granular activated carbons [34]. Table 3 shows the attrition test data of Van Wagenen et al.

Van Wagenen et al [34] reported very good *in vitro* adsorption characteristics for creatinine using Witco

Table 3. Attrition test data using compressed air to agitate the carbon granules [34]

Carbon brand and grade	Mesh size	Average weight loss, $g \pm 1$ SD	Average weight loss, %	Trials N
Witco 517	12 × 24	2.52 ± .31	12.6	10
Columbia LCK	12 × 24	3.14 ± .21	15.7	9
Witco 337	12 × 24	3.53 ± .21	17.65	9
Witco 125	12 × 24	3.97 ± .44	19.85	9
Pittsburgh SGL	12 × 24	4.55 ± .79	22.75	7
Norit	12 × 20	7.42 ± .37	37.10	7
Darco	12 × 24	11.92 ± .21	59.6	4

517 and Columbia LCK (Fig. 1). Denti et al [38], Walker [36] and other investigators found good creatinine clearances with the carbon they selected. Figure 2 depicts the adsorption characteristics of uncoated and coated carbon for molecules of different sizes, showing that for increasing molecular weight compounds it is mainly diffusion through the polymeric coating that decreases the carbon's adsorption capacity [37]. If 200 g of carbon is used at a flow rate of 100 ml/min, creatinine clearance can be maintained at over 100 ml/min for three hours [12].

The surface morphology of different carbons varies markedly, depending mainly on the type of material and the form and duration of activation. Some, as mentioned previously, have fewer microparticles on the surface initially than others. Van Wagenen et al [34] have documented this for a number of the previously discussed carbons.

The University of Strathclyde group [19, 36, 40] chose an extruded activated carbon because it would have a smooth surface, a more regular geometry and more control in the formation of the macropore structure. Benzene desorption and mercury porosimetry experiments were reported [40]. Investigating BAC-MU, a very spherical activated carbon of uniform size and minimal impurity manufactured by Mitsubishi International Corporation, Japanese investigators [46, 47] found that in comparison to coconut activated carbons tested, the adsorption capacity especially for middle molecular weight compounds was much higher for BAC-MU and the microparticle generation rate was five times lower.

Van Wagenen et al [34] found that the shape of the majority of the microparticles was quite irregular for the larger particle sizes ($>20\mu$) and more uniformly
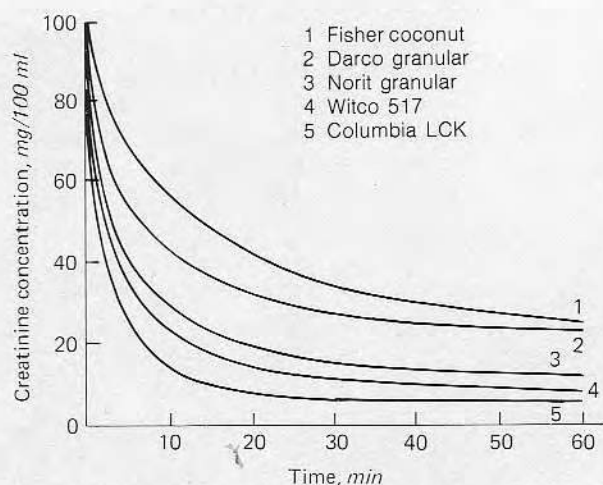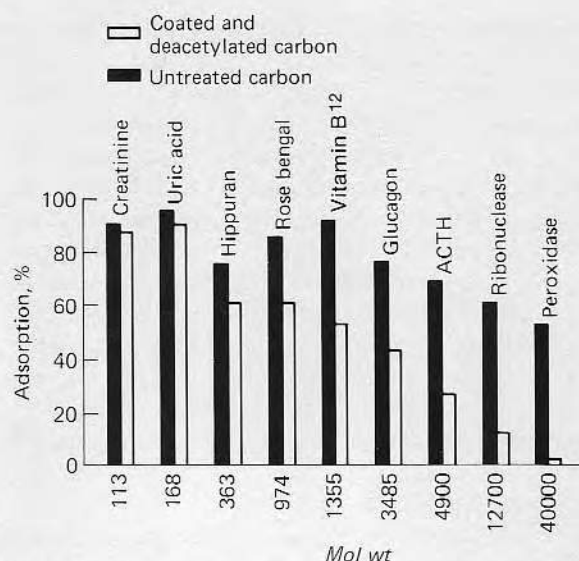
Fig. 2. *Adsorption characteristics of uncoated and coated deacetylated carbon for molecules of different sizes [37].*

ellipsoidal in the case of smaller particles. Figure 3 represents the particle size distribution of microparticles generated using Witco 517 carbon when a carbon/water slurry was agitated and the solution filtered through a 0.22μ Millipore filter. Almost 35%

1 Fisher coconut
2 Darco granular
3 Norit granular
4 Witco 517
5 Columbia LCK

Fig. 1. *Radiolabeled creatinine solute depletion from aqueous solution by various grades of granular activated carbon as a function of time [34].*
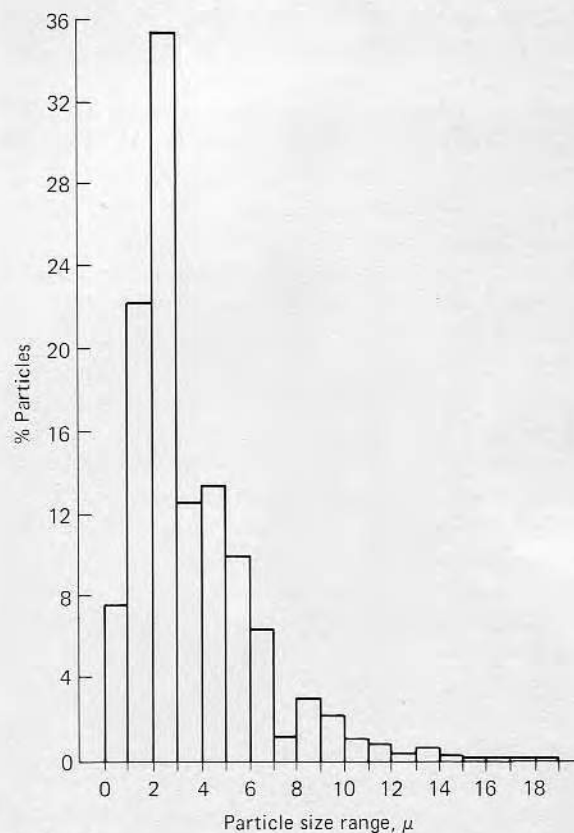
Fig. 3. *Particle size distribution of microparticles generated when Witco 517 carbon is agitated in water [34].*

of all the microparticles are in the 2 to 3μ range, 94% are in the 1 to 7μ size range and less than 5% of all the microparticles are larger than 10μ. This does not necessarily relate to sizes generated during hemoperfusion, as the *in vitro* test conditions are different. Gilchrist et al [19] reported that the particulate generation with the 100 g Strathclyde column was 1 particle/5 ml, mainly in the 2 to 5μ range. Denti et al [38] reported that the release of particulate matter with uncoated carbon was a 8.6μg before washing and 3.8μg after washing. Coated washed carbon generated 0.4μg. The amount of carbon was 125 g, the flow rate was 50 ml/min and the time was six hours. Using a coulter counter, Denti found that the microparticulates generated came mainly from the perfusion circuit and not from the coated carbon. Van Wagenen, Coleman and Andrade [41] reported similar results and found that a column of well-cleaned, strong activated carbon (200 g) perfused at a flow of 150 to 200 ml/min for three hours generated 200 to 500 μg carbon particles, in the 1 to 2μ range. Watson et al [39] have graphed the concentration of 2 and 5μ particles leaving the wash fluid of their column as a function of time. It is difficult to compare the microparticle generation rates obtained from different investigators, as different amounts of carbon, different flow rates and different volumes of perfusate have been used. The microparticle generation rate should be expressed in micrograms of microparticles generated per gram of activated carbon per hour per ml of perfusate. The flow rate used should also be stated. It has been recommended that there should be no more than 1000 particles/ml at 2μ or no more than 100 particles/ml at 5μ for i.v. fluids [42, 43]. The number of microparticles generated by carbon hemoperfusion should be less than these values.

Water-extractable ions should be removed from the carbon before hemoperfusion begins. As different activated carbons use different starting materials, e.g., peat, petroleum and coconut, the ion contamination of the carbons will vary widely. Smith and Nephew have shown that for their activated carbon, although derivatives of copper are not extracted by water or saline, these derivatives may be leached out by plasma or serum [39]. To remove water-extractable materials, Denti, Giovannetti and Luboz [18] employed the following washing technique:

(*a*) Wash in concentrated hydrochloric acid.
(*b*) Wash in boiling water until pH rises to 6–6.5.
(*c*) Prolonged wash in deionized water.

Denti et al concluded that acid washing is sufficient for decreasing the ion release to safe levels [18].

With regard to the polymer coating, a wide variety of polymeric materials have been used by different investigators. Many of the coatings do significantly decrease the number of microparticles and increase the blood compatibility and do not severely decrease the adsorption capacity of the carbon.

A very strong carbon may not require a strong coating, whose function is to reduce microparticles— such a carbon requires only a blood-compatible coating. A weak carbon requires a strong coating to minimize fines production and to act as a blood-compatible surface. If a thin protein coating, e.g., albumin, was used to encapsulate the carbon, the carbon selected must have an intrinsic low microparticle generation rate.

If carbon hemoperfusion is used acutely as in drug overdose, the concern over microparticles and blood compatibility may not be as great as when carbon hemoperfusion is used chronically as to treat chronic uremia or hepatic failure.

The carbon column should have a very low priming volume and very low blood loss, especially if applied to uremic patients. Gilchrist et al [19] reported a 2 to 8 ml blood loss with a 500-ml washback through a 100-g carbon column at an average flow rate of 150 ml/min. The University of Strathclyde group [19] also found a 30 to 40% reduction in platelet levels with coated carbon in preclinical evaluations, and in clinical evaluations no platelet drops in excess of 25% of the initial count were reported. Vale et al [25] reported a mean fall in the platelet level of 38% using 300 g of coated carbon (Smith and Nephew Research, Ltd.) at a flow rate of 100 to 300 ml/min. Chang [15] reported a post-hemoperfusion value of 91.8% ± 11.8% using 300 g of albumin-coated collodion-microencapsulated activated carbon at a flow rate of 150 to 200 ml/min. Andrade et al [12] reported a 20 to 50% platelet drop in the first hour of perfusion using albumin-coated carbon and a platelet drop of 20% or less in one hour of perfusion using polyhydroxyethyl methacrylate–coated carbon. The platelet drop for uncoated carbon was 50 to 70%. Denti obtained a 54% platelet drop after one hour using 125 g of cellulose-coated carbon at a flow rate of 50 ml/min in dogs (unpublished results). Odaka et al [46] reported a 20 to 30% platelet drop and no change in the white blood cell level using 90 g of albumin/collodion-coated spherical carbon clinically. No comparisons can be made between the platelet drops reported by different investigators if different types of animals were used in their experiments. Rosenbaum, Ronquillo and Argyres [17] found that the platelet drop that occurred during coated-carbon hemoperfusion was similar to the drop obtained during conventional hemodialysis treatment.

Care must be taken in sterilizing the carbon column. If autoclaving is used, the high temperatures (120°C) may cause structural changes in the polymer coating. Some coatings are autoclavable; others may not be. If ethylene oxide is used, it will be adsorbed onto the carbon, and if the carbon has a high concentration of chloride ion, ethylene chlorohydrin will be formed, which is toxic. Investigations by Walker [36] showed that it takes three to four weeks for desorption of ethylene chlorohydrin from coated carbon. If the carbon has a low concentration of chloride ion, then the time required for desorption of ethylene chlorohydrin will be less. Another method is radiation sterilization of activated carbon, although no work is available at present. Two percent formaldehyde solution has been used, but care must be taken to ensure that it is completely desorbed [19]. Activated carbon will adsorb gases from the air or impurities from water, and great care must be taken in the storage of carbon, the method of washing and coating to ensure optimal conditions.

Activated carbon can adsorb pyrogens from contaminated distilled water and tap water. To prevent pyrogenic reactions from occurring, a sample of fluid from the outlet of the column should be submitted for a pyrogen test. All the materials used in the column construction, carbon and coating material must be nontoxic, nonpyrogenic and sterilizable.

Conclusions

As the different activated carbons vary in their properties, it is essential in hemoperfusion that the activated carbons be properly evaluated to select the best ones for use. The evaluation tests which were discussed were for cleanliness, washability, attrition resistance, adsorption capacity, microparticle generation and ion elution. Scanning electron microscopy can give useful data on the surface morphology of the carbon. The polymeric coatings should be tested for blood compatibility and tests made on the complete device to ensure sterility, nontoxicity and non-pyrogenicity.

Witco 517, Columbia LCK and Norit RBI are carbons which appear satisfactory for use in hemoperfusion provided that the appropriate handling and preparation is used. Other activated carbons may be used as long as they are thoroughly washed and the microparticle generation rate is less than the limits set for i.v. fluids. If carbon hemoperfusion is used chronically as an assist to treat chronic uremia, concern over the microparticle generation rate, blood loss and blood compatibility will be greater than if carbon hemoperfusion is used acutely to treat poisoning.

The selection of the carbon to be used is only one of the aspects of carbon hemoperfusion that must be evaluated; others include column design, flow rates and pressure drops.

The activated carbons used in dialysate regeneration could have higher adsorption capacities and hence a higher microparticle generation rate, as they are not coming into direct contact with blood.

References

1. Smisek M, Cerny S: *Active Carbon.* New York, Elsevier Publishing Company. 1970
2. Weber WJ, Morris JC: Kinetics of adsorption on carbon from solutions. *Proc Am Soc Civil Eng* 89:31–59, 1963
3. Dedrick RL, Beckmann RB: Kinetics of adsorption by activated carbon from dilute aqueous solution. *Chem Eng Progr Symp Ser* 74, 63:68–78, 1968
4. Holt LE, Holz PH: The black bottle. *J Pediatr* 63:306–314, 1963
5. Yatzidis H: A convenient hemoperfusion micro-apparatus over charcoal for the treatment of endogenous and exogenous intoxications. Its use as an effective artificial kidney. *Proc Eur Dial Transpl Assoc* 1:83–84, 1964
6. Yatzidis H: Treatment of severe barbiturate poisoning. *Lancet* 2:216, 1965
7. Dunea G, Kolff WJ: Clinical experience with the Yatzidis artificial kidney. *Trans Am Soc Artif Intern Organs* 11:178–182, 1965
8. Hagstam KE, Larsson LE, Thysell H: Experimental studies on charcoal haemoperfusion in phenobarbital intoxication and uremia including histopathological findings. *Acta Med Scand* 180:593–603, 1966
9. Hagstam KE, Larsson LE, Thysell H: Charcoal deposition in internal organs after haemoperfusion with the Yatzidis technique in rabbits. *Proc Eur Dial Transpl Assoc.* 3:352–354, 1966
10. Andrade JD, Kunitomo K, Van Wagenen R, Katigir B, Gough D, Kolff WJ: Coated adsorbents for direct blood perfusion: Hema/activated carbon. *Trans Am Soc Artif Intern Organs* 17:222–228, 1971
11. Andrade JD, Kopp K, Van Wagenen R, Chen C, Kolff WJ: Activated carbon and blood perfusion: A critical review. *Proc Eur Dial Transpl Assoc* 9:290–301, 1972
12. Andrade JD, Van Wagenen R, Chen C, Ghavamian M, Volder JGR, Kirkham R, Kolff WJ: Coated adsorbents for direct blood perfusion II. *Trans Am Soc Artif Intern Organs* 18:473–483, 1972
13. Willson RA, Winch J, Thompson RPH, Williams R: Rapid

removal of paracetamol by haemoperfusion through coated charcoal. *Lancet* 1:77–79, 1973

14. Chang TMS: (1966–1969) Refer to references in ref. 15
15. Chang TMS: *Artificial Cells.* Springfield, Illinois, Thomas, 1972
16. Yatzidis H, Psimenos G, Symoulidis DM: Nondialyzable toxic factor in uraemic blood effectively removed by activated charcoal. *Experimentia* 24:1144, 1969
17. Rosenbaum JL, Ronquillo E, Argyres SN: Column hemoperfusion and hemodialysis techniques to treat barbiturate intoxication in dogs. *J Alb Einstein Med Center* 16:67–71, 1968
18. Denti E, Giovannetti S, Luboz MP: Adsorption techniques for the artificial substitution of renal functions, in *Proc 2nd Bioeng Conf.* Milano, Italy, Nov, 20, 1973, to be published
19. Gilchrist T, Johnsson E, Martin AM, Naucler L, Cameron A: Development of the Strathclyde haemoperfusion system, in *Artificial Liver Support,* edited by Williams R, Murray-Lyon IM, London, Pitman Medical, 1975, pp. 319–328
20. Fennimore J, Munro GD: 1 Design problems, in *Artificial Liver Support,* edited by Williams R, Murray-Lyon IM, London, Pitman Medical, 1975, pp. 330–336
21. Coleman DL, Andrade JD: Platelet retention of albuminated glass beads. *Circulation* 50 (suppl 3): Abstr 1138, 1974
22. Maini R, Winchester J: Removal of paraquat from blood by haemoperfusion over sorbent materials. *Br Med J* 3:281–282, 1975
23. Winchester JF, Edwards RO, Tilstone WJ, Woodcock BG: Activated charcoal haemoperfusion and experimental acetaminophen poisoning. *Toxicol Appl Pharmacol* 31:120–127, 1975
24. Vale JA, Rees AJ, Widdop B, Goulding R: Use of charcoal haemoperfusion in the management of severely poisoned patients. *Br Med J* 1:5–9, 1975
25. Vale JA, Rees AJ, Widdop B, Goulding R: The use of charcoal haemoperfusion in the management of severely poisoned patients, in *Artificial Liver Support,* edited by Williams R, Murray-Lyon IM, London, Pitman Medical, 1975, pp. 352–355
26. Andrade JD, Coleman DL, Kim SW, Lentz DJ: The coating of activated carbons for optimal blood compatibility, in *Artificial Liver Support,* edited by Williams R, Murray-Lyon IM, London, Pitman Medical, 1975, pp. 84–92
27. Chang TMS: Biocompatible microencapsulated (coated) charcoal for haemoperfusions in patients, in *Artificial Liver Support,* edited by Williams R, Murray-Lyon IM, London, Pitman Medical, 1975, pp. 94–102
28. Abouna GM, Gilchrist T, Pettit JE, Boyd ND, Todd JK, Courtney JM, Maini R: Haemoperfusion with activated charcoal in treatment of experimental acute hepatic failure, in *Artificial Liver Support,* edited by Williams R, Murray-Lyon IM, London, Pitman Medical, 1975, pp. 180–184
29. Gazzard BG, Weston MJ, Murray-Lyon IM, Record CO, Williams R: Experience at King's College with charcoal haemoperfusion—overall results in 37 patients, in *Artificial Liver Support,* edited by Williams R, Murray-Lyon IM, London, Pitman Medical, 1975, pp. 234–241

30. Greenbaum MA, Gordon A: A regenerative dialysis supply system. *Dialysis Transplant* 1:18, 1972
31. Stephen RL, Jacobsen SC, Atkin-Thor E, Kolff WJ: Portable/wearable artificial kidney (WAK)—initial evaluation. *Proc Eur Dial Transpl Assoc* 12:1975, in press
32. Sparks RE, Mason NS, Litt MH, Meier PM, Lindan O: Removal of uremic waste metabolites from the intestinal tract by encapsulated carbon and oxidised starch. *Trans Am Soc Artif Intern Organs* 17:229–235, 1971
33. Decker WJ, Combs HF, Corby DG: Adsorption of drugs and poisons by activated charcoal. *Toxicol Appl Pharmacol* 13:454, 1968
34. Van Wagenen RA, Steggall M, Lentz DJ, Andrade JD: Activated carbons for medical applications: *In vitro* microparticle characterization and solute adsorption. *Biomat Med Dev Artif Organs* 3(3):319–364, 1975
35. Merrill JP: Treatment of drug intoxication by hemoperfusion. *N Engl J Med* 284:911, 1971
36. Walker JM: Evaluation of carbon haemoperfusion and urea removal systems. Ph.D. Thesis, University of Strathclyde, Glasgow, 1974
37. Denti E, Luboz MP, Tessore V: Adsorption characteristics of cellulose acetate coated charcoals. *J Biomed Mater Res* 9:143–150, 1975
38. Denti E, Luboz MP, Tessore V, Castino F, Gaglia PF: Adsorbents in hemoperfusion *Kidney Int* 7:S401–S405, 1975
39. Watson PA, Kolthammer JC, Western NJ, Warren R: Safety evaluation, in *Artificial Liver Support,* edited by Williams R, Murray-Lyon IM, London, Pitman Medical, 1975, pp. 344–349
40. Cameron A. Courtney JM, Gilchrist T, McDowell J, Walker JM: The selection and use of activated carbon to treat kidney diseases and drug overdose, in *Soc Chem Ind, 4th London Internat Carbon and Graphite Conf,* 1974, to be published
41. Van Wagenen R, Coleman DL, Andrade JD: Adsorbent hemoperfusion: nonbiological particulate matter. *Kidney Int* 7:S397–S400, 1975
42. Vessey I, Kendall CE, Peters FE: Particulate matter in intravenous fluids. *Med J Aust* 1:293–294, 1966
43. *British Pharmacopoeia:* Limit test for particulate matter, Appendix XVIC A 123, 1973
44. Dunlop EH, Langley PG: Column design for adsorbent systems and the effect on mass transfer, in *Artificial Liver Support,* edited by Williams R, Murray-Lyon IM, London, Pitman Medical, 1975, pp. 310–318
45. Chang TMS, Migchelson M, Coffey JF, Stark A: Serum middle molecule levels in uremia during long term intermittent hemoperfusions with the ACAC (coated charcoal) microcapsule artificial kidney. *Trans. Am Soc Artif Intern Organs* 20:364–371, 1974
46. Odaka M, Hirosawa H. Tabata Y, Kobayashi H, Soma M. Nomura Y, Sato H. Nabeta K: Hemoperfusion utilizing coated activated carbons, in *Proc Artif Organs Conf.* Tokyo, 1975, vol. 4, A57, to be published
47. Amano I, Kano K, Ono S, Sugiyama B, Shitaji T, Saito A, Manji T, Maeda K, Ota K: Basic investigation on adsorptivity of coated activated carbons, in *Proc Artif Organs Conf,* Tokyo. 1975, vol. 4, A56, to be published